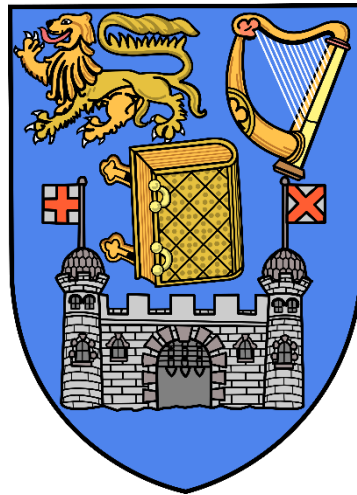# Reconfigurable Test Execution Systems
Machine and Process Development

By

Cian Martin

Department of Mechanical and Manufacturing Engineering

Parsons Building

Trinity College Dublin

Declaration

I declare that this thesis has not been submitted as an exercise for a degree at this or any other university and is entirely my own work. I agree to deposit this thesis in the University's open access institutional repository or allow the library to do so on my behalf, subject to the Irish Copyright Legislation and Trinity College Library conditions of use and acknowledgement.

_____

Cian Martin, 23th February 2017

Acknowledgements

I would like to take this opportunity to thank my supervisor Prof. Garret O'Donnell for his advice, guidance and tutelage throughout this project. I would also like to express my thanks and gratitude to the following people for their contribution:

To Dr. Jeff Morgan for his constant assistance, creative input and Labview support.

To Rory Stoney for his technical and machining skills and also for facilitating this opportunity.

To Seamus O'Shaughnessy, Barry Aldwell, Rob McDowell and Daniel Trimble for their time and support.

Contributors

This thesis is a result of an industrial partnership between Trinity College Dublin and Ceramicx. The CIRCLE end-of-line test system was developed by the following:

- Cian Martin   Masters student   Mechanical Engineer.
- Dr. Jeff Morgan   Post-Doc   Software Engineer.
- Dr. Garret O'Donnell   Associate Professor   Principal Investigator.
- Robert McDowell   Masters Student   Mechanical Engineer

Electrical and mechanical design and manufacture was undertaken by Cian Martin. Software routines described within were developed by Dr. Jeff Morgan. Early concept CAD was developed by Robert McDowell.

Abstract

Reconfigurable manufacturing systems (RMS) are a key enabling technology to meet new challenges in a global market. These emerging products and markets are defined as having short development cycles, being highly customisable and manufactured in sufficient quantity to meet the demands of a diversified consumer base[1]. RMS's are designed for rapid adjustment of functionality and production capacity in response to new process technology, customer requirements and market conditions. The RMS has several characteristics which are distinct from other forms of manufacturing execution systems. These include; modularity, integrability, customization, convertibility and diagnosability. Such requirements are achieved through leveraging recent technological advances in cloud computing and Internet of Things (IoT) and the concepts of cyber-physical systems and Industry 4.0. To achieve a holistic RMS, these design principles must be applied to each phase in the manufacturing process, from initial materials processing to end-of-line testing.

The objective of the work presented in this thesis was to design an end-of-line test execution system (TES) based on modular, reconfigurable and plug and produce concepts. The TES is designed for utilisation in an Irish SME for the automated test of infrared ceramic heating elements. The TES was constructed with a view for integration and expansion and comprised an asynchronous conveyor system with a number of modular test stations. Several process measurement systems were integrated into each test station. These systems were characterised and specific process parameters were identified for successful product testing as part of the commissioning of the TES. This investigation provided critical insight into the material properties and functional performance of the product. The TES developed within this research and the product database created as a result of its operation will provide a platform for future research in reconfigurable manufacturing and test systems.

Table of Contents

Nomenclature

Abbreviation	Description
A	Amps
ATE	Automated Test Equipment
BRIC	Brazil, Russia, India, China
CAD	Computer Aided Design
CAE	Computer Aided Engineering
CCD	Charge Coupled Device
CIRCLE	Ceramicx Infra-Red Heater Characterisation Laboratory Equipment
CMM	Coordinate Measuring Machine
CMOS	Complementary Metal-Oxide Semiconductor
CPS	Cyber-Physical System
DAQ	Data Acquisition Device
DML	Dedicated Manufacturing Line
DUT	Device Under Test
ERP	Enterprise Resource Planning
FMS	Flexible Manufacturing System
FPA	Focal-Plane Array
GPIO	General Purpose Input Output
ICT	Information and Communication Technology
IoT	Internet of Things
mA	Milliamp
MCB	Miniature Circuit Breaker
MEMS	Micro Electro-Mechanical Sensors
NI	National Instruments
PSU	Power Supply Unit
R&D	Research and Development
RCD	Residual Current Device
RMS	Reconfigurable Manufacturing System
SNR	Signal to Noise Ratio
SOP	Standard Operating Procedure
TES	Test Execution System

1 Introduction

1.1 Product test systems

Globalisation in the late 20th century has resulted in ever greater competition in manufacturing technology[2]. Pressure to reduce research and development time, component lead times and time to market have forced a rapid evolution in manufacturing processes and techniques. These pressures have arisen as more dynamic markets and shorter product life cycles require manufacturers to compress the time required to propose, develop, manufacture, market and deliver products[2]. In modern production, being first to market leads to extended product lifecycles, better market penetration and a higher added value for products[3]. However, in this race to market, quality must be maintained. New technological advances have enabled manufacturers to undertake more comprehensive quality and performance testing by incorporating digital data into manufacturing processes with the use of enabling technologies such as Internet of Things (IoT), Big Data and, most recently, concepts such as Industry 4.0.

Current production methods need to adapt to meet changing market demands. Common dedicated manufacturing lines (DML), designed to manufacture single products in high volume, are too inflexible to meet changing trends. Flexible manufacturing systems (FMS), which are general purpose and software reconfigurable, are often too slow for large scale manufacturing and come with a high initial cost. The ideal manufacturing system needs to be responsive to market variability, able to acquire and manage production resources, and offload excess resources in alignment with demand. Likewise, test systems incorporated into the manufacturing process must also be able to reconfigure in line with product volume and variety as well as changeable client and regulatory demands.

The reconfigurable manufacturing system.

Through modular physical construction, a reconfigurable manufacturing system (RMS) is designed for rapid change in structure. Hardware and software components can be modified in order to quickly adjust production capacity and functionality within a product or part family[4]. By following six core design principles, the RMS can outperform other production systems in terms of structure, scalability and productivity[5].
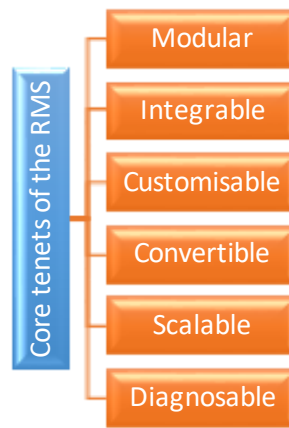
Figure 1.1-1 Tenets of the RMS [5]

These principles give the RMS system the ability to adapt to new requirements as products, assembly methods and test requirements develop. Modules are easier to update and maintain compared to a full system rebuild. New tests and features can be added quickly and meshed into the system and software architecture. The RMS incorporates quick changeover mechanisms and can switch between multiple test sequences depending on product requirements. Speed is key in this process and features such as automated part sensing and calibration can reduce change-over and maintenance downtime. The RMS can also change in accordance to product demand and volume. Adding additional processes or duplicating existing processes reduces bottlenecks and increases overall throughput, at a lower cost than purchasing multiple machines.

As RMS's are frequently adapted, changed and expanded upon, diagnosability is crucial to detect machine failures and conflict between hardware and software modules[6]. The ever changing nature of the RMS puts pressure on the machine designers to account for modules and modes not yet conceived when designing the initial structure. These unknown specifications must be taken into account to avoid limitations to reconfigurability, and can be achieved through over specification of core components and application of generous safety factors.

By leveraging the advances in communication, Internet of Things (IoT), Big Data, and Industry 4.0, RMS's will be the smart manufacturing system of the future, automatically calculating required production, then reconfiguring and adapting to predicted demand.

1.2 Big Data and Industry 4.0

Industry 4.0 has become a synonym for the transformation of today's factories into tomorrow's smart factories, which can meet the current challenges of short product lifecycles, customisation and global competition. Industry 4.0 is a concept of vertical integration across the entire product value chain, binding suppliers, designers, manufacturers and logistics through smart, adaptive communications networks. As the first three industrial revolutions were enabled by innovations surrounding mechanisation, electricity and IT, the enabling technology of Industry 4.0 is the Internet of Things (IoT), a network of microcontrollers, actuators, sensors and communication equipment which can acquire large amounts of real-time information. IoT is a concept based on a collection of intelligent, independent nodes, each with the ability to acquire and wirelessly communicate data from the physical world. This data is then received and uploaded to servers or web based applications for storage and analysis[7]. These nodes are characterised as being cheap to manufacture and deploy, having limited processing power and long battery life. Approximately 90% of all industrial processes are supported by ICT[8].
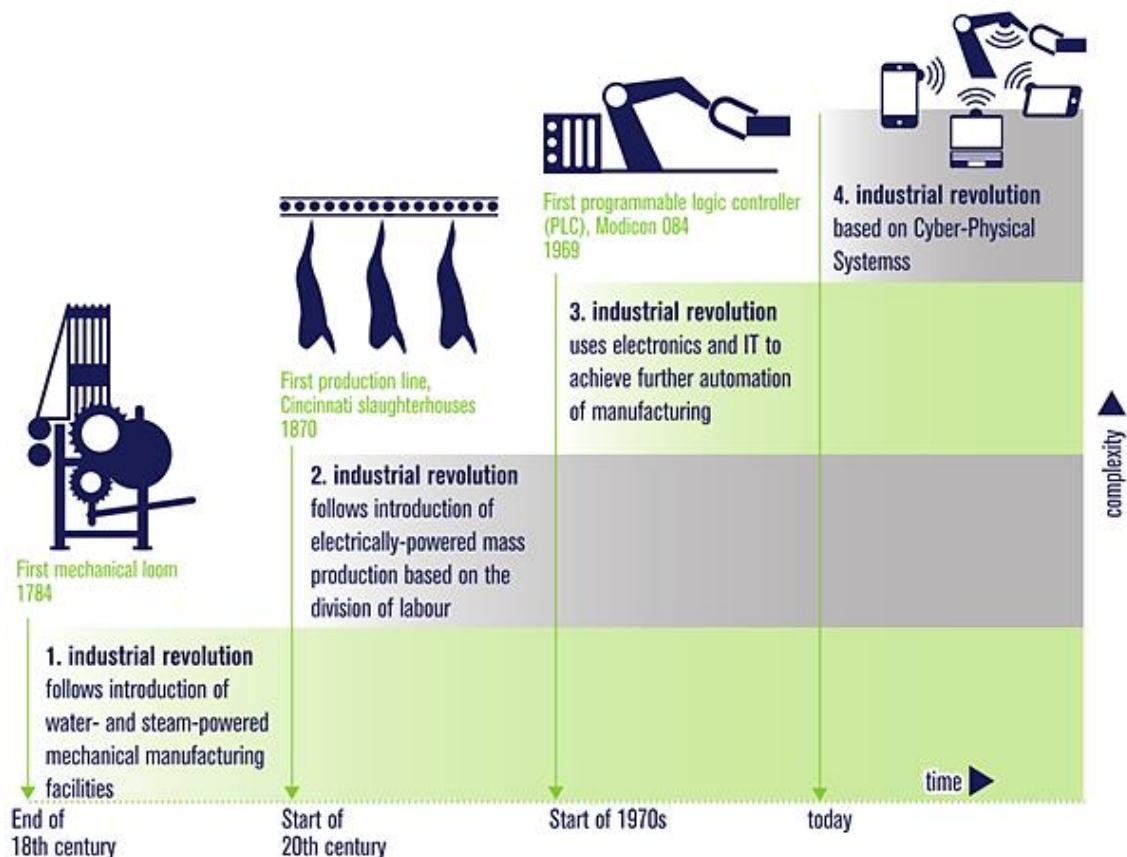

Figure 1.2-1 The fourth industrial revolution[9]

3

These systems link physical production and test environment with layers of local and cloud based software, creating an amalgamation of the real and virtual worlds. This is known as a cyber-physical system (CPS). A CPS enabled factory is comprised of smart machines, warehousing systems and production facilities, which are end-to-end ICT integrated and capable of autonomously exchanging information and self-configuration[10]. This approach ensures that every step of the production process, from inbound logistics, to production, marketing, outbound logistics and service, is quantifiable and traceable, allowing for flexibility and an analytical, data-driven approach to manufacturing management.

Industry 4.0
• Horizontal integration through production networks
• End-to-end integration of engineering across the entire value chain
• Vertical integration and networked manufacturing systems
• Decentralised production

Cyber-physical systems
• Software integration of production processes
• Optimised decision making
• Process monitoring, feedback and control resulting in deterministic behaviour
• Big Data harvesting through large sensor networks
• Cloud computing and smart analytics
• Self-configuring for resilience and self-adjusting for variation

Reconfigurable manufacturing systems
• Modular, scalable, integrable, convertible, customisable, diagnosable hardware and software systems
• A physical system capable of rapid changes in structure
• Can tailor configurations based on required action and output
• Communicates through CPS's to optimise allocated resources
• Upgradable with plug-and-play hardware and software

Figure 1.2-2 Industry 4.0 development tree[11]

A fundamental aspect of the smart factory is that the CPS is constantly aware of its own topology, state and capabilities, and the identity and requirements of connected equipment and processes[12]. Production decisions may be automatic as new data is made available, i.e. where a delayed inbound delivery automatically informs the factory scheduling program of a new delivery time, resulting in a shift in production schedule

to account for the delay. The flexibility and reconfigurability afforded by these CPS's is predicted to overcome the current rigid planning and production processes of traditional factories.

Through increased communication and streamlined "plug-and-produce" features, Industry 4.0 stays true to the lean manufacturing philosophy, while adding data retrieval, process monitoring and automated quality controls, giving precise information on individual products and processes. This enables the cyber physical systems to automatically analyse orders and allocate parts, calculating the optimum balance between machine utilisation and continuous flow of goods, thus removing the restrictions inherent in lean manufacturing for custom or single orders and allows for continuous trimming of materials and supply chains, reducing waste.

1.3   Prospective insight in RMS

Considering the capability of manufacturing systems to be designed for plug-and-produce, modularity and reconfigurability, and the emergence of industry 4.0 which enables significant data extraction from processes and products; there is an unrealised opportunity to use captured data to drive process improvement. The scope of this research is based on developing a novel test execution system using principles of modular, reconfigurable manufacturing and Industry 4.0 philosophies. This is achieved by taking data as specific times during functional performance testing, with an aim to provide insight about the quality of the product and of the production process, creating a feedback loop designed to drive efficiency and quality management.

1.4 Aims and objectives

The aim of this research was to design and develop a modular, reconfigurable test execution system (TES) for end-of-line testing of discrete products. This design of this system was based on the current state of research surrounding reconfigurable manufacturing systems, cyber physical systems and Industry 4.0.

The objectives of this project include:

- Development of initial test execution concepts and specifications based on modular, reconfigurable and plug-and-produce principles for product handling and test.
- Translation of concepts into fully functional designs and the realisation of functional product handling systems and automated test stations.
- Characterisation of the test station performance and demonstrating the potential of Industry 4.0

A use case from an Irish SME provided the main technical context for the novel TES development, which required high volume testing of IR heating elements in a manufacturing environment.

2 Literature review

2.1 Manufacturing execution systems

Manufacturing methods and techniques are constantly in development as companies, industries and economies seek to gain greater and more efficient output. Many current strategies have their origins in the USA which began a rapid shift towards automation in the 1970's in response to cheap labour coupled with efficiency and quality assurance methods which had emerged from Japan, China and other East Asian nations. These economies have continually strived for manufacturing excellence and their innovations have been copied and developed across the world to the present day as nations seek to maintain and expand manufacturing capability and economic growth[13].

2.1.1 Information technology

In the late 1960s, US companies began to invest heavily in robotics and manufacturing software to streamline manufacturing processes and compensate for higher labour costs. The population of industrial robots grew from 200 in 1970 to nearly 5,500 by 1981 and were mainly employed in the automotive industry[14]. Proprietary computer aided design/engineering (CAD/CAE) packages were first developed by Ford, McDonnell Douglas and Lockheed[15]. These packages linked computer aided manufacturing (CAM) with computer numerical control (CNC) packages to convert digital designs into physical objects. Manufacturing equipment became software reconfigurable, forming flexible manufacturing systems (FMS). FMS are units of automated manufacturing and robotic systems, designed to enhance process efficiency and operator safety. The use of new industrial robots across a range of applications continued to expand due to their ability to perform quick, accurate and repeatable tasks while removing workers from difficult and repetitive jobs such as component assembly, welding and heavy material handling.

As technological improvements increased in breadth, industrial control systems (ICS) were introduced to provide monitoring and high-level control. Supervisory control and data acquisition (SCADA), distributed control systems (DCS) and programmable logic controllers (PLC) gathered and monitored process data in real time and relayed information back to centralised control hubs.
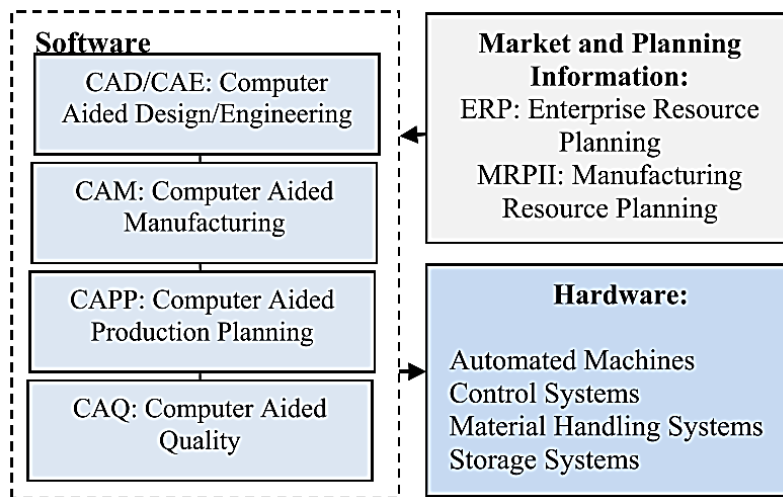
Figure 2.1-1 Elements of computer integrated manufacturing (CIM) [8]

This culmination of robotics, CAD/ CAM, unattended FMS and ICS is defined as computer integrated manufacturing (CIM)[16]. CIM was created in 1973 as a means to automate, optimise and integrate the operations of a total manufacturing system. CIM took inputs from a business's enterprise resource planning (ERP) system and design and manufacture software before releasing finalised work packages to production machinery, stock keeping and logistics systems[13].

2.1.2 Production philosophy

While manufacturing technology continued to develop in the US, countries with limited industrial might and resources strove instead to hone their production processes and eliminate waste of any type. Lean manufacturing was successfully implemented in the 1980s in Japan and focussed on the strict integration of workers into the production process and continuous improvement on value-adding activities by avoiding waste[10]. Waste is divided into seven categories; transportation, inventory, motion, waiting time, over-production, over-processing and defects. Lean manufacturing shifted focus towards demand oriented production, pulling products strictly controlled networks of manufacturing and assembly cells rather than pushing unnecessary amounts of components into the production line[16]. Each cell is comprised of a number of processes and a worker to operate these processes. The processes are structured to remove bottlenecks and optimise the flow of material and products through each cell to the final assembly line, while ensuring each worker is moving efficiently and working at capacity[17]. In essence components are fed to processes only when required and the product is continually drawn towards the shipping area, resulting in lower stock and storage requirements, and greater emphasis on scheduling

and process control. The presence of a worker at every production step allows quality control (QC) checks throughout the process. Parts are measured intermittently and those which are faulty are rejected throughout the process, rather than allowing an inferior part to complete production. Faults can also be traced to their origin and processes continually adjusted to improve throughput and yield. Responsibility and accountability is placed on the individual worker to identify and trace faults. This all-encompassing QC approach is called total quality management (TQM) and is instrumental to the continued application of lean manufacturing today[16].

While lean manufacturing is suited for high production runs and fixed processes, for products with smaller production runs or short production cycles, an agile manufacturing system is preferred. Agile manufacturing has higher flexibility and customization in terms of volume and product variety, at the expense of speed, wastage and stock levels, which are characteristic of the lean model. To gain the benefits of both lean and agile systems, products can be designed to be assembled identically for most of the production process, while steps that implement customisation or additional features are pushed to the end of the assembly line. This amalgamation is called the Leagile system. The Leagile system implements a "decoupling point" between the upstream lean and the downstream agile system. Upstream lean assembly lines run according to lean principles, quickly and efficiently producing modules and products as required by the downstream agile line. The agile line retains the necessary component surplus to customise products to order and also reconfigure and realign in accordance with market demand[18].

2.1.3 Manufacturing system configurations

As IT and production philosophy developed, their influences began to show in the approach taken to the design and architecture of manufacturing systems. Dedicated Manufacturing Lines (DML), suited for a single task are common in large scale manufacturing, with high throughput and cost per part. DLM's are cost effective provided market demand is high and consistent, but product variety is difficult and with an ever changing market, DLM often do not operate at full capacity. To counter the drawbacks of DLM's, flexible manufacturing systems (FMS) increase the variety of components that can be produced on the same system. While the physical construction of the machine is still fixed, flexibility is achieved through changes in software. FMS are common in many manufacturing lines where production volumes

are low or intermittent, where they are capable of realigning to changes in design or manufacturing demand. However, as the physical construction is fixed, FMS are rarely developed specifically for a particular part or product. Rather they are a multi-purpose general manufacturing machine. FMS also rarely have parallel machining operations, and complex part manipulation and multiple tooling can be expensive and difficult to program. Limitations due to single tool operation and issues with production capacity and scalability mean that FMS are usually unable to quickly respond to increased market demand.

DML	FMS
Limitations: • Not flexible – *for a single part* • Fixed capacity – *not scalable*	**Limitations:** • Expensive • Slow – single-tool operation
Advantages: • Low cost • Fast – multi-tool operation	**Advantages:** • Convertible • Scalable capacity

Figure 2.1-2 Comparison of DML and FMS[6]

As production volume increases and decreases over a product's lifespan, DML and FMS both require proper forecasting to ensure optimal production volumes. Quick changes in demand can result in either line under-utilisation or product scarcity. A more ideal manufacturing system needs to be responsive to market variability and able to acquire production resources and offload excess resources in alignment with demand. By viewing the developments of manufacturing IT, production philosophy and manufacturing system configurations, an overall view of the enormous challenges faced by manufacturers can be attained. There is a constant drive towards reducing waste and cost, while also increasing flexibility in volume, quality, yield, performance, throughput and consumer satisfaction. In the last decade, manufacturing has moved towards computational models to forecast production requirements, manage inventory and maintenance and allot manufacturing time. However, much of this data is still located on local servers or isolated within individual machines unable to communicate externally to leverage recent advances in cloud computing and data analytics. The use of this untapped potential together with the growth of the Internet of Things (IoT) and Industry 4.0 has led to a recent resurgence in western manufacturing countries.
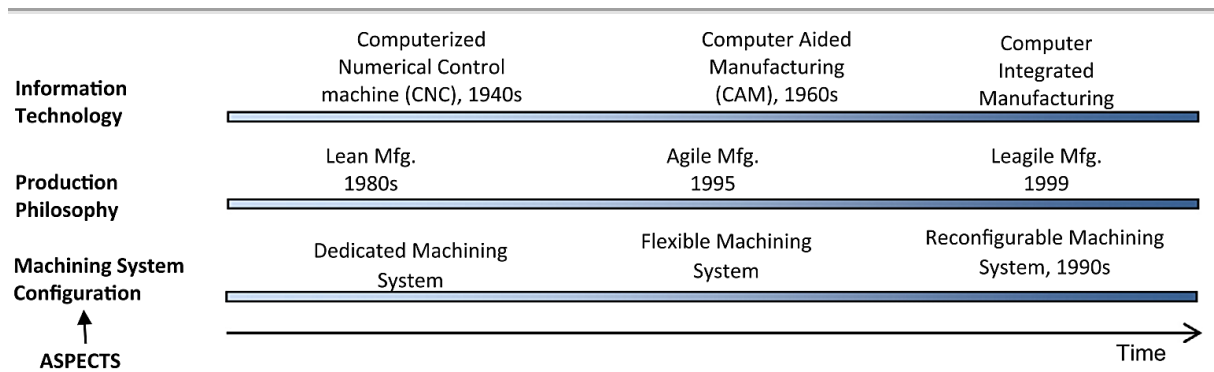
Figure 2.1-3 Evolution of manufacturing systems[13]

2.2 Reconfigurable and intelligent manufacturing

Recent growth in global markets has resulted in a dramatic increase in customer demand for product variety and customisation. Between 1996 and 2012, product variety has more than doubled, while there has been a 30% decline in average product lifespan[19]. In addition to quality and durability, which are essential features in any product, there are several new design requirements which have emerged in recent decades:

- Shortened lead times: Getting a product first to market and capitalising on a competitor's lag has several advantages, extending product lifecycle, better market penetration and higher added value for products[3]. This leads to higher profit margins and a greater return on investment.

- Greater variety: Manufacturers are required to produce a greater variety of products to meet more personalised and unique needs. What was previously known as customisation has now become customerisation, as companies use new communication methods to establish a dialogue with customers to create products that are intrinsic and personal to the individual[20].

- Unpredictable volume: As product life cycles fall and market share narrows the demand for an individual product diminishes. The demand for products can also increase or decrease rapidly, depending on changeable trends and fashions. This emphasises the need to move from large, expensive, fixed tooling to a flexible, holistic manufacturing approach.

- Lower product cost: A large globalised marketplace offers many opportunities for customers to buy similar products at a lower cost. It has become more common for customers to buy online direct from Chinese factories through websites such as Alibaba and Taobao. Manufacturers are required to minimize

production costs and promote associated services to prevent cheaper alternatives from eroding market share[20].

The change in manufacturing away from large scale, mass produced products and the development of advanced manufacturing technologies has led to a resurgence in manufacturing in the western world which has been in steady decline since the 1980's due to globalisation[21]. BRIC countries (Brazil, Russia, India, China) saw robust growth by promoting their cheap labour and materials costs at the expense of more developed nations. Between 1991 and 2011, BRIC average manufacturing value increased by 179% and represented 40% of world manufacturing, while traditional industrial countries averaged 17% growth and share of world manufacturing decreased by 20%[22].
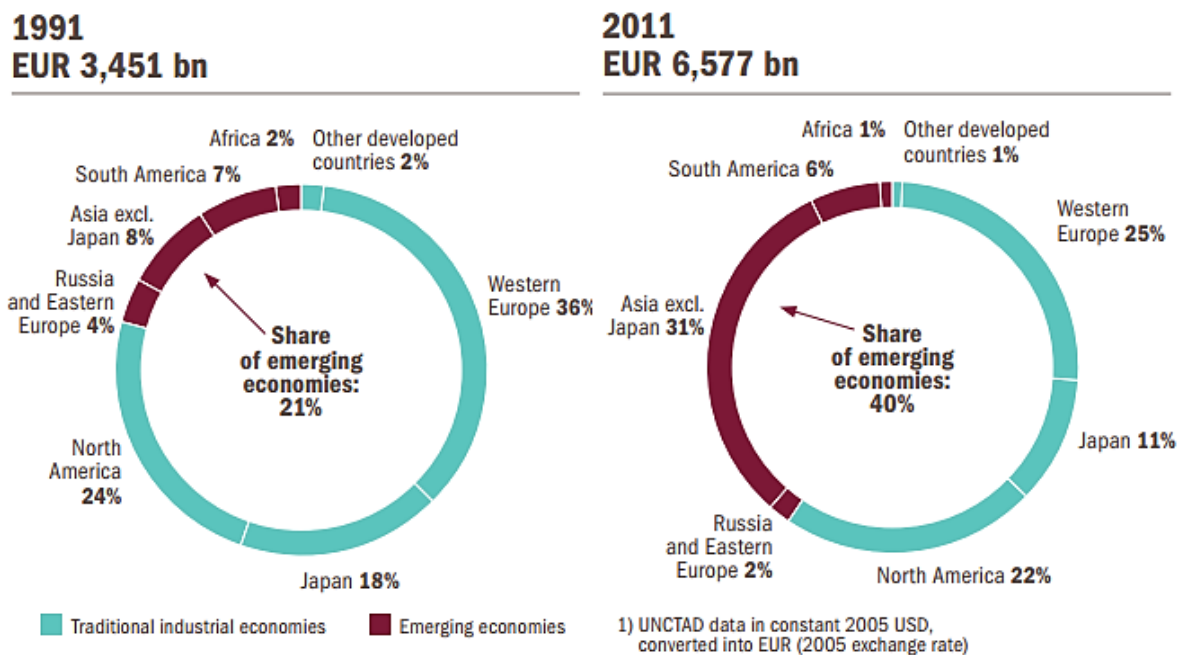
Figure 2.2-1 Rise of emerging economies as industry players[22]

This decrease is more noticeable in France, Spain and the UK where the rate of industrialisation and industrial employment has fallen from 15% in 1991 to 11% in 2011, outsourced to BRIC countries or to new EU entrants like Poland, Romania and Czech Republic. Deindustrialisation has had serious repercussions by creating trade imbalances, weakening economies, reducing in the size of a skilled labour workforce, depressing wages and creating a mismatch of local supply and demand. However, this trend is set to change thanks to recent advances in manufacturing technology.

As the manufacturing industry becomes increasingly advanced and sophisticated, traditional powerhouse manufacturing countries, such as the US, Germany, Japan, and the UK are seeing a resurgence in global rankings. By leveraging the innovation, talent, and strong industrial ecosystem clusters, these nations are competing with renewed strength and surpassing their low-cost BRIC rivals[23]. These leading manufacturing nations are continuously investing in R&D through public means while incentivizing the private sector to conduct its own research through development of collaborative innovation partnerships, which are yielding a resurgence of manufacturing potential.
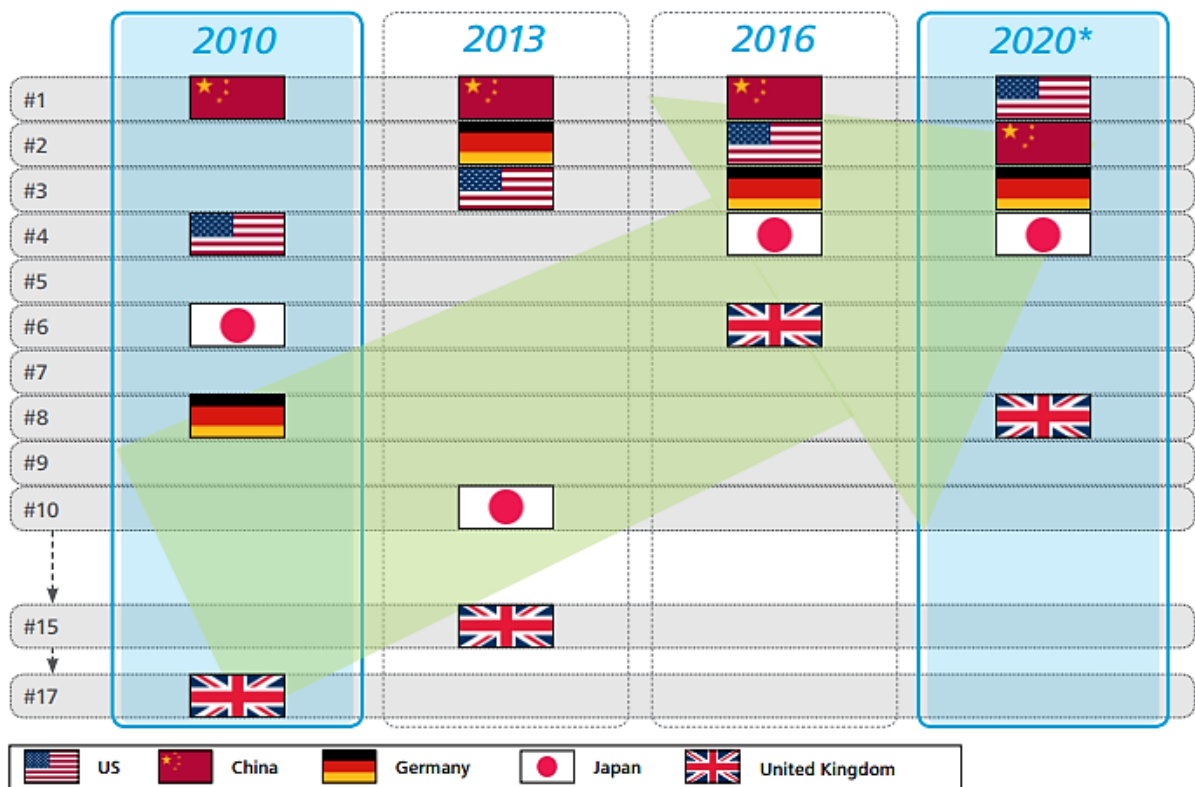

Figure 2.2-2 Deloitte manufacturing powerhouse rank and future forecast[23]

A major aspect of the growth in manufacturing potential in Europe has been the development of Industry 4.0, a German led initiative focussed on imbuing traditional manufacturing technologies with the potential of information and communications technology (ICT) and internet based platforms[9].

2.2.1 Industry 4.0

The vision of Industry 4.0 is one where traditional manufacturing systems are evolved through a full integration of physical, IT and internet based services. IT systems are already heavily integrated in manufacturing, but the adoption of Industry 4.0 can

connect these systems to internal and external processes, and supplier and customer networks[24]. Vertical integration through the amalgamation of ICT and Enterprise Resource Planning (ERP) is used to support the manufacturing process by creating a holistic network, which constantly adjusts to supply and demand[25]. These smart systems are capable of managing complexity, are less prone to disruption and are able to manufacture goods more efficiently, as operators and machines gain the ability to communicate to manage resources and responsibilities.
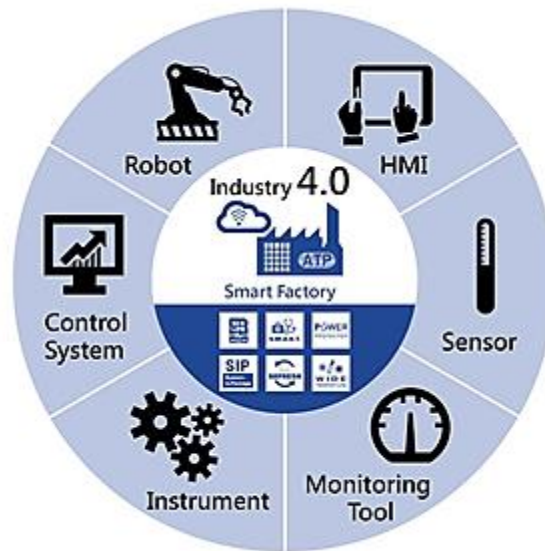

Figure 2.2-3 Features required for Industry 4.0 [26]

By simulating steps in the manufacturing process from control of design, configuration, ordering, planning, manufacture and delivery phases, a smart factory can predict their influence on production. This allows for flexibility, transparent decision making and optimised productivity and efficiency.

These optimisations will have knock-on effects to the quality and range of associated products. Flexibility allows for mass customisation or alterations for specific markets at a relatively low cost[24]. Virtually controlled physical processes can be decentralised and remain coordinated, potentially leading to geographically independent production, local or mobile manufacturing cells and proto-factories[27]. This may potentially lead to a shift away from current, inefficient global shipping and logistic methods. Huge economic potential is associated with the fundamental reorganisation of the value chain that Industry 4.0 represents. Acatech has projected that German productivity could grow by 30%. The Fraunhofer Institute and the Federal Association for Information Technology (Bitcom) calculated that German gross value added (GVA)

could well be boosted by €267 billion by 2025 with the successful introduction of Industry 4.0[25].

Industry 4.0 has many facets and should be differentiated from a range of smaller concepts such as Internet of Things, Factory 4.0, the maker movement and Ubiquitous Manufacturing[24]. These smaller concepts enable Industry 4.0 to achieve a core goal of constant digitization and linking of all productive units in an economy.

One of the largest enabling factors for Industry 4.0 is the recent growth of the Internet of Things and the rapidly growing service infrastructure which has been created to analyse captured data. New technological improvements such as the widespread application of wireless communication networks such as GPS, GSM, and Wi-Fi, the plummeting cost of MEMS such as accelerometers, proximity, temperature and pressure sensors, microphones, and gyroscopes, low power communications such as BLE, RFID and LTE, and the cheap availability of computation horsepower though embedded controllers from ARM, Intel and Microchip[8] have created an industry estimated to be worth over $300bn by 2020 and tipped to impact 6% of the global economy[28]. IoT and the rise of Big Data analysis have made the development of high resolution manufacturing systems possible. The convergence of the real and virtual world through the internet, cloud services, machine learning, data acquisition systems, robotics and intelligent manufacturing systems have created the environment for smart, self-managing, deterministic cyber-physical systems[29].

2.2.2 Cyber-physical systems

The concept of Industry 4.0 relies heavily on the introduction of these cyber-physical systems (CPS) to manufacturing environments. CPS are integrations of computation and physical processes, where computational systems are used to monitor and control physical processes through smart communication and feedback loops which add new capabilities and performance[11]. These systems are actively collaborating and communicating between themselves and internet-based data accessing and data processing services to create an ecosystem of robustness, autonomy, self-organization, self-maintenance, self-repair, transparency, predictability, efficiency and interoperability [29].
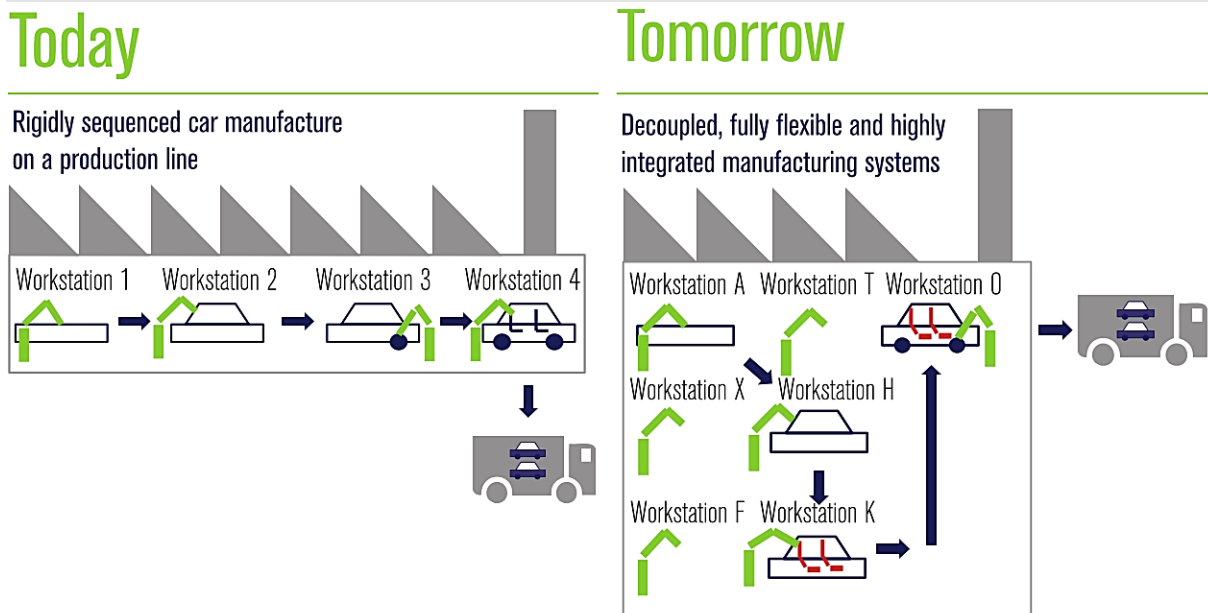
Figure 2.2-4 Industry 4.0 dynamic manufacturing[9]

The main challenge in manufacturing is the vertical integration of processes at all stages of product delivery so they may communicate more efficiently. Typical processes include fabrication of parts, assembly, packaging, transport, quality control, marketing and sales. These activities are operated by producers, system integrators, sub-suppliers, logistics/supply chain experts, and many others. At the heart of these activities is the production of the product itself[11]. CPS can integrate these processes by acquiring information from each facet of product delivery and acting autonomously, through the ability to manipulate and negotiate with other elements of the system, to respond to internal and external changes[30].

A 5 level CPS architecture, published by Bagheri et al., provides a broad methodology for deploying a cyber-physical system in a manufacturing environment[31].

1. Smart Connection: CPS rely on their ability to gather accurate physical data, through sensors, controllers or ERP systems. The protocols to gather, collate and relay this data should be as seamless as possible to facilitate a reliable, consistent data flow.

2. Data to Information Conversion: To infer meaning from this data, specific algorithmic methods can be implemented to disseminate information in order to gain environmental self-awareness.

3. Cyber: The cyber level is a central information hub where gathered information is used to create knowledge and insight into the operation and status of

individual system modules. Analytical models can monitor overall system performance, highlighting shortfall and surplus.

4. Cognition: Through the use of analytical knowledge, the CPS can become truly deterministic and self-aware. This knowledge is used to make data driven decisions for top-to-bottom system and resource management.

5. Configuration: This final stage is the physical manifestation of the decisions made in the Cognition level. The CPS has the capability to automatically adapt and reconfigure real-world machine and system processes.
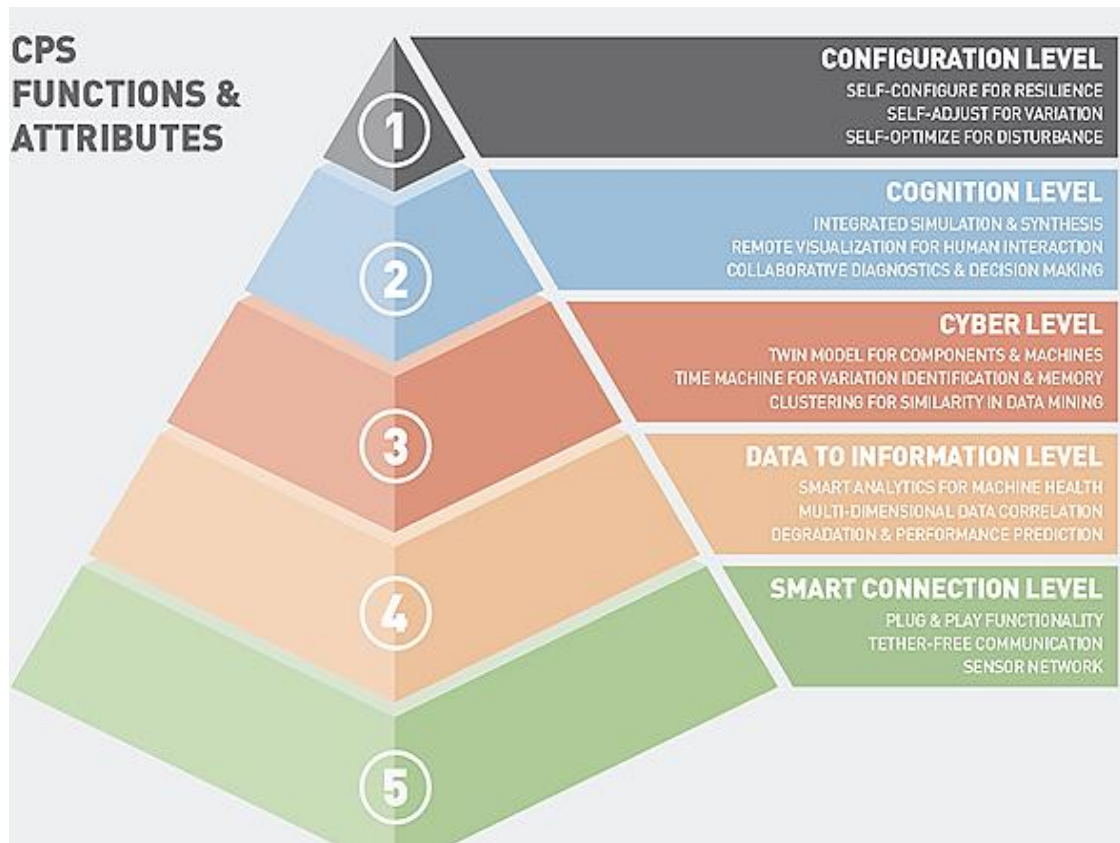
Figure 2.2-5 5 level architecture for CPS in manufacturing[31]

This architecture describes a closed loop system where physical data is brought into a virtual world, converted, conditioned, analysed and finally acted upon to create a physical output.

In addition to factory automation, examples of CPS include:

- Advanced medical devices such as prosthetics which providing real-time control and sensory feedback.

- Aerospace systems which integrate flight systems and air-traffic control.

- Integration of smart vehicles and intelligent highway management systems for near-zero automotive traffic fatalities, minimal injuries, and significantly reduced traffic congestion and delays.

- Robotic control architecture which mesh potentially hundreds of sensors with multiple computing elements, balancing processing requirements, creating 3D environmental maps for navigation and managing redundancy.

- Intelligent process control which can monitor systems to predict maintenance schedules, correctly diagnose potential system failure and remove human operators from hazardous environments[32][33].

While CPS's are generally characterised as a collection of vertically integrated software based systems; in terms of data collection, numerous CPS enabled physical devices are required to provide data input and a resultant physical response[11]. One such system which shares the intelligent, modular and scalable concepts proposed by CPS is the reconfigurable manufacturing system.

2.2.3   Reconfigurable manufacturing systems

The concept of reconfigurable manufacturing systems (RMS) was most comprehensively examined by Koren in 1999, who introduced a system which could be reconfigured in both functionality and capacity in a cost effective way[5]. This system would combine the high throughput and repeatability of a DML with the flexibility and configurability of a FMS. RMS was defined as a system "designed at the outset for rapid change in structure, as well as in hardware and software components, in order to quickly adjust production capacity and functionality within a part family in response to sudden changes in market or in regulatory requirements"[5]. The RMS has also been defined as systems "capable of tailoring their configurations to meet the resource demands of an ever changing mix of products…based on a concept of scheduling manufacturing processes rather than manufacturing products"[34].

	Dedicated	RMS/RMT	FMS/CNC
System Structure	Fixed	**Adjustable**	Adjustable
Machine Structure	Fixed	**Adjustable**	Fixed
System focus	Part	**Part Family**	Machine
Scalability	No	Yes	Yes
Flexibility	No	Customized	General
Simultaneously Operating Tool	Yes	Yes	No
Productivity	High	High	Low
Lifetime Cost	**Low** for a single part, when fully utilized	**Medium** or production at me lium-to-high volume new parts and vari- able demand during system lifetime	**Reasonable** for simultaneous pro- duction of many parts (at low volume); otherwise – **High**

Figure 2.2-6 Comparison of dedicated, reconfigurable and flexible manufacturing systems.[6]

As mentioned in the introduction, RMS characteristics are based on modularity, scalability, integrability, customisability, convertibility and diagnosability[5].

1. Modularity allows for hardware and software elements to be reordered, reconfigured and added to, as process demands change. Modularity also provides a measure of system redundancy as each module acts as an individual unit, where multiple units comprise a complete system.

2. Scalability implies the system can react to changing demand and has the ability to acquire new production resources, scale up with rapid increases in requirement and scale down through offloading resources to other processes.

3. Integrability means that the system is designed from the outset to accept new modules and technology through a forward planning design architecture which accounts for future expansion and requirements.

4. Convertibility requires a system that allows for quick changeovers between current product types and families and quick adaptability to future products.

5. Customisability is the intersection of these characteristics which create a system capable of realignment for each new, unique process.

6. Diagnosability which quickly identifies the sources of quality and reliability issues which occur in large systems[35].

With the increased interest in RMS, several design frameworks have been theorised which form a support structure that directs the development of a scalable and convertible manufacturing system. The design process involves design analysis and

synthesis to map specifications, constraints, variables and overall design objectives to discover the optimal solution from all possible modular configurations.

Many design frameworks break the design challenge into three sections. The framework proposed by Abdi and Labib [36] is comprised of the following steps:

1. Strategic Level: Use market analysis to quantify the required capacity. Select the appropriate manufacturing system type based on performance measurements such as cost, quality and production time.

2. Group products into product families according to commonalities. Generate multiple configurations and evaluate the performance of each based on factors such as cost, space, time to build and reconfigurability to hone the final RMS configuration. Select the most optimal reconfiguration required to produce each family.

3. Design the RMS using the required configurations as a template. Integrability and an open machine control architecture are the major paradigms for successful implementation of the reconfigurable manufacturing system [37].

This design methodology is reiterated throughout the service life of the machine as new products require new processes.

The three step design methodology was later expanded on by authors such as Deif [38], who's methodology aimed to predict the market size and production capacity required, then focus on the system design with a predictive model of future production requirements, and Bi [20] who introduced the concept of uncoupled, loosely coupled and strongly coupled systems as metrics of available modularity. In this methodology an uncoupled system corresponds to a single module which fulfils a single, simple requirement. A strongly coupled system is comprised of many modules which when correctly configured can fulfil a single, complex requirement. This approach is used to break down the challenge of configuration design when assessing potential requirements over the lifetime of the RMS [20].

RMS software control architectures follow a similar modular approach to account for future expansion, updates, protocols and software which may need to be integrated.

1. The architecture should be modular and each software routine maintained as an encapsulated controller able to fulfil a single function. The system is capable of calling and sequencing these routines to accomplish system wide objectives.

2. The control system should be distributed, as system components are often decentralised and physically separate.

3. The control architecture should be open as control components may be developed by a variety of vendors using a variety of programming languages, communications networks, databases, and protocols. An open architecture allows control components to be seamlessly updated with new features and behaviour.

4. The control system should be scalable and upgradeable as adding, removing and upgrading hardware components will be required when the functionality, capability or enabling technologies change.

5. The control system should be self-reconfigurable as system configurations may be realign frequently according to demand[20].
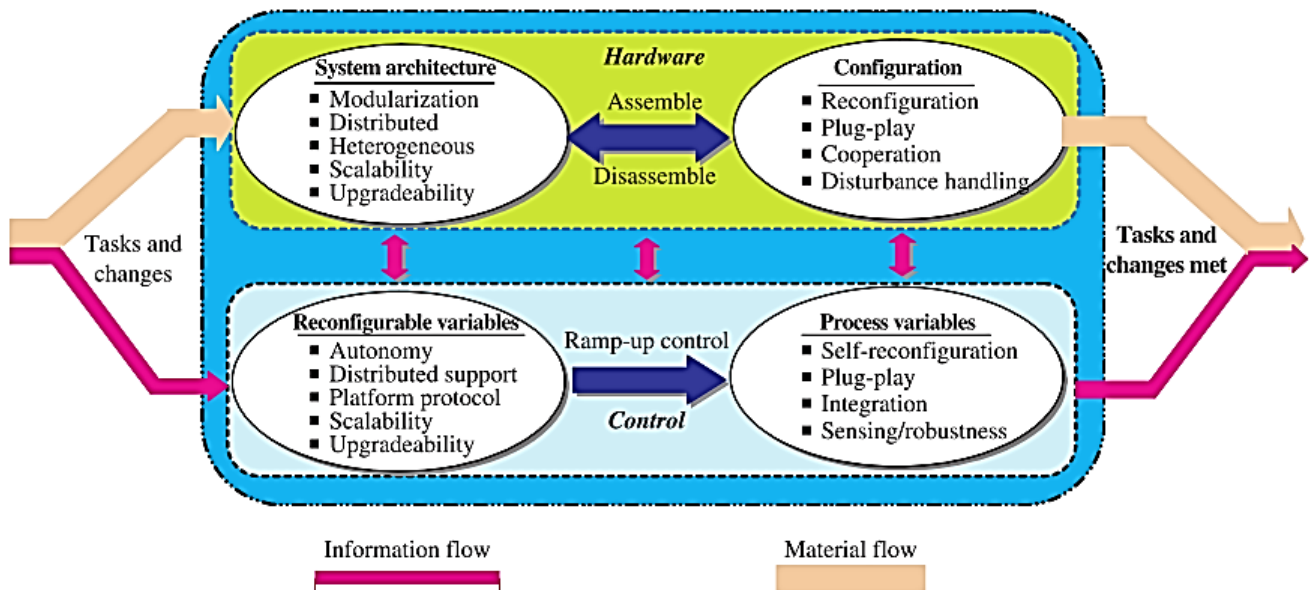

Figure 2.2-7 Hardware and software requirements of an RMS[20]

In a changing and uncertain manufacturing environment, the RMS paradigm is the best approach to meet these key challenges due to the level of reconfigurability and flexibility available to adapt to new requirements.

Currently, the concept of RMS has had little penetration into the manufacturing environment. Much of the emphasis to date has been the theoretical exploration of the RMS concept and how it aligns to various manufacturing paradigms. In 2014, SmartFactory[KL], the largest research and demonstration centre for Industry 4.0 technologies[39], constructed the first modular, plug-and-produce assembly line for the manufacture of customised business card holders. The production process was

achieved by a collection of unique modules, each built by an individual vendor to predetermined specification, namely; a fixed construction footprint, the OPC UA protocol for machine-to-machine (M2M) communication and a universal plug-in connector for standardized provision of power, compressed air and communications [12].

Figure 2.2-8 SmartFactory^{KL} RMS[39]

Similar learning factories have been constructed across Europe to develop and demonstrate the concepts of RMS, CPS and Industry 4.0. These sites provide training in realistic manufacturing environments and allow for a greater freedom for experimentation and innovation, without the restrictions inherent in a real-world industrial setting[40]. Examples of such learning factories include:

- The Process Learning Factory CiP at the Institute of PWT, Darmstadt, which focusses on Lean Manufacturing and advanced design

- The Learning Factory for Energy Productivity and the Learning Factory for Lean Production at The Institute for Machine Tool and Industrial Management of the Technical University of Munich

- The iFactory in the Intelligent Manufacturing Systems Centre at the University of Windsor, Canada, which is a transformable manufacturing platform, for the configuration, modelling and analysis of products, processes and manufacturing systems[41].

Learning factories such as these are rarely representative of real-world factories, instead exist to link academic research and industrial development, with the objective of moving education and research processes closer to real industrial problems[42]. The ideas and strategies tested by these learning factories can be used by any company facing the challenge of remaining competitive and efficient in the face of continuous change and expanding product variety[41].

2.3 Big Data

"Data is the new oil" and the volume, variety and complexity of data is exploding at record rates[43]. Big Data is the proliferation of data from various systems, devices and applications and it is constantly increasing in size, diversity and complexity. This makes it challenging to capture, manage and process within a tolerable period of time using traditional software solutions[44].
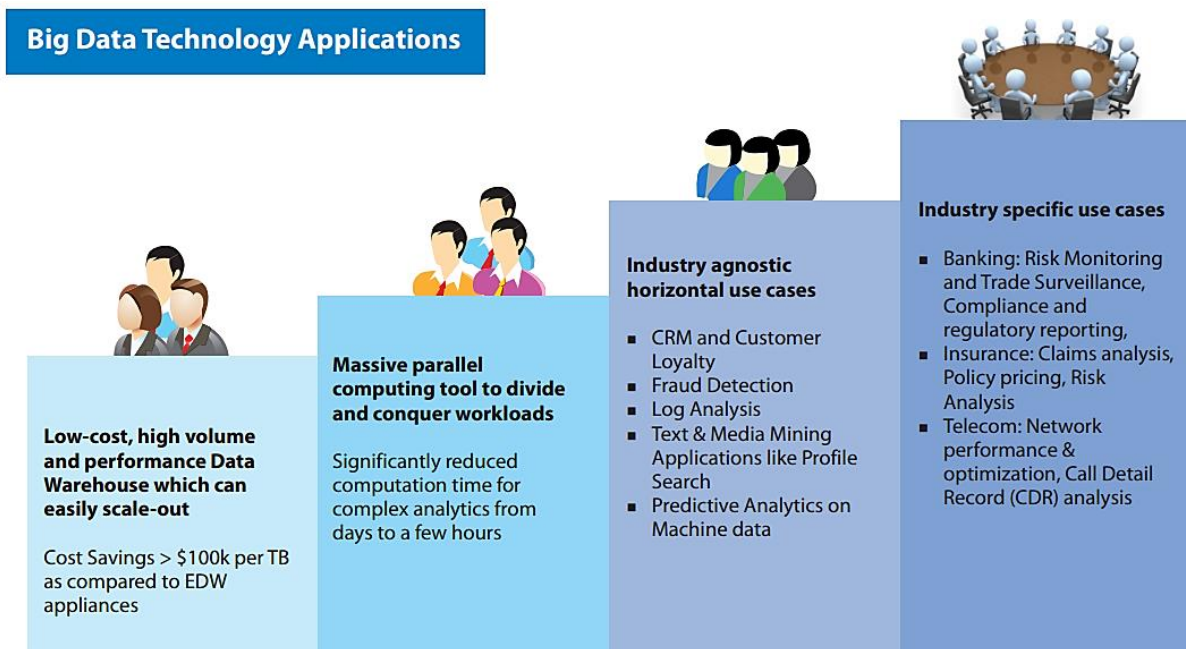

Figure 2.3-1 Evolution of Big Data in enterprise[45]

2.3.1 The potential of Big Data

Traditionally, businesses have relied heavily on experienced personnel to lead the decision making process. However, such experience is often lost over time with potentially disastrous consequences. Big Data promises a smart analytical system that can be used to transition from an experience-based approach to an evidence-based decision making process. By utilising Big Data and new algorithmic analysis techniques, fast, fact-based decision making can have tremendous business value. Analysis of captured data can give insights to drive decision-making in areas such as:

- Empirically proving long term quality standards.
- Maximizing yield through fine-tuned processes.
- Recovering capacity by identifying and engineering out bottlenecks and flow restrictors.

- Predicting process failure and downtime by comparing historic performance against current measurements.
- Managing supply chain execution through vertically integrated data harvesting services[46].

To correctly leverage Big Data, businesses need the ability to support a multitude of structured and unstructured data types, the capacity to compress and store these data sets and the capability to exploit this data through historical analysis of critical trends to enable a real time predictive analysis[44]. Several challenges inherent to the structure of Big Data must be overcome before this analysis can be realised.

Much of the captured data is unstructured, or non-numeric, which must be converted into a compatible format for quantitative analysis. It is generally recognised that the larger the data sample, the more accurate the analysis, meaning as much data as possible from as many sources should be retained for future use. The volume and velocity of this information coupled with the need for faster analysis can stress the necessary infrastructure and potentially overwhelm a business' IT capacity. Variability can also be problematic, with seasonal or event triggered surges than can be difficult to coordinate and may require flexible storage and processing capability. Finally, this ever increasing flow of data from an expanding range of sources must be mapped, linked and matched to discern meaningful relationships, trends and causal factors[46].

2.3.2 Big Data in manufacturing

Cyber manufacturing is concept that aims to apply Big Data to a manufacturing context by harvesting data from an interconnected CPS to achieve resilient, fact-based decisive performance[47]. Big Data has been identified as a main enabling factor in the development of CPS's. This will enable a control system to create predictive models design to compensate or intervene in physical processes or notify personnel should a particular system move outside a pre-determined threshold limit.
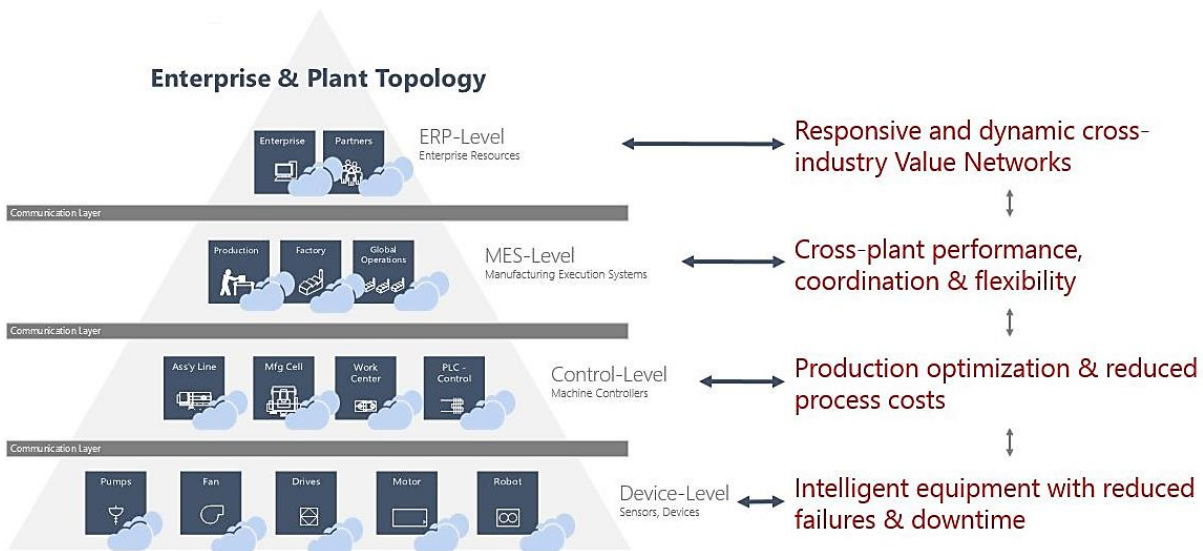
Figure 2.3-2 Positive impact of Big Data on manufacturing[48]

Currently, there are few standardised communications protocols that can be deployed across a variety of manufacturing assets. A vast majority of connected equipment use a wide range of sensors, hardware and software, leading to different data formats and acquisition requirements[47]. Recently, groups such as the MTConnect Institute and National Instruments have laid the foundations for industry wide, open architecture solutions. The Digital Manufacturing and Design Innovation Institute (DMDII) and National Institute of Standards and Technology (NIST) have endorsed open-source solutions and published a road map which illustrates the necessary development required to create a interoperable framework for smart manufacturing systems[49].

Utilising Big Data in manufacturing has become increasingly popular, resulting in massive gains in efficiency and cost savings. Intel has harnessed big data for use in predictive analytics to reduce the number of quality assurance (QA) tests required on each processor, saving $3 million in manufacturing costs for a single line of Intel Core processors. By expanding this process across all semiconductor fabrication plants, Intel expects to save $30 million annually[50]. Tesco currently collect 70 million refrigerator related data points, which are analysed to provide metrics for performance, predict and schedule servicing and reduce energy costs saving up to €20 million annually[51].

2.4 Test systems

2.4.1 Dielectric voltage withstand testing

When an electrical potential difference is applied to an electrical device, the natural capacitance of the insulation material changes. For 50Hz AC voltages, the charge/ discharge cycle occurs 50 times per second, never reaching a steady state. This can cause the insulation to ionize, leading to the insulation material to lose its resistive properties, resulting in breakdown and a large flow of capacitive leakage current[52]. Electrical devices also exhibit resistive leakage current, which is often several orders of magnitude less than capacitive leakage current due to advances in insulation material science[53].
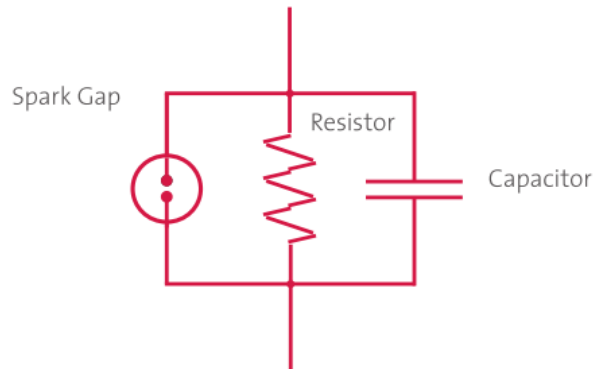

Figure 2.4-1 Basic insulation scheme in electrical products[53]

Sufficiently high levels of leakage current can be lethal to humans, so a dielectric voltage withstand test is performed on nearly all new electrical and electronic products. The test methodology is described in consumer and quality standards such as:

- Underwriters Limited (UL)[54]
- Low Voltage Directive (EN 50116)[55]
- ASTM D149-97a[56]
- Portable Appliance Testing (PAT)[57] which is required by many OH&S regulations.
- Safety, Health and Welfare at Work (General Application) Regulation 2007 S.I. No. 299/2007[58] in Ireland.

The test voltage is defined in the applicable safety standard and is based on the AC input voltage, the grade of insulation used in the equipment and the accessibility of the secondary voltages. This voltage is a multiple of the working voltage of the electrical or electronic device, as a safety margin to replicate voltage surges and transients[53].

Grade of insulation	Working voltage	U < 130V r.m.s.	130V < U < 250V r.m.s.	250V < U < 1000V r.m.s.
Operational		1000	1500	see values in IEC 950 Table XV Part 2
Basic, Supplementary		1000	1500	see values in IEC 950 Table XV Part 2
Reinforced		2000	3000	3000

Figure 2.4-2 Test voltages for electrical strength IEC950 [59]

The dielectric voltage withstand test is performed using a high potential (hipot) tester. The dielectric test can be performed with AC or DC voltages, depending on the test standard and hipot tester specifications. The AC Hipot tester is used for proof testing as it provides real world, 50/60Hz test conditions. The AC voltages can cause slight deterioration in the insulation, uncovering flaws in devices that may be unnoticed in DC testing. By comparison, DC Hipot testers provide an initial surge of charging current that quickly drops off as the equipment under test becomes charged. The steady DC output can also be gradually increased throughout the test to provide a qualitative measure of leakage current at various input voltages. A DC Hipot tester is comparatively cheaper, although the device under test must be electrically discharged at the end of the test for safety reasons[60]. A current monitor records the current losses in the system and compares the result to a pre-set threshold value[53].

The maximum threshold value is determined based on the equipment classification:

❖ Class I devices are defined as equipment that provides basic insulation and are connected to the protective earth conductor in the building wiring. They can produce leakage current up to 3.5mA, except in the cases of heating devices where the limit is 0.75 mA or 0.75 mA per kW, with a maximum of 5 mA[57].

28

❖ Class II devices are protected with double or reinforced insulation in lieu of a protective earth connection and can produce up to 0.25mA of leakage current[59].

❖ Class III devices are powered from a Separated Extra Low Voltage (SELV) source, such as a power transformer, which will not exceed 50 V and are usually required to be less than 24 or 12 V. They can produce leakage current up to 0.25mA[57]

*Note that these leakage currents are at the rated voltage, not the hipot test voltage.

While the limits specified in electrical standards constitute the maximum allowed leakage current for a particular device category, there is no correct threshold current setting for individual devices. In practice, the value at which the dielectric material suffers a breakdown, resulting in a large rush of current, must be determined empirically and the resulting dielectric voltage withstand threshold is based on this result[53].
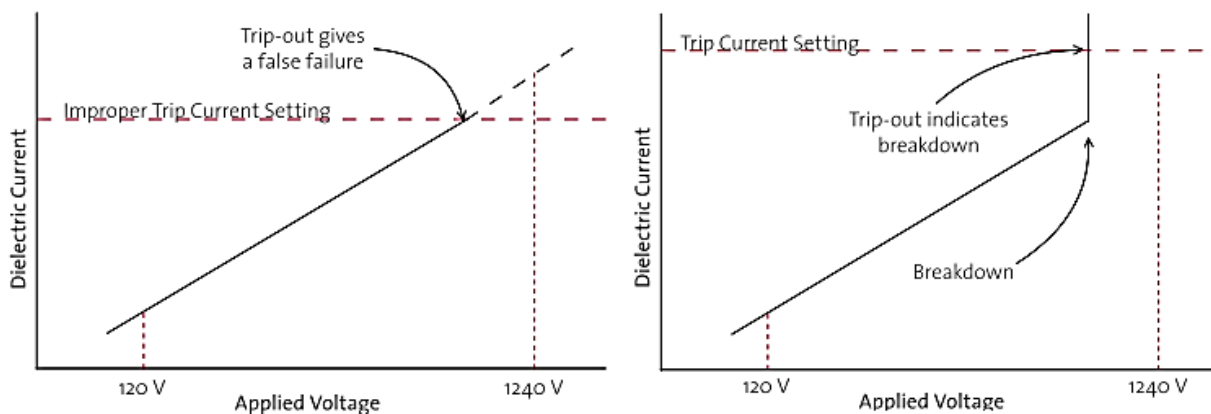

Figure 2.4-3 Incorrect thresholds may lead to false failures[53]

Consideration must also be given to environmental factors, such as temperature and humidity. The resistance of insulating materials has been observed to decrease with an increase in temperature and also with an increase in humidity[56]. When a product is required to operate in an environment above room temperature, a dielectric strength-temperature relationship should be determined across the range of expected operating temperatures. The presence of moisture also can have a marked and unpredictable effect on resistance values, especially for materials which are hygroscopic or deliquescent[60]. Absorbed moisture or moisture present on the surface of the material will contribute to dielectric loss and an increase in surface conductivity[56].

2.4.2   Non-contact thermal measurement and analysis

Any object with a temperature above absolute zero (-273.15°C) emits electromagnetic radiation which is proportional to its intrinsic temperature. Part of this radiation is in the infra-red spectrum. This infra-red radiation can be used to infer the temperature of the object. Non-contact temperature measurement is a preferred option for the following reasons:

- ❖ Temperature measurements can be taken on moving or distant objects.
- ❖ Measurements can be taken in hazardous and inaccessible environments.
- ❖ Response times are usually very fast compared to traditional contact thermometers.
- ❖ The measurement device has no influence on the temperature of the measured object, is non-destructive and there is no mechanical wear[61].

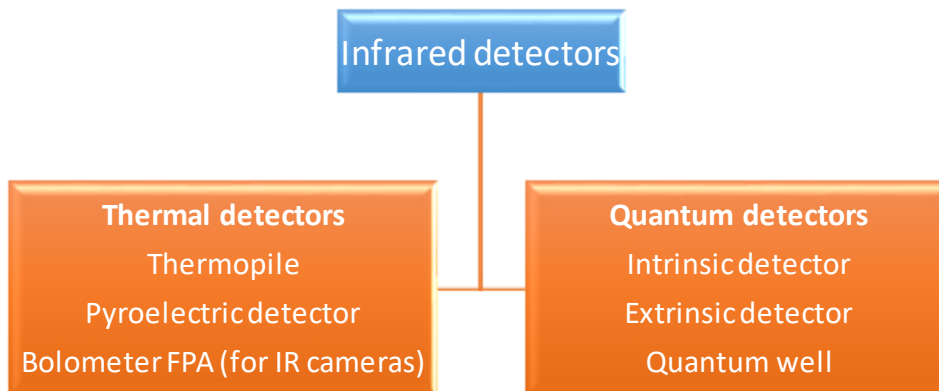There are two main types of non-contact infra-red detectors.

Figure 2.4-4 Types of non-contact thermal detectors

Thermal detectors are devices which absorb emitted electromagnetic radiation. This causes a heating effect which changes some physical property within the device. The temperature change is then translated in various ways to an electrical signal, which is then conditioned and analysed[62]. Basic thermal detectors are wavelength independent as they depend on radiant power and not spectral content, although they are usually paired with window material such as fused silica or sapphire, which allows the passage of a specific wavelength, such as infrared[63].

Thermal detectors are mainly classified into:

1. Thermopile detectors that change in voltage.
2. Bolometers that change in resistance.
3. Pyroelectric detectors that change in dielectric surface charge.
4. Diodes that change in voltage-current characteristics. [64]

Where thermal detectors measure electromagnetic waves, semiconductor-based quantum detectors measure photons of infrared radiation.

Quantum detectors are classified into:

1. Intrinsic detectors that operate over wide range of wavelengths.
2. Extrinsic detectors with very long wavelength operation.
3. Quantum well detectors, which have uniform responses and can be tuned to a desired wavelength[65].

Photons strike the surface of the quantum detector material, changing its electronic energy distribution. This results in an quantifiable electrical output[65]. Quantum detectors exhibit both perfect signal-to-noise performance and a very fast, nanosecond response times[62]. However, quantum detectors require cryogenic cooling, necessary to prevent thermal generation of charge carriers. These internal thermal transitions can compete with the optical transitions, introducing signal noise to non-cooled devices. Current methods of cooling result in devices that are bulky, heavy, expensive and inconvenient to use[63]. While cooling requirements are the main obstacle to the more widespread use of quantum based thermal detectors, the low cost of CMOS processes and increases in MEMS development has resulted in an explosion in production of thermal detectors, such as thermal imaging devices[63]

Thermal imaging devices are capable of visualising IR radiation and are a preferred measurement method due to the large quantity of information that can be gained from a thermal image. Thermal cameras use a focal plane array (FPA) image sensor which is a monolithic CCD or CMOS based array of 20,000 to 1 million specially calibrated micro bolometers[66]. Changes to the bolometer's temperature results in a corresponding change in electrical signal output, which is converted by a digital signal processor to a false colour image, where each bolometer is represented as one pixel[62].
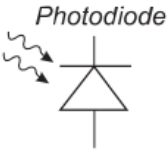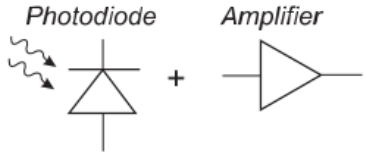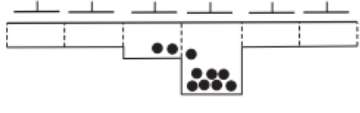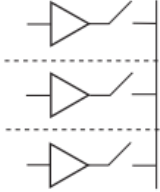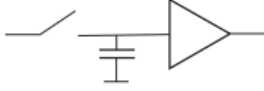
	CCD approach	CMOS approach
Pixel	*Photodiode* Charge generation and charge integration	*Photodiode* + *Amplifier* Charge generation, charge integration and charge-to-voltage conversion
Array readout	Charge transfer from pixel to pixel	Multiplexing of pixel voltages: Successively connect amplifiers to common bus
Sensor output	Output amplifier performs charge-to-voltage conversion	Various options possible: - no further circuitry (analog out) - add. amplifiers (analog output) - A/D conversion (digital output)

Figure 2.4-5 Comparison between CCD and CMOS based image sensors[66]

CMOS-based sensors have gained traction over CCD-based sensors due to the increasing pixel density and increasing read out speeds. As each pixel is an individual circuit the CMOS FPA has a higher SN ratio than CCD which uses a pixel-to-pixel charge transfer cross detector[66]. The data captured by thermal cameras can be analysed through thermal data analysis software. Software can enhance the thermal image data by providing in-depth temperature analysis such as individual pixel intensity values, colour maps and electromagnetic frequency spectra while thermal video can show dynamic temperature shifts. Thermal imaging software can be used in process management to trigger alarms and change process variables.
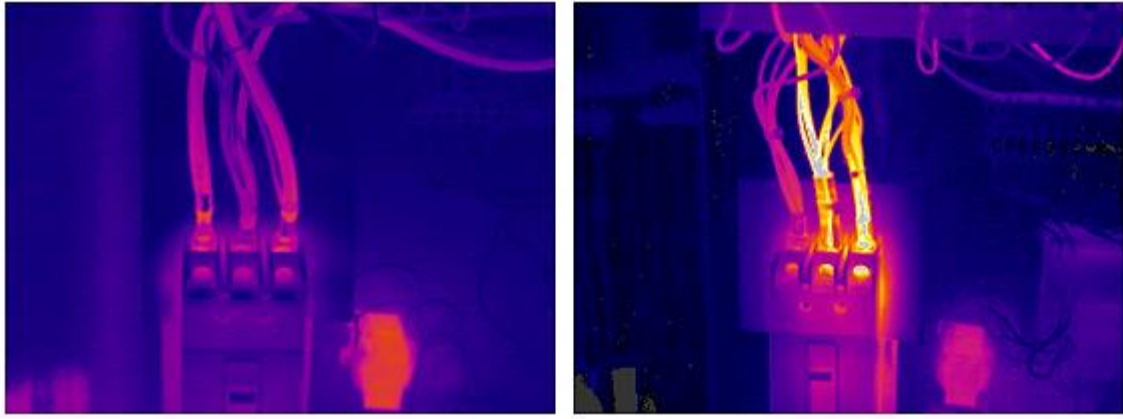
Figure 2.4-6 Thermal image of preventative maintenance on power distribution box [67]

The IR emission value is converted to a temperature value in software based on the emissivity value of the object. Emissivity defines the relation between the actual radiation value and that of an ideal object, one which radiates the maximum electromagnetic energy possible at every wavelength and has neither reflective nor transmissive properties[62]. This ideal is known as a "black body". Emissivity is expressed as a value between zero (shiny mirror) and one (black body). It is impossible to gather accurate readings on surfaces with an emissivity of about 0.5 or lower, due to reflections and distortions which increase signal noise[68]. Thermal measurement devices are critical tools in gaining instant diagnostic insight into electrical and mechanical systems in both manufacturing and test processes.

2.4.3 Computer vision and image processing

In industry, the quality of the product relies heavily on manufacturing precision[69]. Many products undergo varying degrees of visual inspection as the pass through the manufacturing process. However, visual inspection can be ambiguous, subjective and are unable to generate concise data[70]. For these reasons, computerised 3D inspection has becoming prevalent in manufacturing.

Multiple technologies to generate 3D images have been developed. These systems are generally grouped into the following categories:
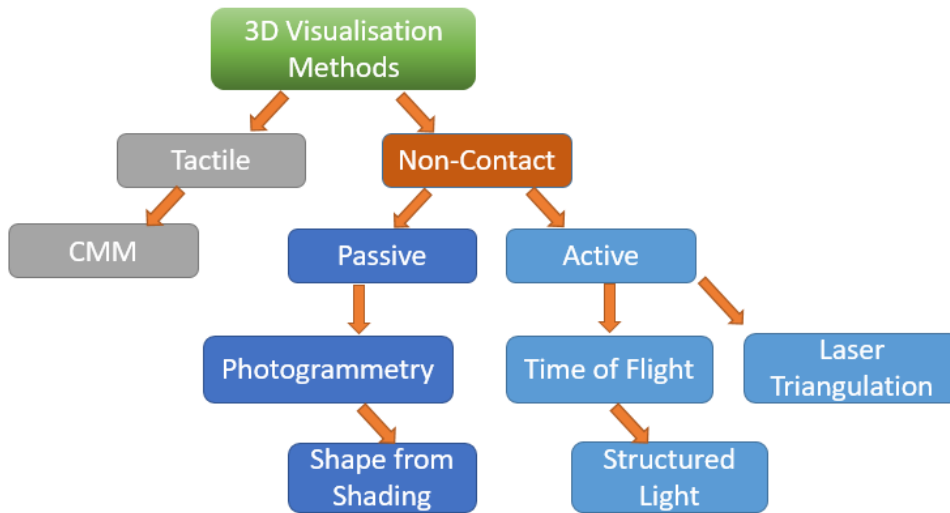
Figure 2.4-7 3D image capture techniques[71]

1. Contact based; These techniques require tactile interaction to determine object geometry:

   ❖ Coordinate Measuring Machine: A CMM uses a touch probe mounted on a CNC axis to measure the surface of an object to micron accuracy. As CMMs are traditionally heavy, expensive and slow, they are used more often in product geometry verification, rather than 3D reconstruction[72].

Figure 2.4-8 CMM touch probe operation[73]

2. Non-Contact based: These techniques can use electromagnetic or acoustic waves to determine object geometry and can be sub-divided into passive and active systems.

a. Passive systems operate using only natural or ambient lighting to illuminate the object[71]. Such techniques include:

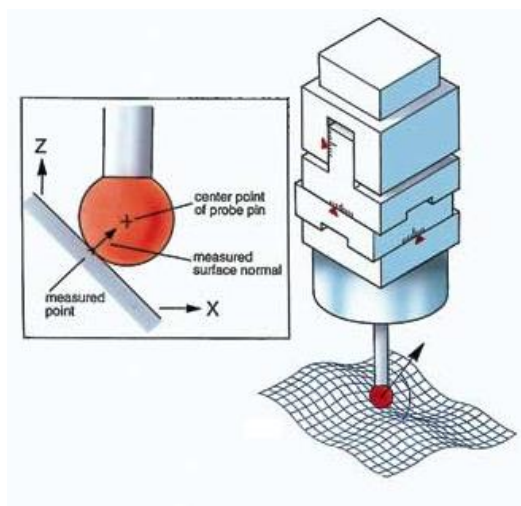❖ Photogrammetry: This process uses a camera or multiple cameras to capture images of the object at multiple angle as shown in fig. 2.4-9. These images are processed in software using spatial intersection, triangulation and bundle adjustments to create a 3D image.
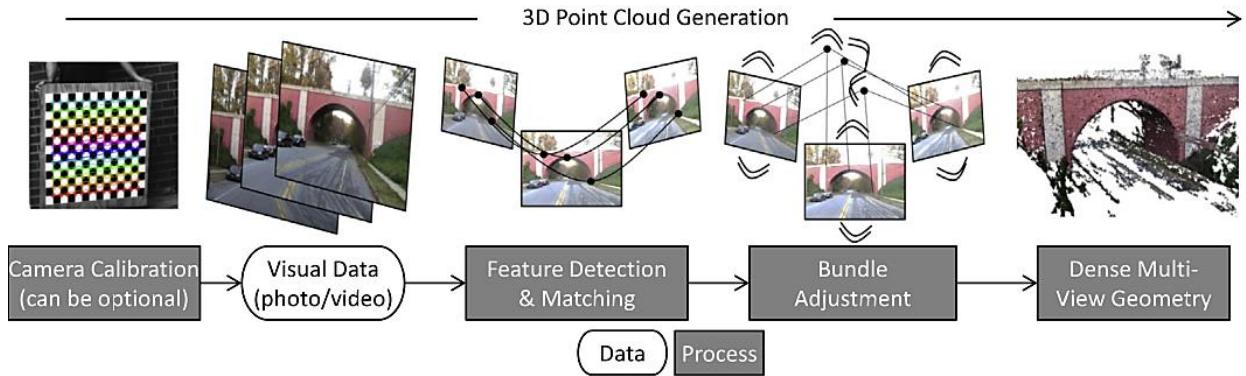
Figure 2.4-9 Photogrammetry method[74]

❖ Shape from Shading: Here, software is used to determine image depth and shape by modelling the gradual shading variations in a greyscale image, where darker pixels correspond to greater depth (fig. 2.4-10). A similar Shape from Focus technique uses the degree of image blur to crop background information, leaving only the object in focus[72]. Due to specific lighting requirements and the degree of light control required for reproducibility, these methods are less prevalent than photogrammetry.

Figure 2.4-10 Shape from Shading converts 2D greyscale image to 3D depth map[75]

b. Active systems use directed energy such as laser, patterned light projection, sonar pulses or magnetism to detect and measure the object[76].

❖ Time of Flight: This technique measures the time or phase difference for a light pulse to travel from an emitter to the object, then back to a receiver. Points on the object's surface are scanned sequentially to construct a point cloud, from which a 3D image is created[77].

❖ Laser Triangulation: Similar to Time of Flight, a physically separate optical emitter which is placed a known distance from a receiver projects a laser line onto the object, shown in fig. 2.4-11. The line is detected by the receiver, which uses trigonometry to calculate the coordinates of the illuminated spot[76].

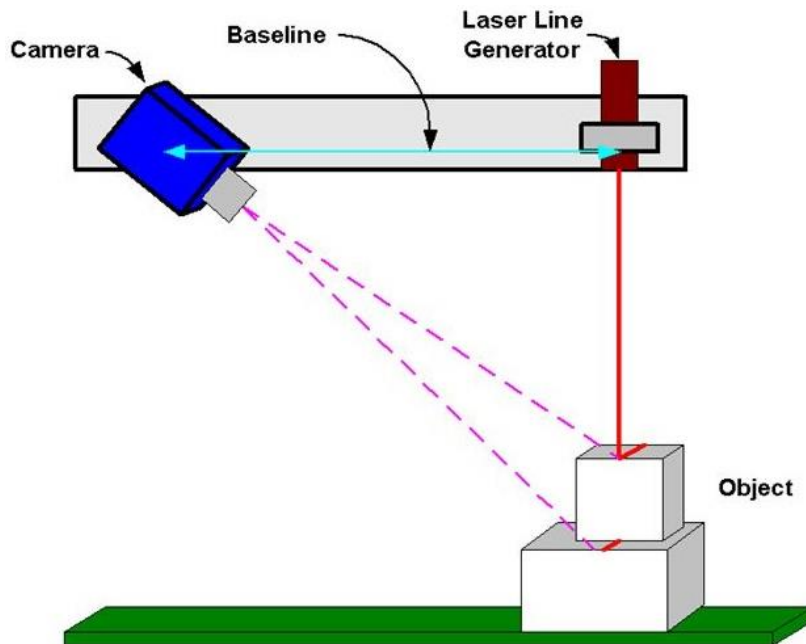*Figure 2.4-11 Laser triangulation technique*[78]

❖ Structured Light: This technique projects a checkerboard or grid image onto the object of interest. A camera captures an image of the object and the projection. The features and curves on the surface of the object deform the uniform, parallel lines of the projection, and thus geometry can be extracted directly from analysis of the deformed grid pattern.[79]
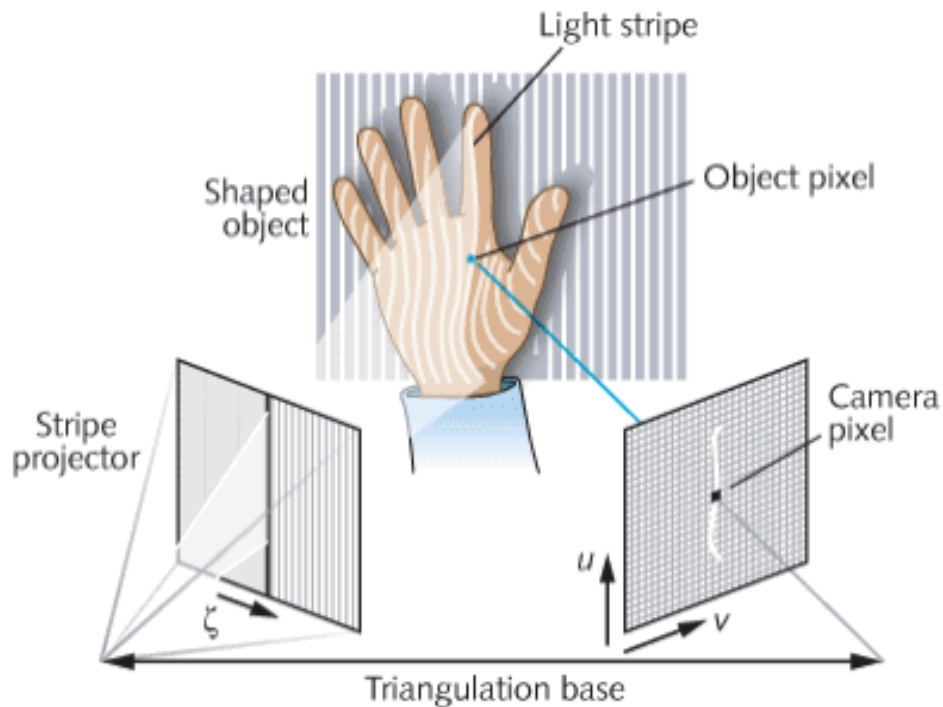
Figure 2.4-12 Structured light projection and image capture[80]

These reconstruction methods can quickly capture the shape of a product and provide empirical characteristic information on the product and by extension, the manufacturing process[81]. Technological advances in accurate, automated 3D systems in the mid-1980s began a trend of close range 3D mapping adoption in industry[70]. These systems used high-res digital metric SLR cameras with wide-angle lenses, retro-reflective object targets or image point measurement operators to extrapolate image measurements within minutes. Such systems were incorporated in a variety of industrial fields including automotive, aerospace, and survey and mapping and civil engineering.

The successful implementation of 3D imaging in manufacturing requires a multidisciplinary approach to create a calibrated toolchain of image acquisition hardware and data reconstruction and analysis software.

1) Imaging sensor: This determines the camera sensor type, resolution data transfer speed, field of view, spectral information and acquisition time. Consumer and semi-professional camera traditionally have poor mechanical stability, require intermittent calibration and captured images require software compensation for measurement inaccuracies due to lens distortion or sensor drift. Professional metric cameras minimize geometric image distortion and give highly repeatable images[70]. Purpose built photogrammetric cameras

incorporate highly stable metric construction, multiple imaging sensors, lighting fixtures and image processing hardware.

2) Illumination and targeting: Specific lighting direction, intensity and wavelength can be used to highlight features of interest in passive systems. Image targeting points can also be added to improve accuracy and repeatability of results.

3) Imaging configuration: Defines the number of cameras or images, desired accuracy, calibration points and reference targets. These targets are coloured to contrast against the object or are retroreflective. Targets may be replaced with software processes such as edge detection and pattern matching[82].

4) Image processing: Automation of target recognition, lighting controls, image capture and data collation and presentation in software.

5) 3D reconstruction: This defines the software method for determining 3D coordinates, through point cloud generation, spatial intersection and triangulation, and bundle adjustments.

6) Data analysis: Translating 3D model into a CAD environment for user interaction and analysis

7) Accuracy verification: Comparing image results against reference artefacts with acceptable tolerances.

To accurately scan a physical object, special care must be taken to optimise ambient conditions to better highlight the characteristics of the object's surface. This can reduce glare from glossy surfaces and surroundings, or focus light on specific features while cast shadow on others. 3D scanning has experienced significant technological advances in recent years with developments in handheld scanners for on-the-job reconstruction, drone mounted scanners for aerial scanning and faster, more accurate software packages for reconstruction such as Geomagic and RealityCapture.

2.5   Literature review conclusion

This literature review dictated the conceptual design for a modular, reconfigurable test execution system based on the principles of Industry 4.0 and Big Data. This system fulfils many of the key trends which are believed to significantly influence automated test systems in the coming years, notably heterogeneous computing, production test data harvesting, automated test management software and production characterization[83]. While RMS learning environments are in development, there is a lack of focus on end-of-line automated reconfigurable testing systems. This test

execution system aims to integrate the recent developments in RMS theory with automated test equipment (ATE) common in dedicated manufacturing processes such as those found in electronics and mechatronics industries.
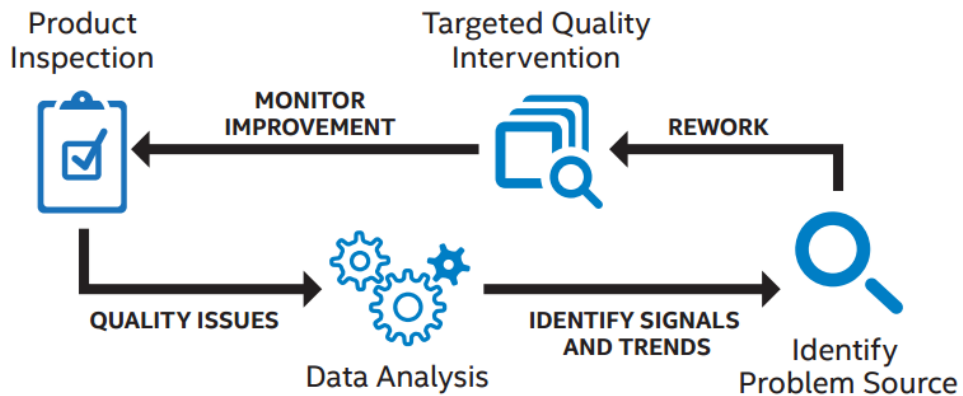
Figure 2.5-1 Closed loop quality control[84]

The data generated from this TES will be proactively analysed for quality analysis on product and process, creating a feedback loop for continual quality improvements. Such techniques have already shown great promise in the semiconductor industry, allowing companies to leverage the power of Big Data analytics to collect and act on increasing yield and productivity while improving overall quality[83].

3 Reconfigurable test execution system design concepts

3.1 Design challenge

Ceramicx infrared heating elements are efficient, robust heaters which provide long wave infrared radiation from 2-10 microns in wavelength. The IR elements typically operate between 300°C and 700°C with a range of power outputs from 125W to 1400W. The IR elements are available in a number of profiles and sizes from 60 x 60 x 8mm for the Quarter Flat Element (QFE) to 250 x 125 x 25mm for the Large Full Trough Element (LFTE). An example of these IR elements are seen below in fig. 3.1-1:

Figure 3.1-1 Ceramicx range of ceramic IR elements

The IR heating elements are constructed from an iron-chrome aluminium resistance wire that is wound on a mandrel into a tight coil. This coil is encased in an inorganic filler material comprised mainly from aluminium oxide (AL_2O_3) and silicon dioxide (SiO_2). Both compounds exhibit relatively good strength, are chemically and thermally stable and have excellent electrical insulation[85]. Al_2O_3 is widely used in passive electronic components such as capacitors[86] and hygrometry devices[87], in biomedical applications and most popularly in refractories, which consumes one quarter of all alumina production[88]. SiO_2 is a primary component in glass manufacture, metal casting moulds, refractory materials and cement[89]. The AL_2O_3 and SiO_2 are mixed into a slurry with water, potassium and calcium, then cast in a mould. The form is air dried until it has a moisture content of <15%, then removed from the mould. This is known as a green element. The element is fired in a kiln at 950°C to

biscuit, dipped in a coloured glaze, and then re-fired to create a finished product. Fig. 3.1-2 and fig. 3.1-3 show the results of an energy dispersive spectroscopy (EDS) analysis on a finished IR element:

Elements Detected wt%						
1	O	Al	Si	K	Ca	Total
Spectrum 1	66.7	11.72	17.63	0.98	2.96	100
Spectrum 2	67.86	9.43	19.83	1.06	1.83	100

Figure 3.1-2 EDS analysis of IR heating elements before firing

Elements Detected wt%								
1	O	Al	Si	K	Ca	Na	Mg	Total
Spectrum 1	63.51	6.87	23.76	1.22	2.88	0.87	0.89	100

Figure 3.1-3 EDS analysis of ceramic glaze after firing

The IR heating elements are used in a diverse range of industrial and engineering applications such as thermoforming, packaging, curing and drying. Ceramicx IR heating elements are available in a number of families of different shapes and dimensions including trough, hollow, flat ceramic elements and bulb elements. Quartz elements are constructed by winding the resistance wire through a series of quartz glass tubes that are held in an aluminized steel case. Ceramicx also produce a range of ancillary products such as connectors and mounting components to support their range of IR elements. The ceramic trough, hollow and flat elements constitute 80% of Ceramicx IR heater sales. Fig. 3.1-4 below gives an indication of the part families under consideration with the project:
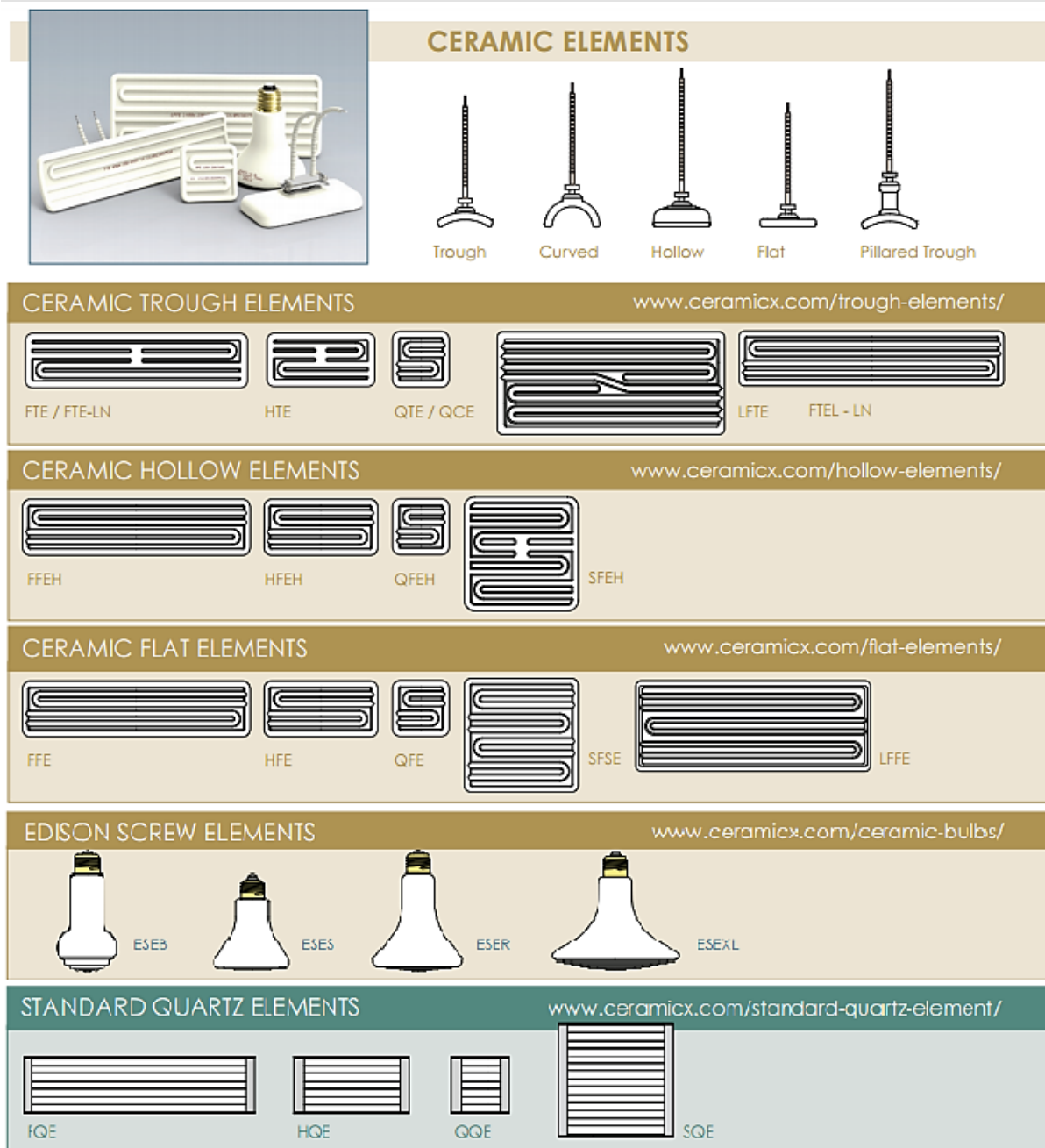
Figure 3.1-4 Ceramicx range of IR heaters[90]

Ceramicx also integrate these IR heaters into a range of space heaters and custom furnace ovens for businesses, creating energy savings of up to 30-40% and increasing IR activity for heating, thermoforming and curing processes as seen in fig. 3.1-5.
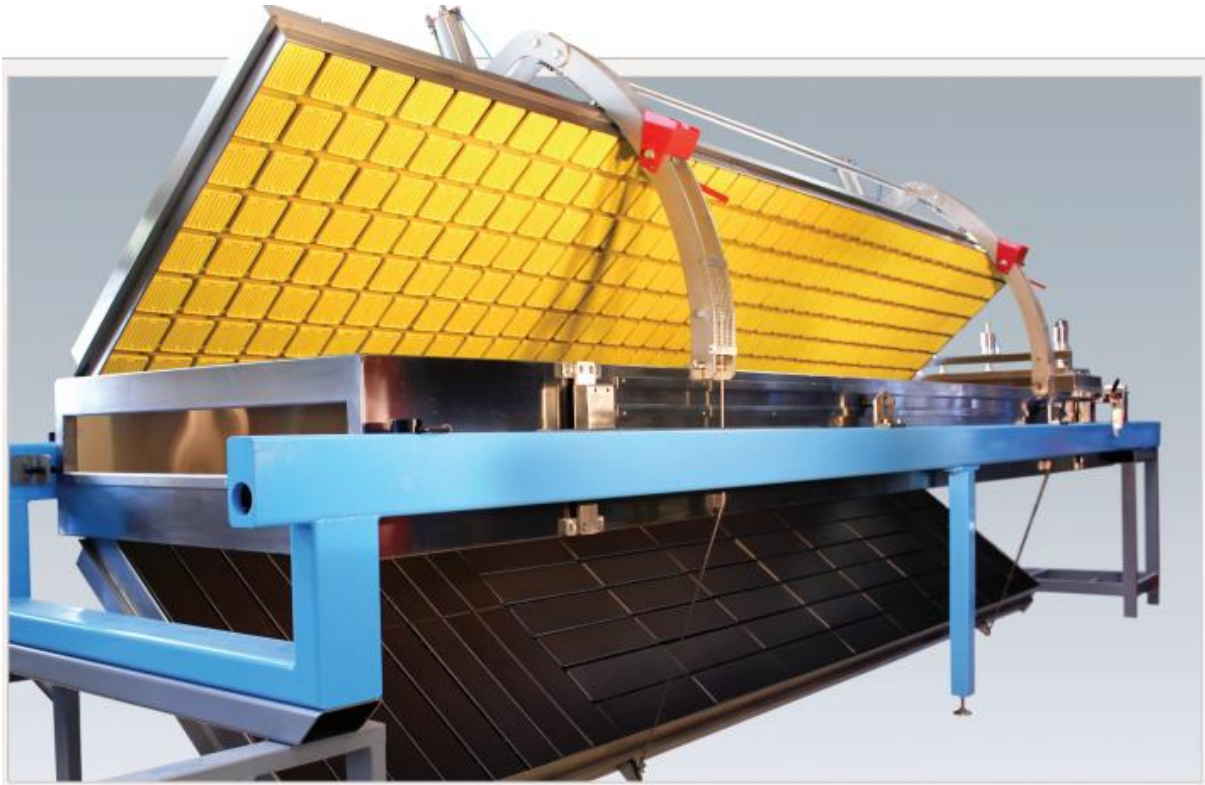
Figure 3.1-5 160kW oven designed and manufactured by Ceramicx [90]

3.1.1 Outline technical specification for product testing.

The IR element's test requirements were considered in the context of modularity, reconfigurability and plug-and-produce, whereby there should be minimal use of dedicated fixturing for products, automated machine reconfiguration for part changeover and a high level of captured data for cloud based processing and analysis. The final design should also increase throughput, reliability, ease of operation and integrate into the current Ceramicx manufacturing environment.

3.1.2 Design concepts

Concept 1: Optimise current test system

Several concepts were considered for this project with the final concept utilising series and parallel testing to achieve maximum machine output. The first concept focussed on optimising the test system in place at the time, increasing throughput and reliability by retrofitting new control software and data analytics.

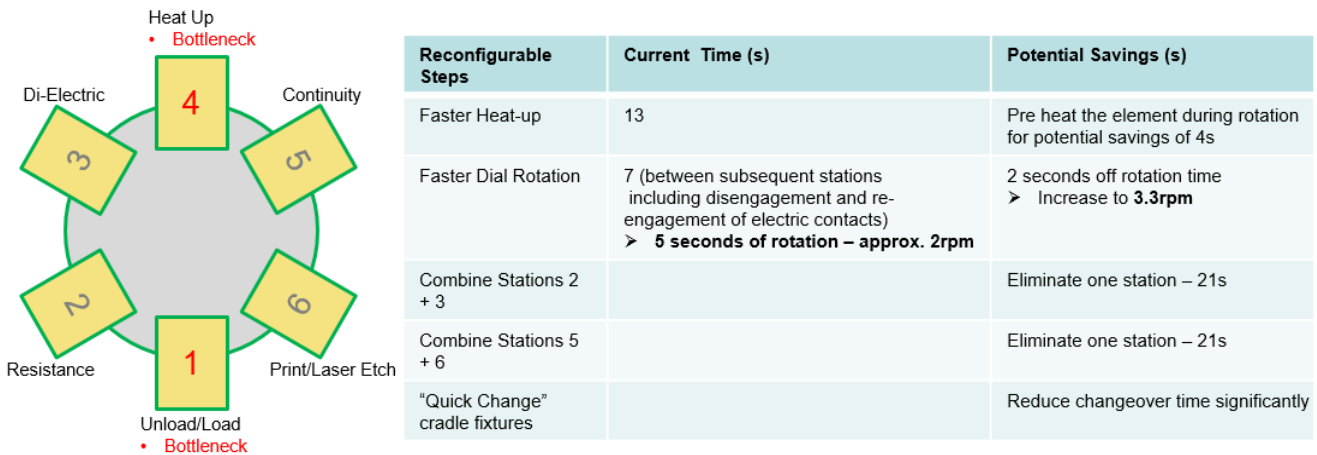| Reconfigurable Steps	Current Time (s)	Potential Savings (s)
Faster Heat-up	13	Pre heat the element during rotation for potential savings of 4s
Faster Dial Rotation	7 (between subsequent stations including disengagement and re-engagement of electric contacts) ➢ **5 seconds of rotation – approx. 2rpm**	2 seconds off rotation time ➢ Increase to **3.3rpm**
Combine Stations 2 + 3		Eliminate one station – 21s
Combine Stations 5 + 6		Eliminate one station – 21s
"Quick Change" cradle fixtures		Reduce changeover time significantly

Figure 3.1-6 Optimised concept

Fig. 3.1-6 shows this concept which achieved greater part throughput, simplified the test procedure and lowered implementation time and cost. However, it does not fulfil the RMS specification and was considered a half-step towards the overall design goals. It was decided these could only be accomplished through a system designed from the outset on the concepts of RMS and Industry 4.0.

Concept 2: Holistic, integrated manufacturing system

Lean manufacturing principles emphasise the removal of waste and creating a system where the product is pulled through each manufacturing process, rather than pushed. This macro-scale concept involved the integration of pre and post manufacturing processes to streamline product flow. This reduced time of transit, the number of part transfers and a better distribution of human resources, potentially reducing the number of operators from six to four by removing the operator from the automated test system as seen in fig. 3.1-7:
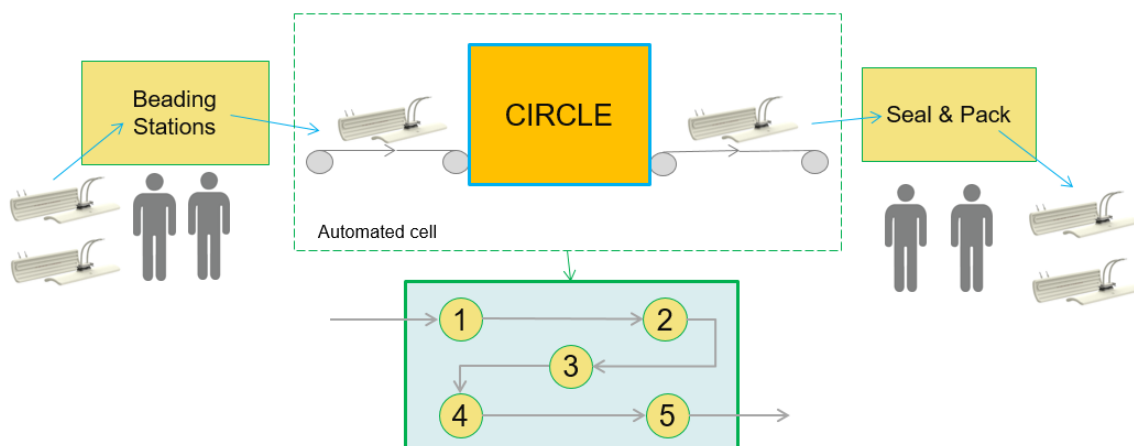

Figure 3.1-7 Concept of continuous part movement

The concept called for a purpose built RMS with automatic, sequential part movement through three phases of production; beading, testing and packing. It was ultimately deemed too complex and expensive to implement, requiring a change to three production stations and large scale reorganisation of factory floor space. However, the concept of a conveyor based RMS was adapted for the final concept.

Concept 3: Multi-pallet and parallel testing

The final design concept settled on a core material handling element based on a looped conveyor concept, with a series of modular, reconfigurable test stations that could interface with the conveyor. An early illustration of this concept is shown in fig. 3.1-8 below:
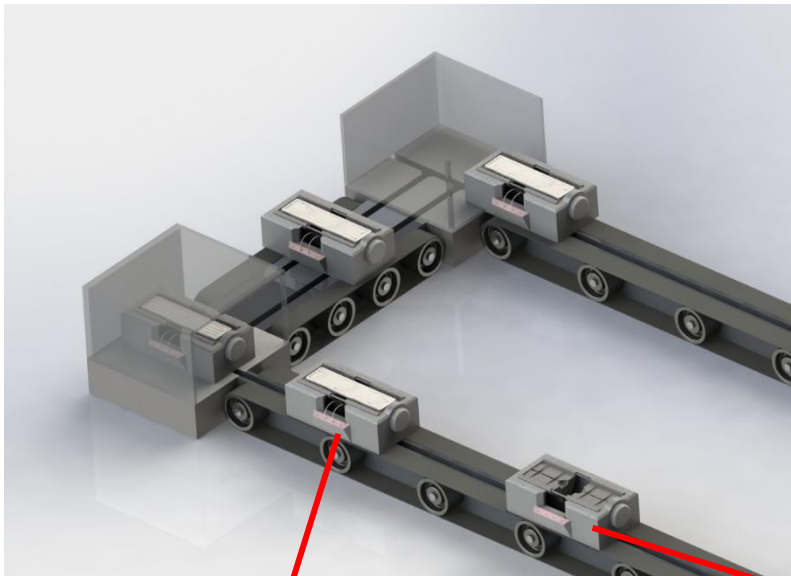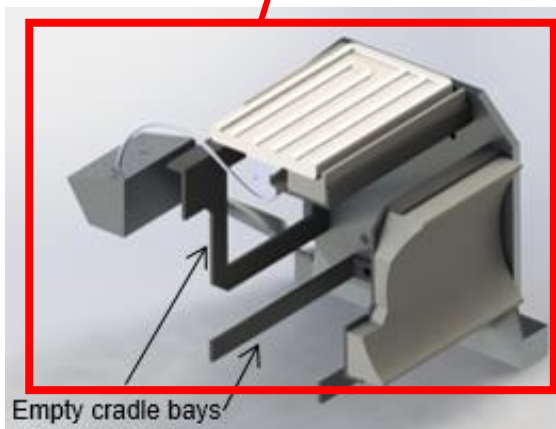

Figure 3.1-8 Early pallet based conveyor system concept

Empty cradle bays

Figure 3.1-9 (a) Cradle with IR element
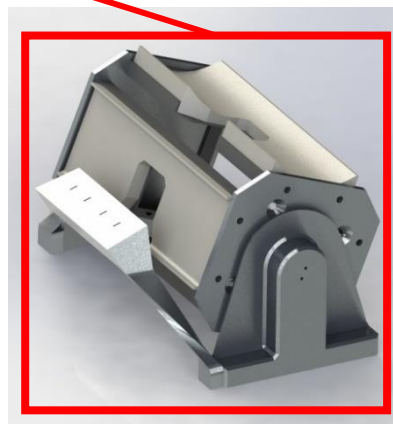
Figure 3-9 (b) Cradle in mid-rotation

This concept focuses solely on the IR element test, while leaving the option for a full factory integrated system open for future implementation. The IR elements are

45

mounted on custom holding fixtures, as seen in fig. 3.1-9, which are then placed on a conveyor system and shuttled by the conveyor through each stage of the testing process. These fixtures futureproof the RMS against changes and new additions to the IR element product line.

Concept 4: Ceramicx Infra-Red Heater Characterisation Laboratory Equipment

It can be seen from fig. 3.1-10 that a looped conveyor system with independent, modular testing stations allows for optimal use of floor space. Workpiece holding fixtures loaded with IR elements travel around the loop completing the required testing stages.

Figure 3.1-10 Final concept CAD design

Each test station has one or more specific test functions:

Test station 1:   Measure heating coil cold resistance and perform a dielectric voltage withstand test.

Test station 2:   Record a thermal image of a heated element followed by a heating coil hot resistance measurement.

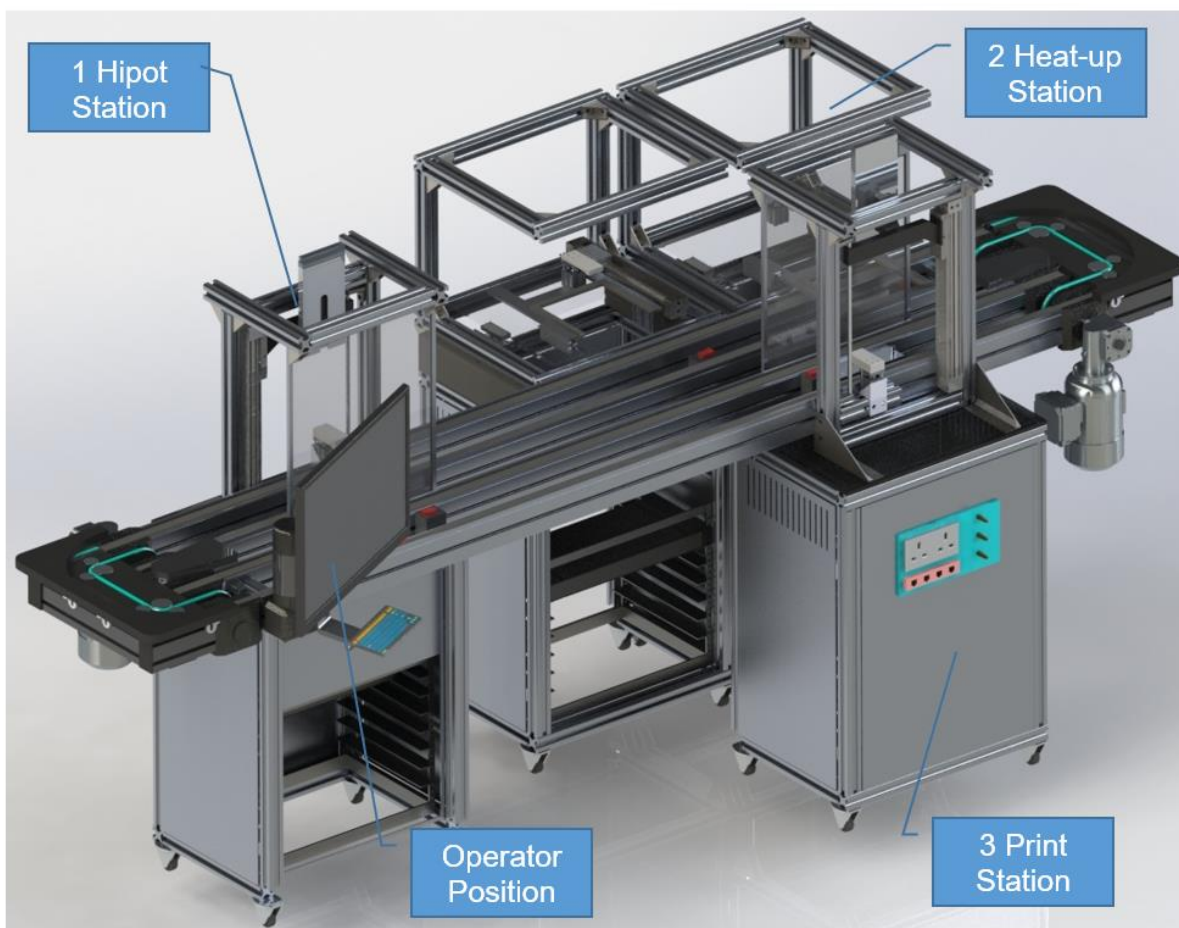Test station 3:   Print a serial number on the front or rear of the element based on successful completion of previous test steps.

The test stations receive instructions and communicate results to a master computer located adjacent to the conveyor. The operator interacts with the master computer through a console in order to setup and monitor the machine's operation, input test parameters, change test steps and incorporate new stations into the test routine. Each of the test stations report data to the master computer, which collates results to a cloud based database. These results are available to multiple stakeholders and provide the basis for unique product technical specification sheets as well as source data for manufacturing analytics, allowing for detailed analysis of the trends associated with production.

3.2   Modular design concepts

In addition to the core functionality required to test heating elements, the CIRCLE system incorporates many Industry 4.0 specifications. The system was designed from the beginning to promote the principles of modularity, hardware and software reconfigurability and heterogeneity, where each station operates independently without interaction with neighboring stations.

3.2.1 Hardware

- The test execution system was designed with scope for expansion and reconfiguration.
- The system was designed with 8 slots that a test station can occupy. In the initial research work, three of these slots were populated with test stations, leaving potential for future hardware expansions should a new product, client or legislation require a new unforeseen test.
- Each station was designed and built in isolation following a standardised template. For example, test stations each have a standard width to fit into a slot and are built on common extruded aluminium skeleton. This formalised the

station footprint, incorporated all relevant safety hardware and included a common component layout reducing design and construction time. A new station built to this footprint should correctly integrate into the rest of the system without large system overhauls, redesign and downtime. This "plug-and-play" design ensures hardware reconfigurability.

- Stations can be duplicated to increase part throughput. While individual stations operate in isolation, duplicate systems can be linked to manage part throughput and test routines. Duplicates operate in a master/slave configuration, sharing computing resources, removing the need for additional system hardware and communication overhead.

- Technical issues can be quickly isolated to individual stations. As each station operates in isolation, issues can be quickly tracked and remedied. This feature also simplifies maintenance as stations can be quickly removed without compromising the overall operation of the test system.

3.2.2 Software

- Each station operates on a common hardware and software platform, specifically the National Instruments (NI) Compact RIO embedded controller and NI LabVIEW graphical development environment.
  Compact RIO Controllers are high-performance embedded controllers with industrial I/O modules, extreme ruggedness, industry-standard certifications, and integrated vision, motion, industrial communication, and human machine interface (HMI) capabilities. These controllers were ideally suited to this application due to their ease of use, reliability and reconfigurability.

	Value	Performance
Processor Performance	Up to 400 MHz	Up to 1.33 GHz dual-core
FPGA Performance	Up to 43,661 logic cells, up to 58 multipliers	Up to 147,443 logic cells, up to 180 multipliers
Operating System	Real-time OS	Windows/Real-time OS
I/O	Up to 8 I/O module slots, 100 Mbit/s Ethernet, USB, RS232	8 I/O module slots, 1000 Mbit/s Ethernet, USB, RS232/RS485, VGA
Power	Up to 9 to 30 VDC supply range, 6 to 25 W consumption	9 to 30 VDC supply range, 20 to 75 W consumption
Ruggedness	-20 °C to 55 °C*, up to 50 g shock	0 °C to 55° C, 50 g shock
Size	Starts at 17.8 x 9.3 x 8.7 cm³*	Starts at 40.4 x 13.4 x 8.7 cm³

Figure 3.2-1 Compact RIO image and technical specification

- The Compact RIO chassis are expandable should new hardware need to be incorporated for additional functionality. Each test station is controlled with an NI cRIO 9066 8-slot chassis, which are loaded with I/O modules specific to the test required. These modules communicated to the station's sensors, test equipment and other hardware. Each chassis has eight module slots, leaving space for further expansion and reconfiguration.

- The LabVIEW architecture allowed for new software plugins to control additional, non-standard hardware.

- As part of a heterogeneous system, each station operated in isolation, requiring no communication with external hardware, save the master console. This simplified the design architecture and removed the possibility of software incompatibility between new and legacy stations.

  Software issues are also isolated to the individual station, simplifying error tracking.

- The operation of each station is comprised of a series of test steps. These steps can be rearranged and altered by the operator to create new routines and behaviours to suit new applications. These new routines can be used to create more intensive tests outside the scope of normal production for in-depth product analysis and data generation.

49

- All test data was collated into a cloud-based MySQL database for future analytics and trending algorithms.

3.3 Realisation of the design solution

3.3.1 Conveyor system

The Test Execution System was designed from the start to foster the principles of Industry 4.0. A Bosch TS Plus asynchronous modular conveyor, comprised two 2.5m sections joined at the end with two 180° turns was used to form a stadium shape. The Bosch TS Plus is a fully modular conveyor system with options to expand and alter the path of the product as needed. The conveyor was split into eight segments of identical sizes, each of which could support a single test station as illustrated in fig. 3.3-1 below:
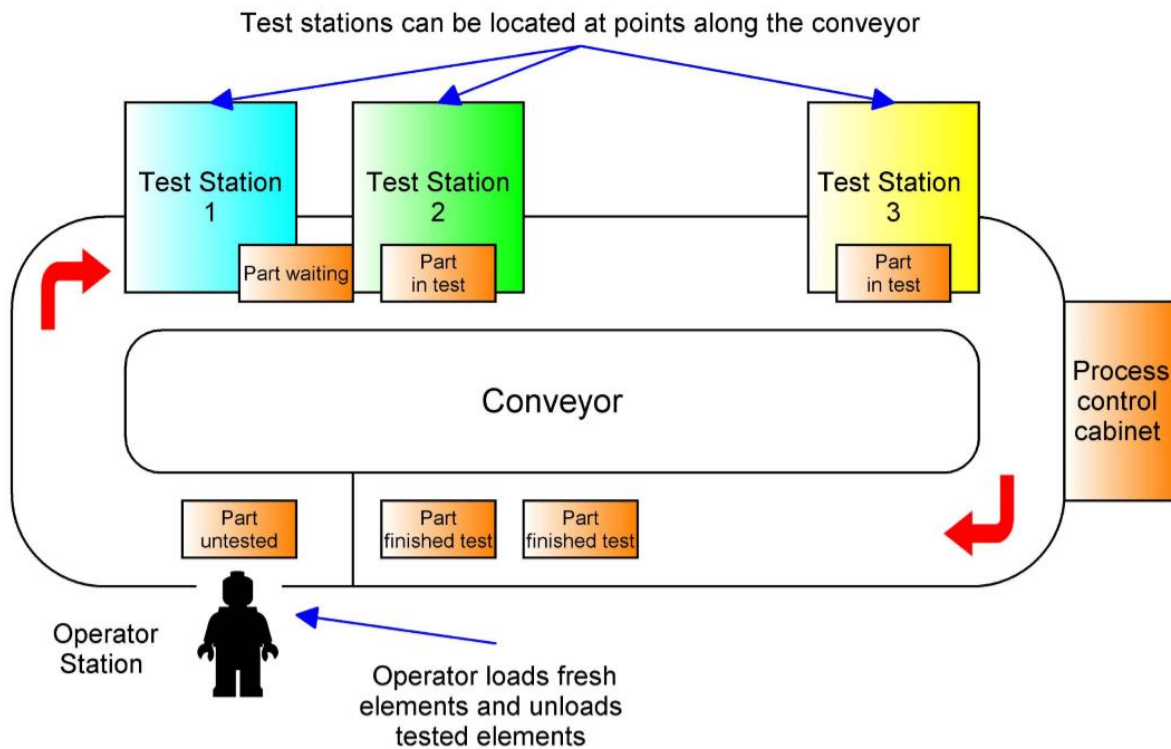
Figure 3.3-1 Plan view of CIRCLE layout

Each segment was fitted with an identical interface plate which provided the test stations with all necessary power, air and data capabilities. The conveyor operated as the backbone of the system, a central hub which provided the necessary infrastructure for any foreseeable test station design which may be required. The conveyor is asynchronous and moved constantly in a clockwise direction, while a network of inductive sensor triggered stop gates managed the flow of pallets through the system.

These gates were controlled by the test station which occupied the slot where the stop gates are located, providing localised control of part movement.

The section view of the conveyor system is shown in the fig. 3.3-2 below:
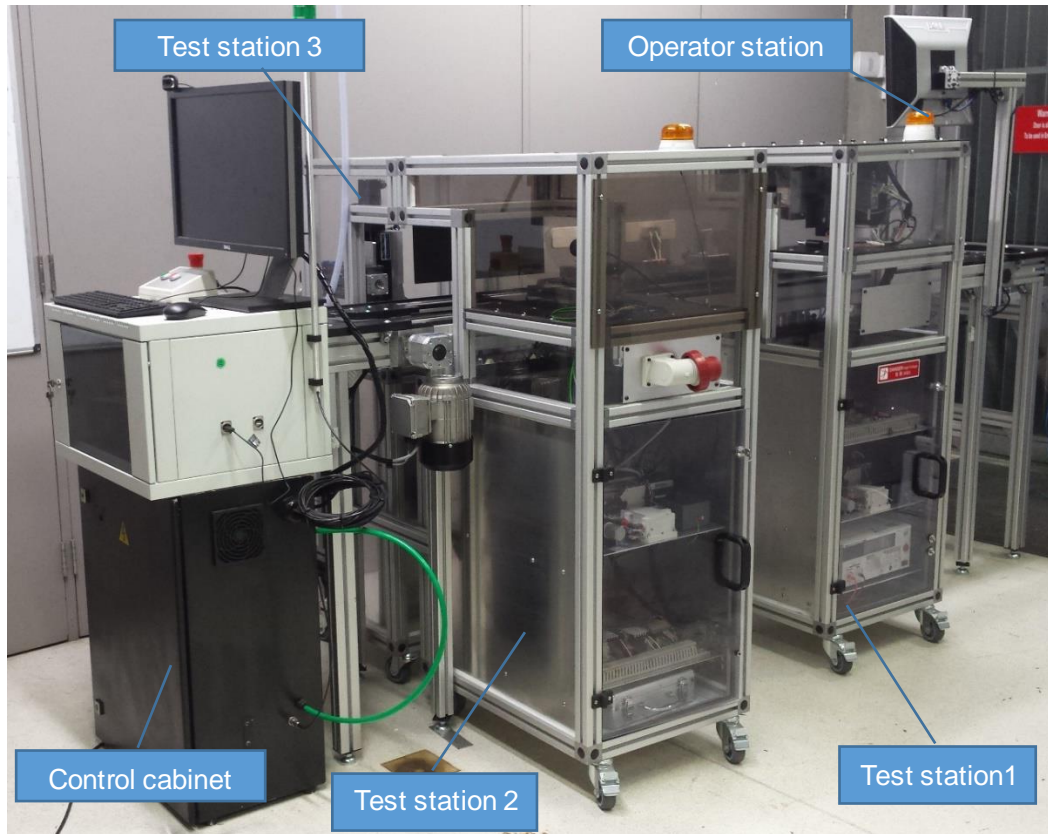
Figure 3.3-2 CIRCLE test execution system

Figure 3.3-3 (a) Test station power and I/O socket
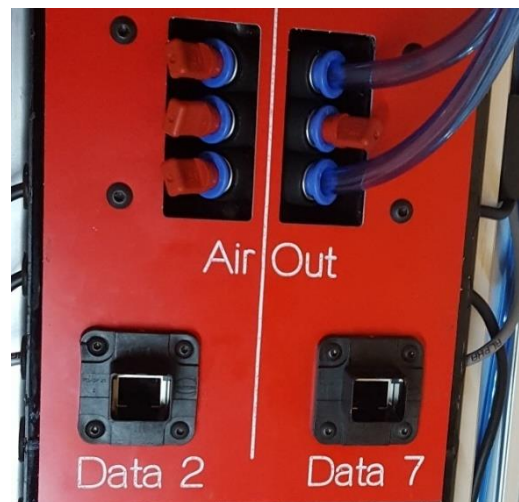
Figure 3.3-3 (b) Test station air and Ethernet socket

The centralised connections were an easy and rapid method of interfacing test stations to the conveyor using robust, industry proven hardware, as seen in fig. 3.3-3.

3.3.2 Conveyor control

A cabinet at the conveyor end controlled and monitored the provision of power and air through the line. The cabinet, shown in fig. 3.3-4, also housed safety components, variable frequency drives (VFD) for the three-phase conveyor motors and low level control for mains power and indicator lights.
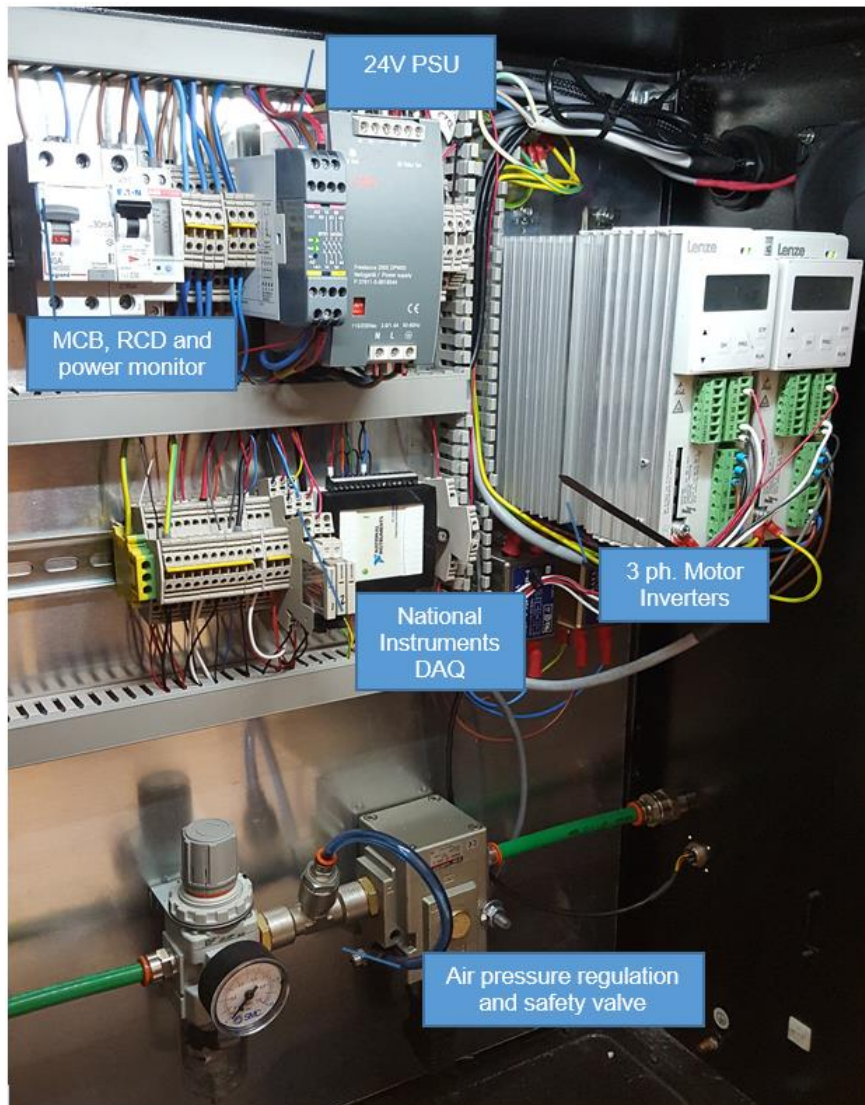
Figure 3.3-4 Control Cabinet hardware

A server rack mounted onto the control cabinet housed a 16 port Gigabit Switch and an industrial computer which controlled the overall operation of the system and acted as a Human Machine Interface (HMI) for the operator. Fig. 3.3-5 shows the main features of the conveyor control system:
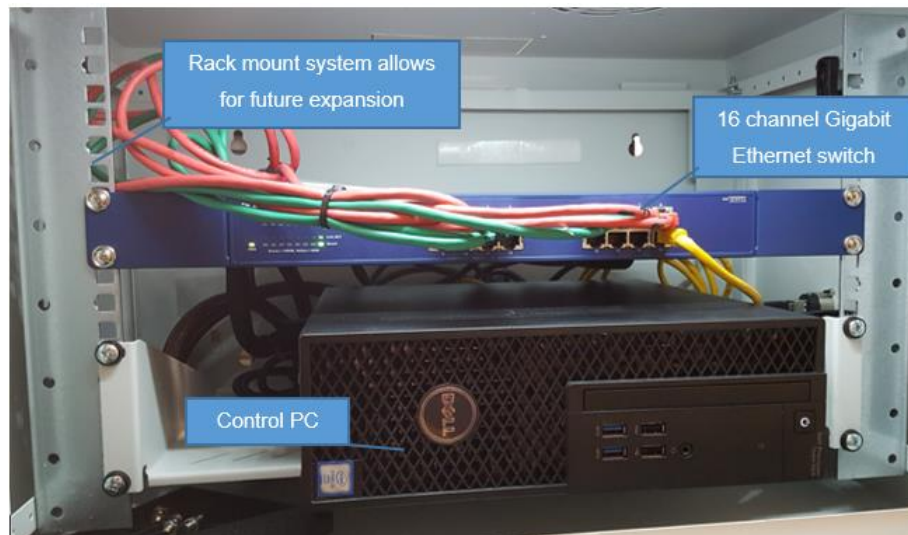
Figure 3.3-5 Server cabinet

3.3.3 Materials handling

A universal Bosch pallet system was used as the basis for materials handling. The pallet base was a standard Bosch TS Plus component, onto which a pressed stainless steel box was mounted. This box was designed for the attachment of brackets which can support the variety of Ceramicx heating elements. These brackets were designed to minimize changeover times between multitude of Ceramicx part types by providing a standardised platform for mounting the ceramic, bulb and quartz elements.

The box also facilitated the electrical contact between each test station and the heating element. This aspect of the design was critical as it drove the design of the various pallet handling mechanisms in each of the test stations.

The electrical contactor and bracket mounted on the Bosch universal pallet system went through several design iterations before the final desing was realised:

1) Early concept CAD (designed by Rob McDowell). This design was based on an early Afag Automation pallet system and used a 3D printed wire holder.
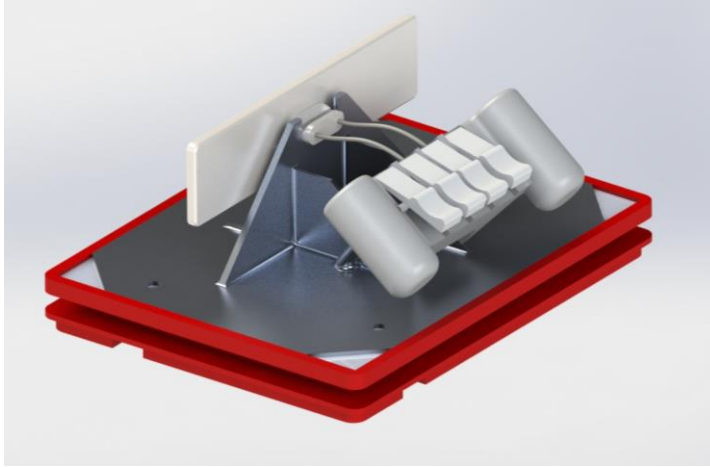
2) It was discovered early on that the most common area for fault was the neck of the IR element. A spring clip was designed to fully enclose the neck in order to catch wire breakout during hi-pot testing. The 3D printer clip was replaced in favour of off-the-shelf quick release connectors.
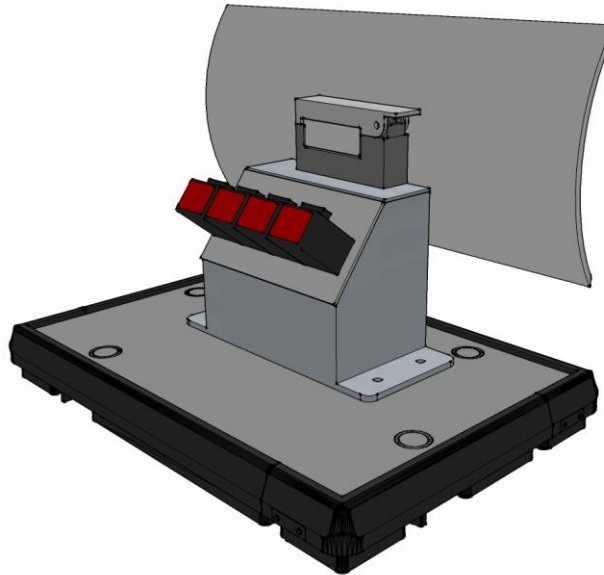
3) It was necessary for the hi-pot tester conductive foam pads to contact as much of the IR element surface to perform a comprehensive dielectric withstand test. This necessitated that the rear of the IR element was exposed to the pad. This iteration placed the IR element on a neck to raise it above the body of the electrical contactor box
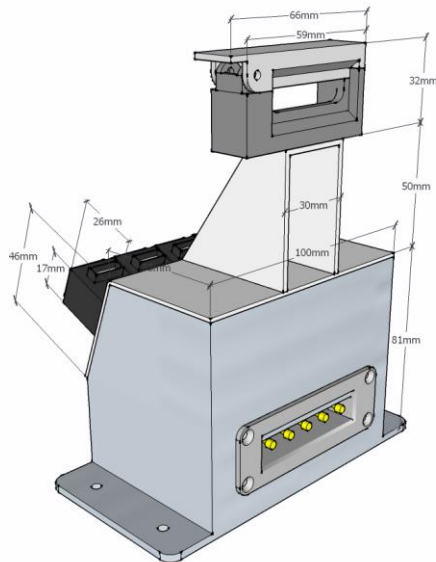
4) Variations of this design were experimented with as the conductive foam pad design was developed in tandem with the pallet design.
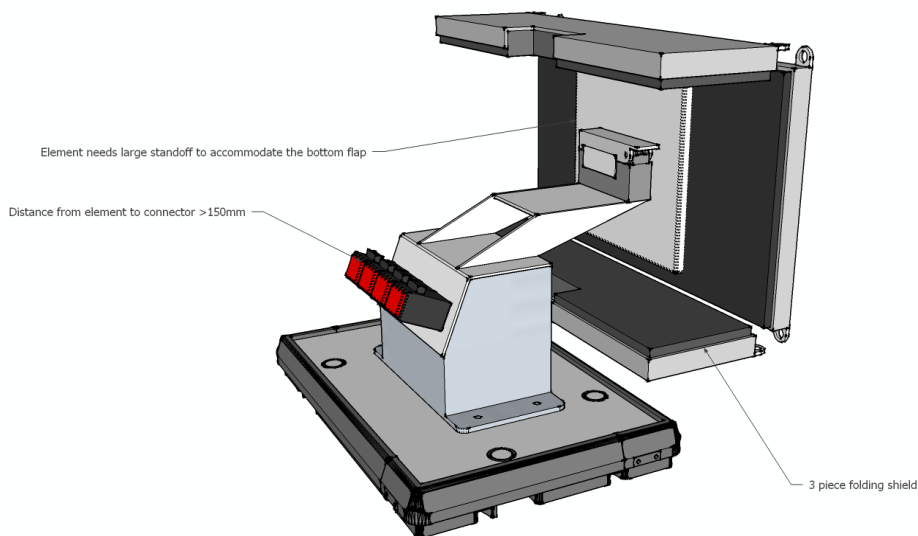
5) The final versions of this design reduced the height of the electrical contactor box, while retaining the neck and IR element clip. These versions were 3D printed from PLA plastic on an Ultimaker 2 3D printer. Multiple parts were assembled and used to test the operation of the test stations.
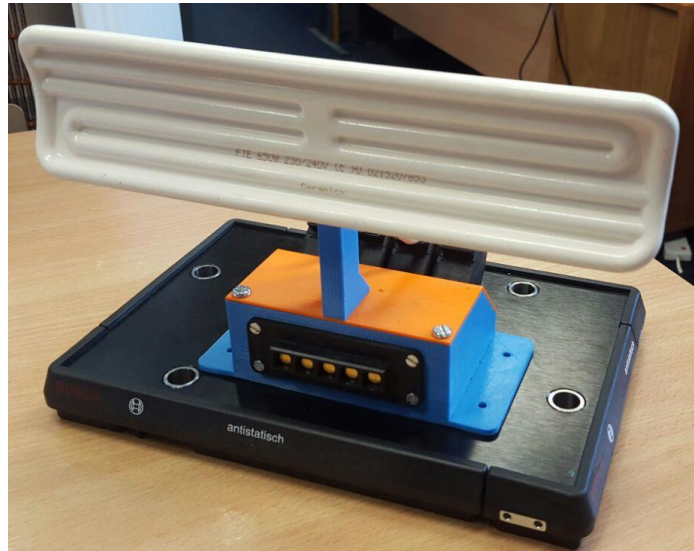
6) The final version was redesigned slightly for ease of manufacture. The assembly was laser cut from 2mm stainless steel and pressed to shape. The electrical contactor was machined from acetal and gold plated pads were push fit to create the female electrical contacter. The male electrical contactor was machined in a similar manner and featured push fit spring pins, which mate with the pads creating an electrical connection between pallet and test station.
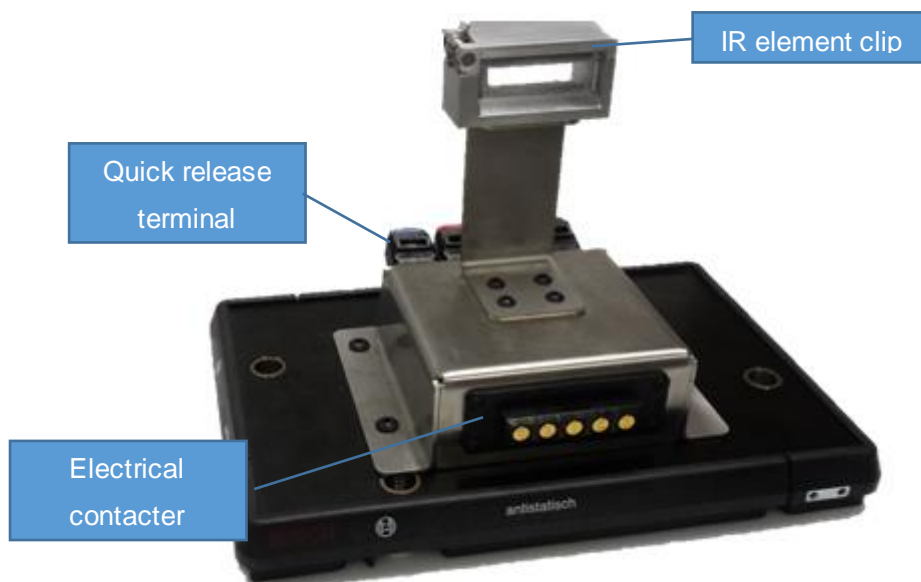
Figure 3.3-6 Ceramic IR element fixture

Test stations

To maintain a modular system and reduce design overhead, each test station was standardised to simplify overall system design and construction. Commonalities between test stations were identified early in the design process and duplicated, preventing design overlap and incompatibility.

- Each test station was dimensioned to fit the standard conveyor slot footprint.
- Test station frames and overall mechanical design was standardised for ease of construction.
- Identical power/ data/ compressed air input panels were designed to simplify construction and reconfigurations.
- Each test station was designed with protective polycarbonate panels to prevent operator access to the internal test equipment and to the conveyor.
- Industry standard safety interlocks were installed on maintenance doors and between the station and conveyor.

Standardised electrical panels, as seen in fig. 3.3-7 were installed to reduce construction time and ease troubleshooting and future maintenance.
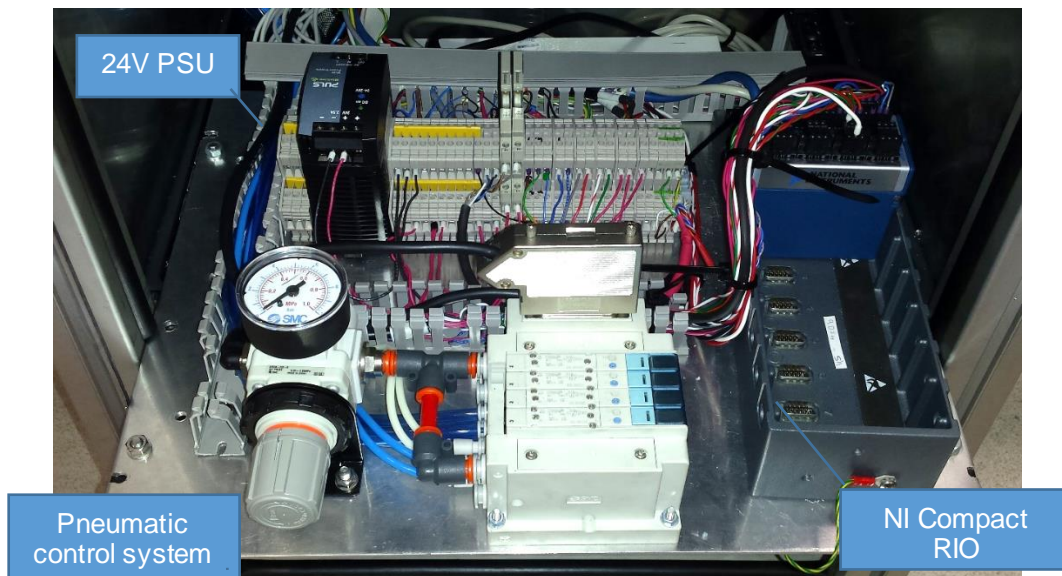
Figure 3.3-7 Test station 1 electrical panel

3.3.4 Test station 1: Cold resistance and hipot test

Test station 1 was used to measure the resistance of the cold element coil and perform a dielectric withstand test to check the integrity of the ceramic coating. This test station featured an electrical contacter linked to a National Instruments NI9219 Universal Analog Input module. This module featured a 0.1% accuracy two-wire resistance measurement and a 1% accuracy K-type thermocouple input. The dielectric withstand

test was performed by a Kikusui TOS5200 hipot tester, located within the test station. Two pneumatically actuated conductive foam pads were used to provide a path to ground for leakage current that is created during the hipot test.

Figure 3.3-8 Test station 1 hipot test system

3.3.5 Test station 2: Heat-up and hot resistance test

Test station 2 was used to check the performance of the heating element by applying a range of operational voltages to the element and recording the heating response with a thermal camera. The test station was constructed using a deep footprint to provide the required focal distance for optimum thermal camera operation. The thermal camera used was an Optris PI400 Thermal Imaging Camera, which has a resolution of 382x288 pixels and a measurable temperature range of -20°C – 900°C. For safety and calibration purposes, two K-type thermocouples were mounted inside the test station and relayed information through a NI9219 module. This module also performed a hot resistance measurement, aimed to characterise the element coils thermal coefficient of resistance and test the integrity after heating. Test station 2 hardware can be seen in fig. 3.3-9:

Figure 3.3-9 Part waiting for test station 2 thermal camera test

Each test station has a standard method for detecting and interfacing with the pallet. This can be seen in fig 3.3-10:
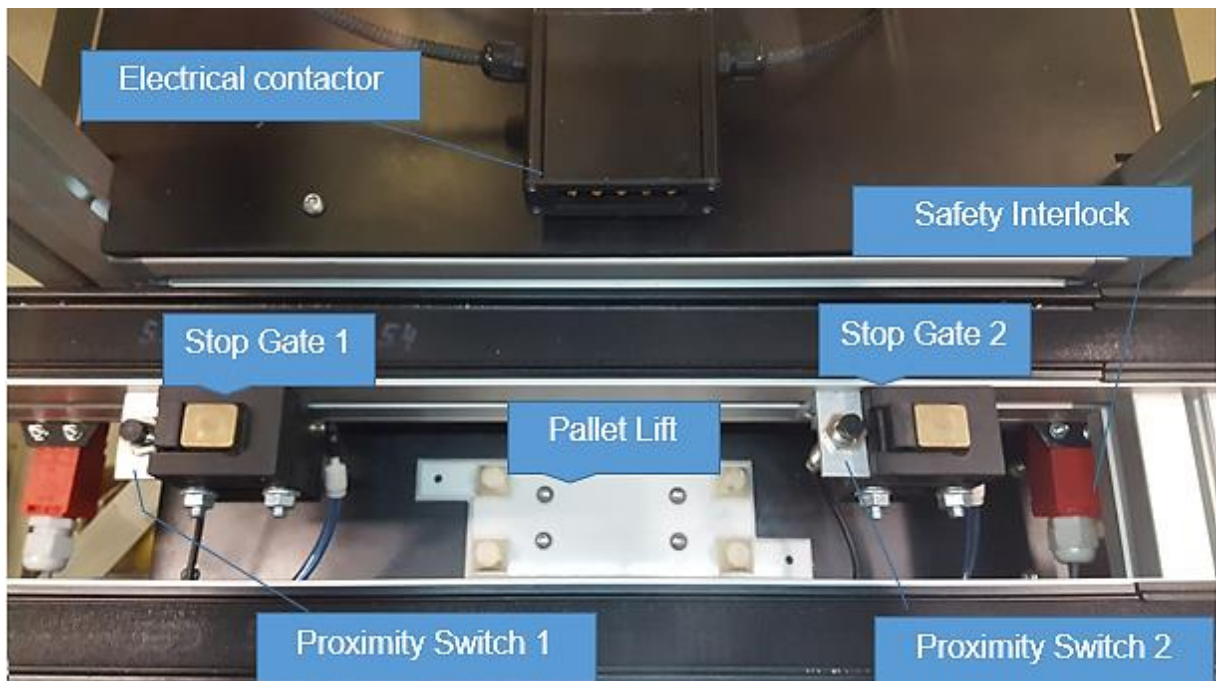
Figure 3.3-10 Plan view of pallet detection and management

3.3.6 Test execution system operation

The CIRCLE test execution system was operated as follows:

The operator loads an untested IR element onto a pallet and releases the pallet onto the conveyor

Each pallet moves through the test stations in the same manner. When all tests are complete the palllet moves to the operator station where the tested part is removed.

The pallet moves to the test station where proximity 1 indicates a part waiting. Stop gate 1 drops, admitting the pallet into the station. All subsequent pallets are held in a queue

After testing is complete, the test station returns the pallet to the conveyor. Proximity 2 indicates the pallet is ready to leave. Stop gate 2 drops and the pallet leaves the test station.

Proximity 2 indicates the pallet is in the test area. The lift actuator raises the pallet from the conveyor into the test station. The test station performs a series of tests according to the test procedure

Figure 3.3-11 Basic test station operation

Additional Features:

Parallel testing: Duplicate stations can be added to increase part throughput. These stations operate by admitting and testing two parts in tandem.

Failed parts: If a test station reports a part failure, the system automatically excludes the part from subsequent testing. The operator is notified of the failure and can remove the part for rework or disposal.

Further Analysis:

Test results, machine performance and process timing results are stored in an XML sheet for further analysis. Test data from each IR element was used to populate a unique technical datasheet which the customer can view online.

4 Test execution case study – Performance investigations

4.1 Characterising leakage current measurements in test station 1

Introduction:

Current flows in a material when a voltage (potential difference) is applied that is strong enough to force the movement of an electric charge, carried by electrons. The flow of charge in a material is measured as electric current. When a high amplitude AC voltage is applied to an insulating material, the alternating current flow causes a charge-discharge cycle which can greatly reduce the insulation's resistance. This rapid decrease in the resistance of the insulation is called a dielectric breakdown. Dielectric breakdown is characterised by a sharp increase in the conductivity of a material due to an applied voltage[53]. The purpose of the dielectric test is to measure a material's ability to withstand dielectric breakdown. The test is performed by placing a large voltage across the device-under-test and recording the leakage current flowing through the insulating material. This test is regularly used in consumer, commercial and industrial electrical equipment to ensure there is adequate separation between a human and potentially fatal electrical current.

4.1.1 Test methodology

The device-under-test is a ceramic IR heating element and the earth leakage investigation is based on examining factors known to contribute to current leakage rates[56][60]. The overall test methodology used in this study is illustrated in the fig. 4.1-1 below:
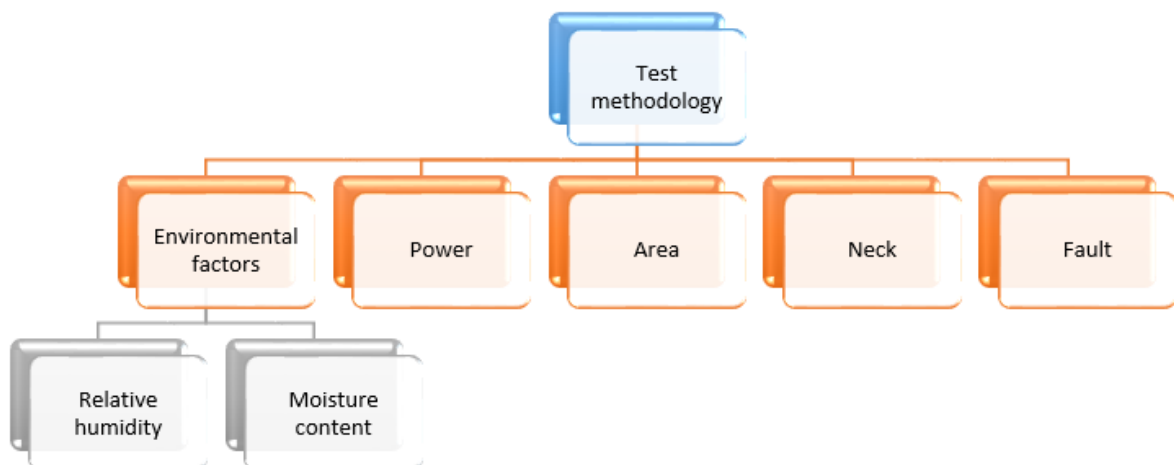
Figure 4.1-1 Test methodology for hipot test station validation

This methodology focussed on various factors which can have a strong influence on leakage current.

4.1.1.1 Test setup

The investigations were conducted using a Kikusui TOS5200 hipot tester, capable of providing 5kV/100mA (500VA at 50Hz) as shown in fig. 4.1-2 below. The Kikusui TOS5200 operated by applying a voltage across the DUT for a pre-set duration and measuring the current flow through the insulating material to earth.

Output range		0.05 kV to 5.00 kV
	Accuracy	± (2 % of set + 20 V)
	Operating range	0.00 kV to 5.50 kV
	Resolution	10 V steps
Max. rated output		500 VA (5 kV/100 mA)
Max. rated voltage		5 kV
Max. rated current		100 mA
Transformer rating		500 VA
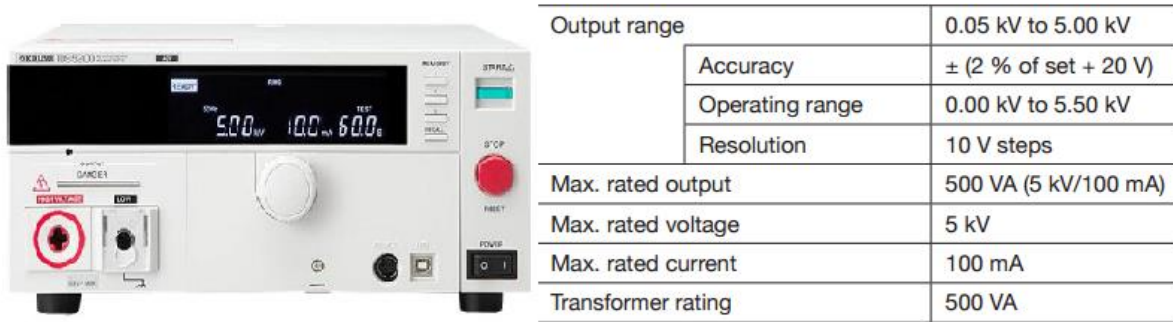
Figure 4.1-2 Kikusui TOS5200 hipot test equipment

Due to the irregular shape and profile of the IR heating elements a path to earth was created using conductive fabric and foam pads. The fabric is comprised of a silver plated tin/nickel alloy thread interwoven with nylon, resulting in a flexible, tear resistant fabric with a surface resistance of <0.5Ωm[91], which can be seen in fig. 4.1-3.

Shieldex Bremen conductive fabric	
Description:	Silver plated nylon fabric Extreme high flexibility
Surface resistance:	<0.5Ωm
Shielding effectiveness	Average 60db from 30MHz to 10GHz
Abrasion resistance	1,000,000 cycles

Figure 4.1-3 Conductive fabric specification and foam pads

Figure 4.1-4 Image of pleated conductive fabric wrapped on foam pad with scale bar (cm)

The foam pads were held in the test station with two aluminium plates, which were connected to a mains earth terminal inside test station 1.

4.1.1.2 Test Procedure

The flowchart for this test procedure can be seen in Fig. 4.1-5, where it is shown that the pallet was lifted by test station 1 into the path of two pneumatically driven foam pads. The pads made contact with the front and rear of the IR heating element while the actuators provide a measure of compression, forcing the foam to deform to the profile of the element. The electrical contacter provided the connection between the Kikusui TOS5200 hipot tester and the heating element. When each test step was complete, the cRio triggered the Kikusui TOS5200 hipot tester to begin, then recorded the resulting leakage current value in milliamps. The element was then returned to the conveyor and released from the test station.
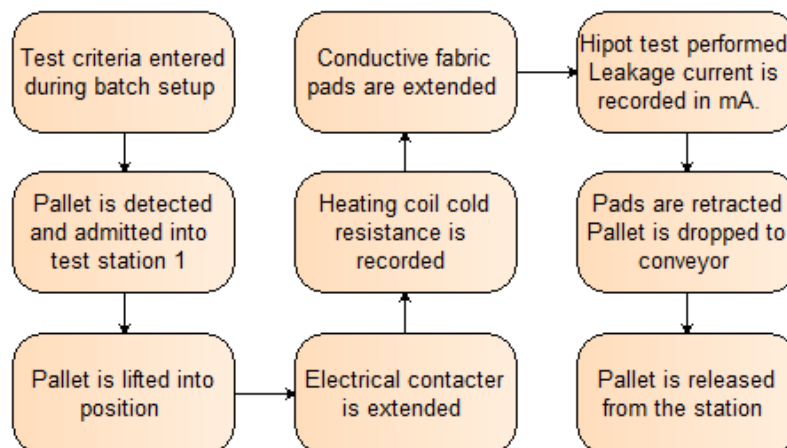
Figure 4.1-5 Test station 1 procedure

4.1.2 Baseline investigations

Before testing, the leakage current inherent in test station 1 was first characterised. There are several electrical connections between the Kikusui TOS5200 and the IR heating element, which add minute amounts of leakage current to the final reading.

Figure 4.1-6 Hipot test current path

The leakage current was recorded at each stage of the current path to quantify this inherent offset. Tests were conducted three times to account for variability in temperature and humidity. Due to the nature of the various electrical connections in test station 1, there was a leakage current of 0.1-0.11mA.

	Test Results (mA)	1	2	3
1	Kikusui 5200 hipot tester (unconnected)	0.021	0.021	0.021
2	Reed relay PCB (Relay ON)	0.056	0.056	0.058
	Reed relay PCB (Relay OFF)	0.056	0.058	0.058
3	Electrical contacter	0.101	0.101	0.1
4	Pallet quick-release terminal	0.108	0.108	0.108

Figure 4.1-7 Hipot test leakage current results

4.1.3 Leakage current investigations.

Preliminary characterisation of the hipot test in test station 1 was carried out to measure consistency of results over time. The parameters of each dielectric test are shown in fig. 4.1-8. This threshold was chosen in accordance to IEC 950 [59] and are consistent with UL 499 Electric Heating Appliances[54] and those used in the sector.

Testing Parameters	
Voltage	1500 VAC
Duration	1 second duration
Threshold Limit	5mA

Figure 4.1-8 Hipot test parameters

64

Temperature and humidity was recorded using a Novus Log Box (Logbox-RHT-LCD) with 0.1% resolution in temperature (°C) and relative humidity (%RH).

4.1.3.1 Characterising the impact of environmental factors on test data:

Test 1: Investigations of repeatable IR element leakage currents:

Square Flat Solid Elements (SFSE) IR elements of two different power ratings were used in these initial tests. These elements were removed from the plastic packaging, then inserted onto the test cradles. The hipot test was repeated 100 times on each part to test consistency of results and integrity of test station components.
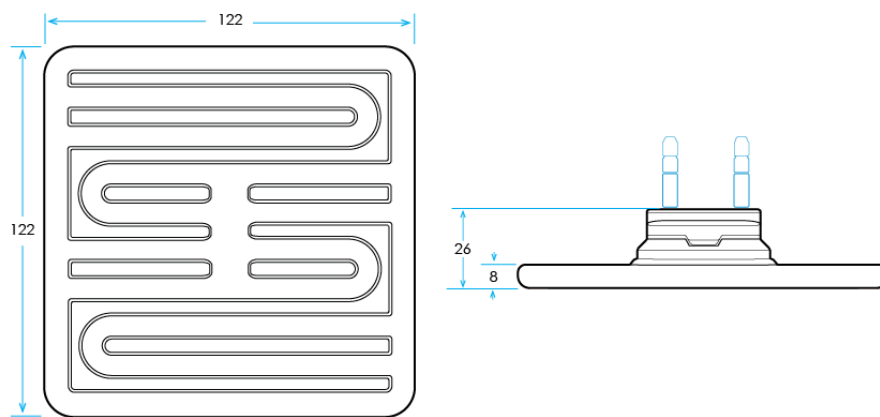
SFSE Technical Details	250W	400W	500W	600W	650W	1000W
Mean surface temperature(°C)	351	480	515	561	596	700
Max power density (kW/m^2)	15	24	30	36	39	60
Max permissible operating temperature(°C)	750					
Average weight	192 g					
Dimensions	122 x 122 x 26 mm					
Useful wavelength range	2 to 10 µm					

Figure 4.1-9 Square flat solid element (SFSE) dimensions and technical data

IR Elements Tested:			
No.	Type	Wattage	Serial No.
1	SFSE	400W	4200
2	SFSE	200W	9380
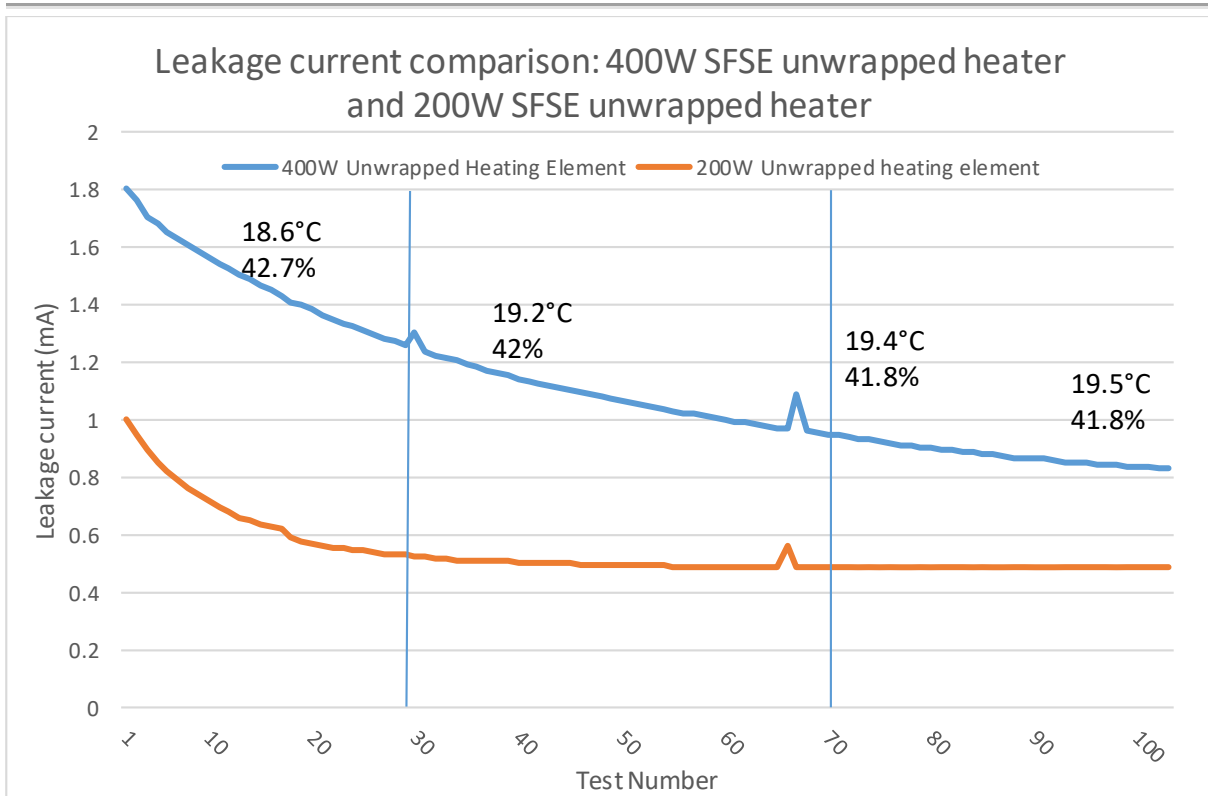
Figure 4.1-10 Comparison testing SFSE 400W and SFSE 200W heater

From fig. 4.1-10 it can be seen that there was significant variation in the earth leakage current over the repeated tests. Some observations include:

- Both IR elements exhibited a similar behaviour pattern, showing a high initial leakage current value, which gradually decayed over the duration of the test.

- The change in temperature is +0.9°C while the change in relative humidity is -0.9%

- The SFSE 200W plateaus at test 30 while the SFSE 400W continued to taper off over the duration of the test.

- Transients seen in at test 30 and test 65 were a result of conductive threads which made contact with the wire leads from the IR elements. These were removed on future tests.

Test 2: Extended investigations of repeatable IR element leakage currents:

A second, longer test was performed under the same conditions using two new, unpackaged SFSE 400W and SFSE 200W IR heating elements. This test was repeated 220 times to examine the long term trend from the hipot test, to ascertain whether the leakage current from SFSE 400W would plateau and to verify the trends established in the previous test.

IR Elements Tested:			
No.	Type	Wattage	Serial No.
1	SFSE	400W	4139
2	SFSE	200W	9297

Leakage current comparison: 400W SFSE unwrapped heater and 200W SFSE unwrapped heater (2)
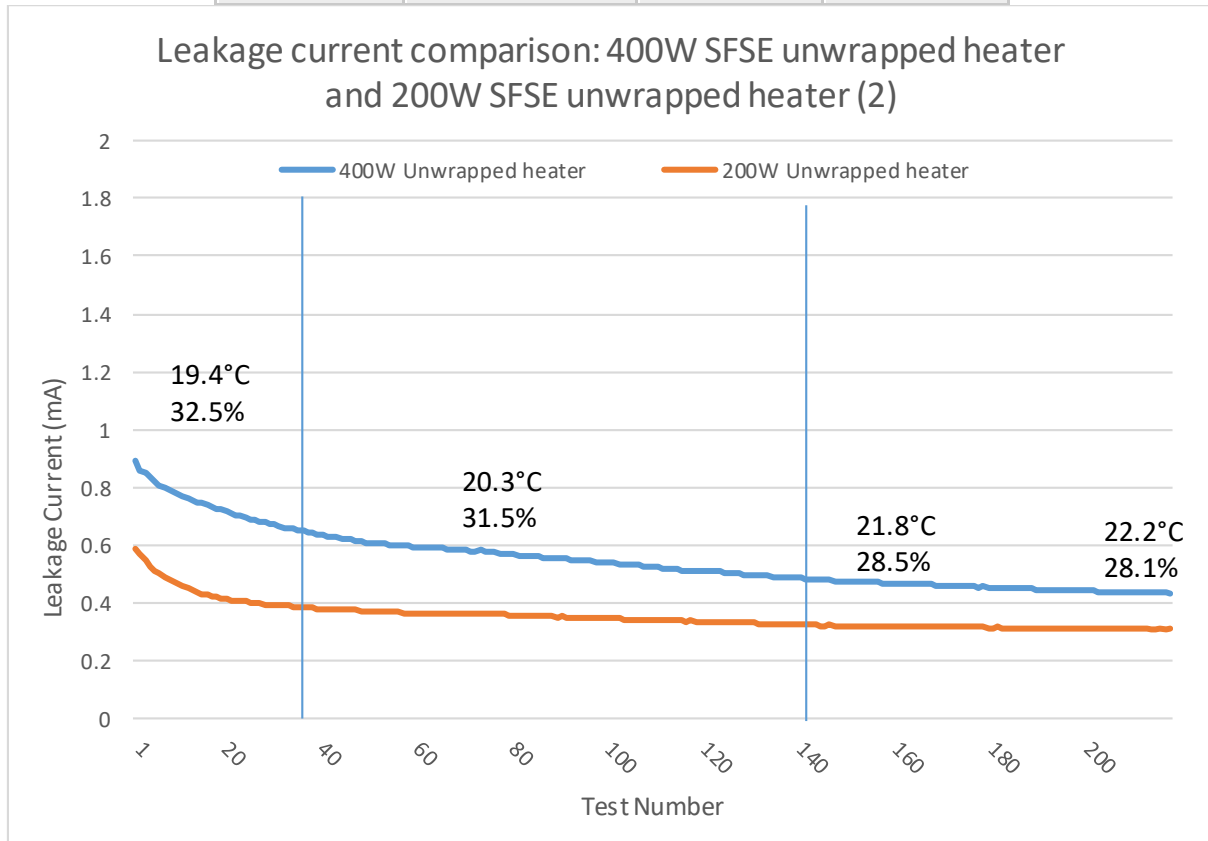
Figure 4.1-11 Comparison testing SFSE 400W and SFSE 200W

- As before, both elements showed a high initial leakage current value that gradually decayed over time. There is an initial high decrease in leakage current, which became more gradual over the duration of the test.

- Both 200W and 400W IR elements never reach a steady state value.

- The leakage current values were 50-80% less than the previous test. This which may be attributed to the relative humidity results which were 10-15% less than the previous test.

- The change in temperature is +1.8°C and remained consistent with the previous test, while the change in humidity is more pronounced at -4.4%C.

Considering the results of test 1 and test 2 in isolation, the leakage current measurements appeared to be consistent and free from signal noise and erroneous readings. However, taken together, there is little correlation between the tests results from identical IR elements. It was theorised that given the leakage current decay trend

and the variation in relative humidity, this discrepancy may be a result of environmental conditions.

Test 3: Investigations of acclimatised IR element leakage currents:

To discount the possibility that packaging is preserving factory conditions, which may cause the IR elements to rapidly change in moisture content when exposed to the lab environment, two new SFSE 400W and SFSE 200W IR element were unpackaged and placed in the testing area for 48 hours to acclimatise. These parts were tested under the same parameters.

IR Elements Tested:			
No.	Type	Wattage	Serial No.
1	SFSE	400W	4178
2	SFSE	200W	9312

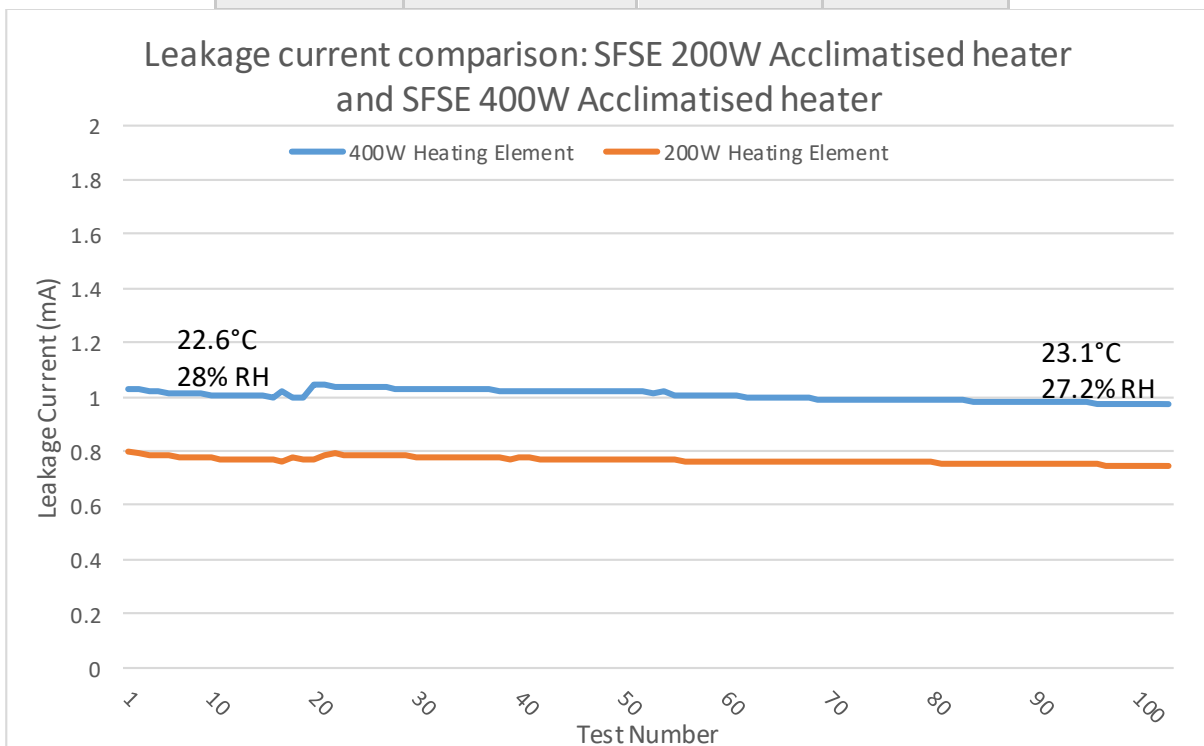*Figure 4.1-12 Comparison Testing SFSE 200W and SFSE 400W*

- The resulting graphs showed much greater consistency, with no decay of note in the leakage current during repeated tests. The leakage current value decreased by <0.02mA for both 400W and 200W IR elements.
- It was noticed that lab temperature and %RH stabilised during this test window.
- The change in temperature is +0.5°C while the change in humidity is -0.8%C

- The difference in the T0:T100 averages is 0.24mA, which remains almost constant through this test, however the average leakage current values for the 400W and 200W element are much higher than previous tests.
- The leakage current for the SFSE 400W remains higher than the SFSE 200W, consistent with test 1 and test 2.

Results:

It can be seen that the SFSE 400W IR element consistently has a higher leakage current than the SFSE 200W. This aligns with expectations that the larger gauge resistance wire within the 400W element presents great opportunity for earth leakage. The non-acclimatised IR elements in test 1 and test 2 track similar exponential decay curves. However, the results of each test batch differ significantly in leakage current value and slope of decay, suggesting that factors outside of the immediate test conditions and test station parameters were changing. The impact of environmental conditions were observed in the results from test 3, where it was possible to remove the decay curve by acclimatising the IR elements.

Despite similarities in trends, the leakage current values showed little consistency between tests. The initial and final test result for each IR element can be seen in fig. 4.1-13. Here it can be seen that there is significant overlap between leakage current results and no consistent pattern between when test data is viewed as a whole.

In spite of differences in leakage current values when test results were compared, there was similarities in the leakage current decay behaviour exhibited by the IR elements. Test results were consistent, free from noise and leakage current outliers. This behaviour, in addition to other controlled test variables indicated that the performance of the test station is reliable, and other influences were involved in the repeatability of the measurements.
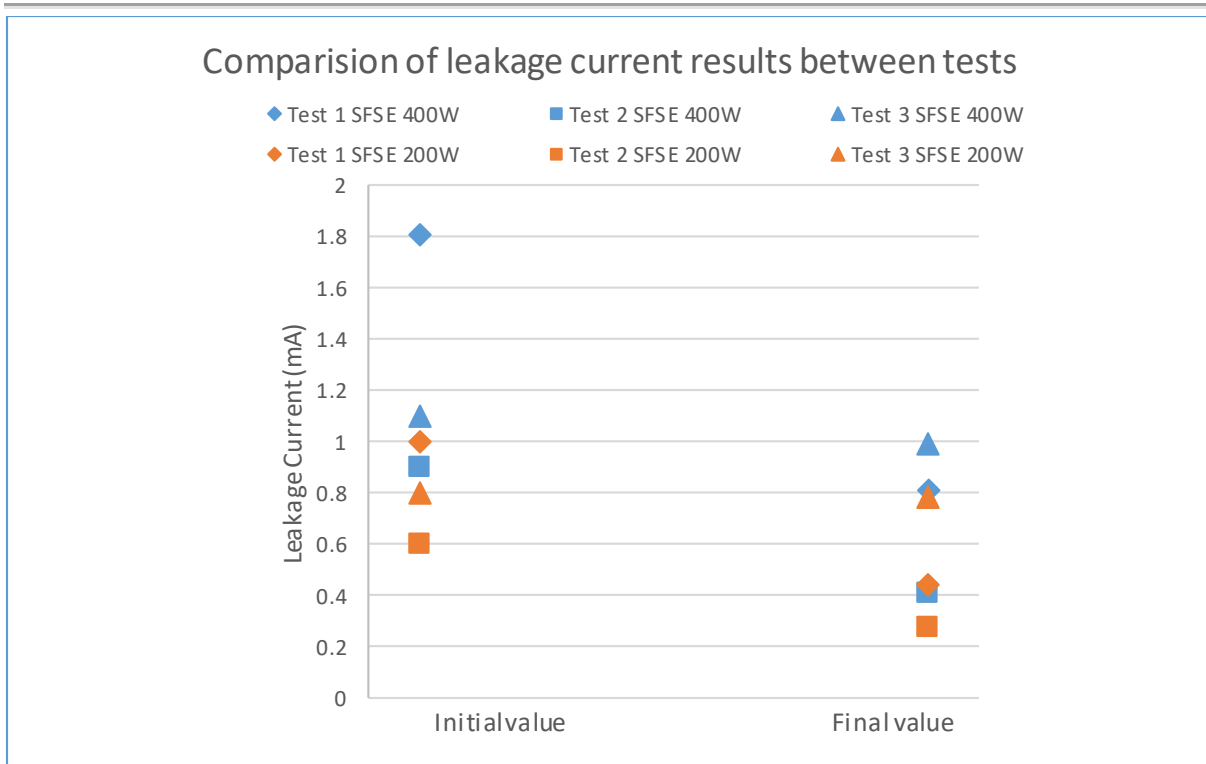
Figure 4.1-13 Leakage current start and end values for Test 1-3

It was hypothesised that the decrease in leakage current values during test 1 and test 2 were partly attributed to the changes in %RH and moisture content as all other factors (element type, size, handling, test parameters) were controlled. The IR elements, which are manufactured from hygroscopic materials, were vacuum sealed in plastic film, which may have preserved the environmental conditions of the factory. Test 3 had consistent leakage current values, which were attributed to acclimatisation of the IR elements to lab conditions. Although these were consistent, they did not match any trends from previous tests, beginning at a higher leakage current value than test 2 and ending at a higher leakage current than both test 1 and test 2.

The variations observed in these investigations presented the hypothesis that moisture absorption could be a factor in the reliable measurement of leakage current.

Test 4: Investigations of moisture free IR element leakage currents:

Investigations were carried out in order to examine whether the presence of moisture was a major factor in the variations of leakage current. Three 1000W Large Full Trough Elements (LFTE) were chosen for testing as they are the largest and heaviest IR heating elements available. Therefore, the LFTE has the greatest capacity to absorb moisture.
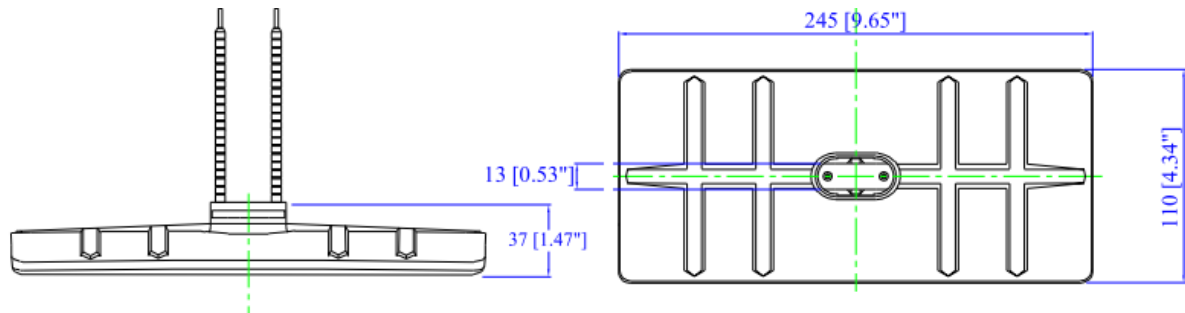
LFTE Technical Details	1000W	1500W
Mean surface temperature(°C)	511	596
Max power density (kW/m^2)	36	54
Max permissible operating temperature(°C)	750	
Average weight	356 g	
Dimensions	245 x 110 x 38.5 mm	
Useful wavelength range	2 to 10 µm	

Figure 4.1-14 Large flat trough element (LFTE) dimensions and technical data

The IR elements were weighed prior to testing, then 40 leakage current measurements were performed on each element. The LFTE elements were heated for three minutes to 400°C to evaporate any moisture or contaminants present within the ceramic, then cooled to 30°C and retested. These results shown in fig. 4.1-15 highlight the impact of absorbed moisture on leakage current.
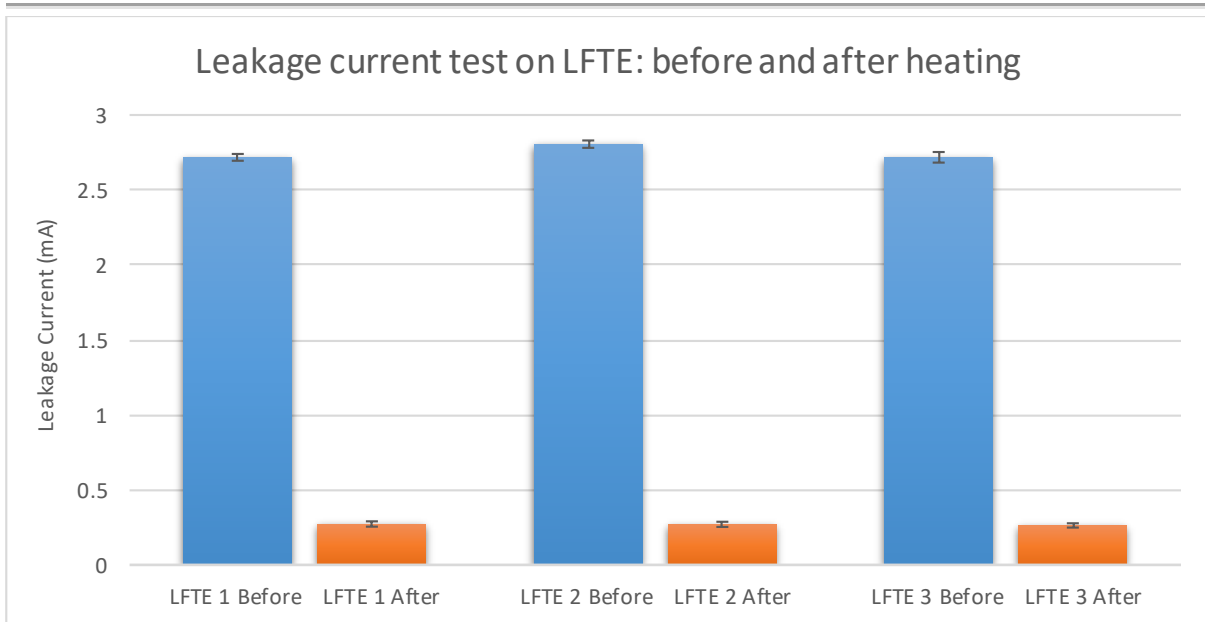
Figure 4.1-15 Changes in LFTE leakage current pre and post heat-up

No.	Type	Wattage	Serial No.	Average mA (before)	Average mA (after)
Average leakage current for LFTE 750W IR elements					
1	LFTE	750W	7504	2.72	0.27
2	LFTE	750W	7507	2.81	0.27
3	LFTE	750W	7509	2.72	0.26

- These results are average of 40 leakage current tests.
- Before heating the elements measure between 2.89 – 2.68mA with a standard deviation (SD) of 0.063mA.
- After heating the elements measure between 0.31 – 0.24mA with an SD of 0.02.
- There is a nine-fold decrease in leakage current value and three-fold decrease in SD after heating.

A final investigation was undertaken to examine if the moisture content hypothesis could be verified by quantifying the change in weight due to moisture absorption. The results are shown in the table below.

SN:	Before heating (g)	After heating	Δw %	After 24 hours	Δw %
Weight comparison of LFTE before and after heating					
7504	361.1	358.3	-0.78	360.2	+0.53
7507	361.3	359.2	-0.58	360.5	+0.36
7509	367.5	365.6	-0.52	366.7	+0.30

Figure 4.1-16 Table showing changing LTFE weight (grams)

This test was repeated for a series of five FTEL IR elements to verify these results.

Heat up test full trough elements (FTEL)					
SN:	Before heating (g)	After heating	Δw %	After 24 hours	Δw %
9979	235.6	234.3	-0.55	234.8	+0.21
9981	235.7	234.3	-0.59	235.0	+0.30
9983	235.8	234.2	-0.67	234.8	+0.21
9995	236.3	235.1	-0.51	235.6	+0.21
9999	238.2	236.5	-0.71	237.1	+0.25

Figure 4.1-17 Table showing changing FTEL weight (grams)

These results support the hypothesis that there was moisture ingress into the IR heating element, which has been shown to be a source of variation in earth leakage values[60]. Given the variable nature of the environment and part handling, it can be concluded that changes in earth leakage values due to moisture can be expected from such a test setup.

Environmental investigation conclusions:

From the results of the previous test it is clear there is a relationship between leakage current results and moisture. Ceramic elements have the capacity to absorb and release moisture depending on the environment, which is evidenced by variations in weight over time and immediately after heating.

This moisture has a significant impact on the leakage current as the only constant leakage current results were recorded in acclimatised elements when lab environmental conditions were maintained at a constant level. Heating for moisture evaporation may be the best method to accurately determine the leakage current value of a ceramic heating element. However, the time required for heating and cooling cycles is too long for a high throughput manufacturing environment.

It was also noted that identical tests run in dissimilar environmental conditions yielded different results. It is unclear whether there is a linear relationship between absorbed moisture/%RH and leakage current, but an approximation can be made that lower moisture/%RH results in lower leakage currents.

4.1.3.2 Characterising the effects of rated power on leakage current.

It can be seen from tests 1-3 that variations in leakage current exist between IR elements of different power and shape. As seen in test 4, smaller variations exist even in identical elements. Investigations were carried out in order to explore the relationship between rated power and leakage current. Ceramicx heating elements range from 125W to 1400W. The Full Flat Element (FFE) range has seven available wattages, ranging from 250W to 1000W. The variation in power is achieved through the use of heavier gauge resistance wire. The increase in cross-sectional area decreases the wire's resistance and increases electrical current carrying capacity, while the total wire length remains constant to fit into the ceramic mould.

Test 5: Investigating the relationship between wattage and leakage current:

In this test fourteen full flat elements (FFE) of wattages from 250W to 1000W were tested to determine the relationship between wattage and leakage current. The IR elements were acclimatised for 48 hours in the testing environment. Ten leakage current measurements were conducted on each IR element to minimize the impact of ambient temperature and relative humidity on results.
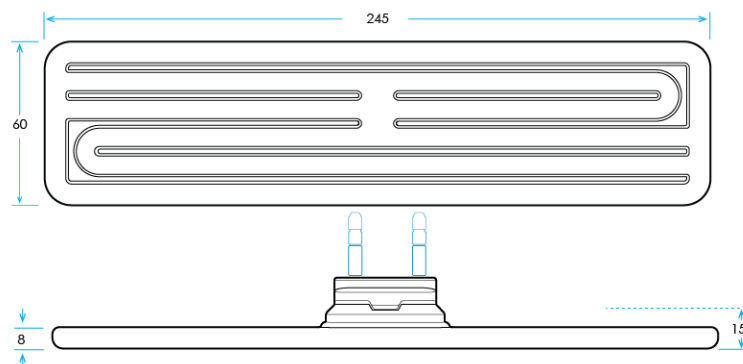
FFE Technical Details	250W	300W	400W	500W	650W	750W	1000W
Mean surface temperature(°C)	351	405	480	515	596	624	726
Max power density (kW/m²)	15	18	24	30	39	45	60
Max permissible operating temperature(°C)	750						
Average weight	182 g						
Dimensions	245 x 60 x 26 mm						
Useful wavelength range	2 to 10 µm						

Figure 4.1-18 Full flat element (FFE) dimensions and technical data

74
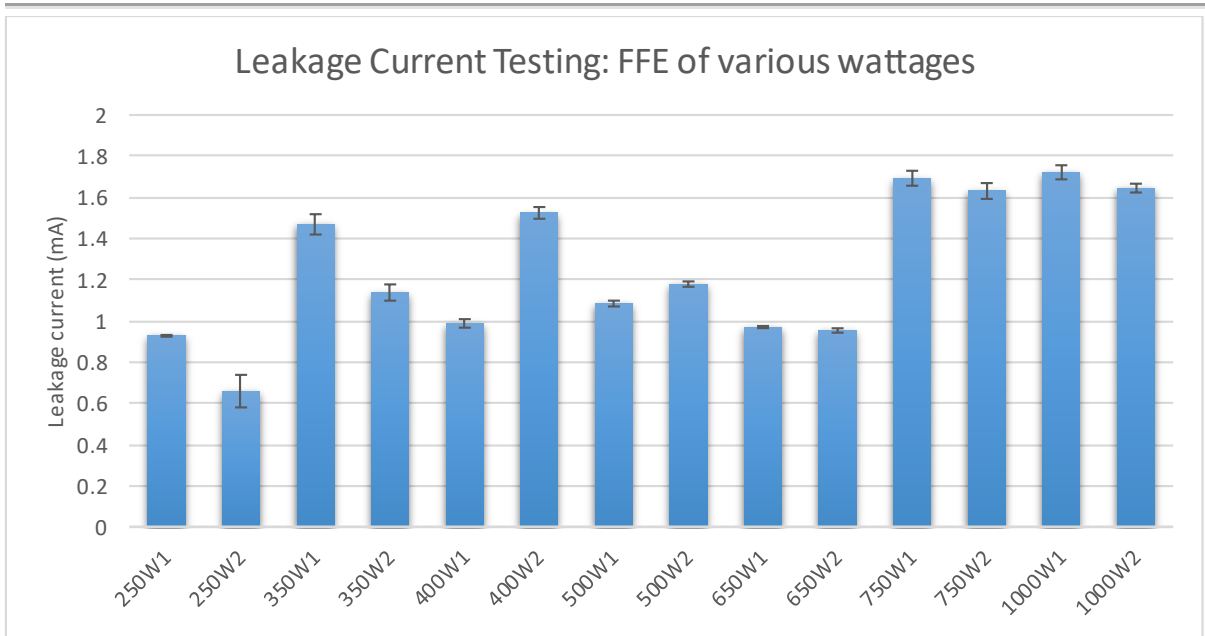
Figure 4.1-19 Comparison test of FFE in various wattages.

IR Elements Tested:							
No.	Type	Wattage	Serial no.	No.	Type	Wattage	Serial no.
1.	FFE	250W	7272	8.	FFE	500W	9749
2.	FFE	250W	7280	9.	FFE	650W	1603
3.	FFE	350W	9076	10.	FFE	650W	1614
4.	FFE	350W	2509	11.	FFE	750W	0776
5.	FFE	400W	0161	12.	FFE	750W	0759
6.	FFE	400W	0816	13.	FFE	1000W	7338
7.	FFE	500W	9750	14	FFE	1000W	7339

- Results shown are an average of 10 measurements.
- There was a slight deviation among these results as shown in the error bars.
- The highest measured leakage current was from a 1000W FFE while the lowest measured leakage current was from a 250W FFE.
- The spread of leakage current results was not consistent in determining a relationship between the level of current flow and leakage current. While the 750W and 1000W FFE had the highest level of leakage current, the 350W and 400W FFE had a higher result than the 500W and 650W FFE.
- There is no evidence of a linear relationship between wattage and leakage current and given the moisture offset seen in previous tests, it may be unwise to infer such a relationship without first removing the presence of moisture.

Test 6: Investigating the relationship between wattage and leakage current in moisture-free IR elements:

To discount the influence of moisture seen in previous tests, each FFE IR element was heated for 3 minutes to over 200°C then allowed to cool to ambient temperature (25-30°C). The elements were then immediately retested under the same conditions.
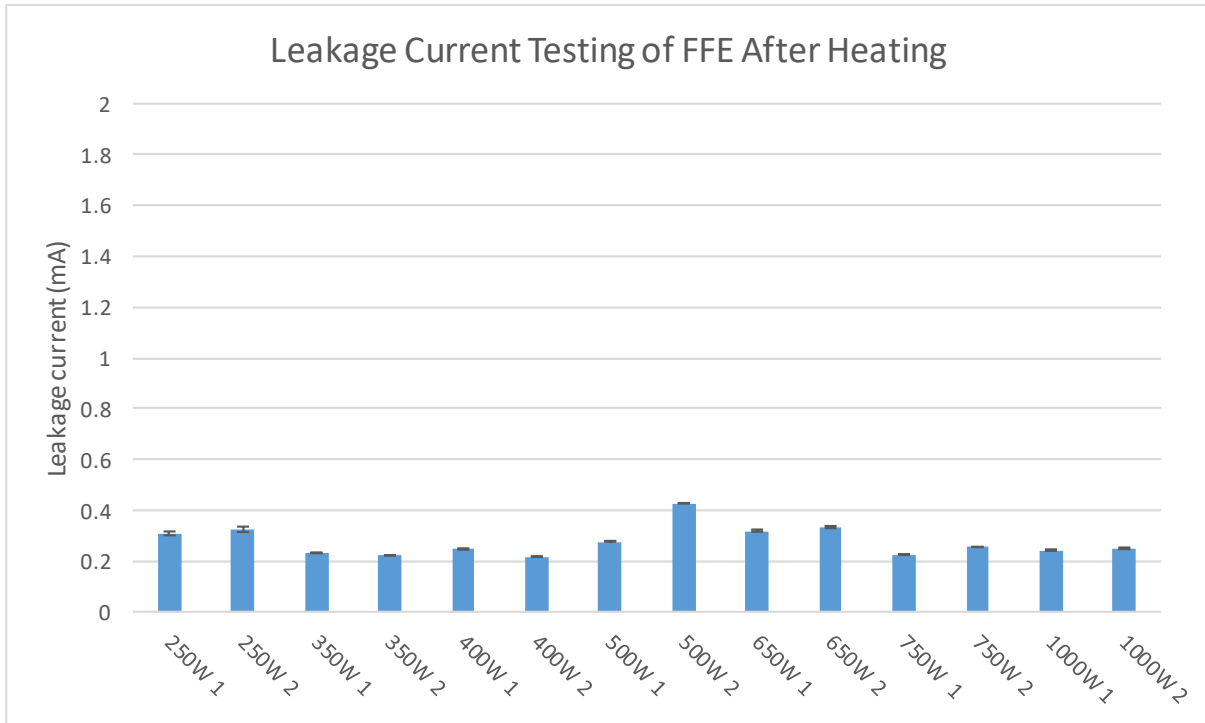

Figure 4.1-20 Comparison test of various wattages after heating

The trend here is consistent with that observed in test 4. All IR elements show a significant drop in leakage current and have a much tighter distribution. A clearer view of these results with a reduced scale can be seen in fig. 4.1-21.
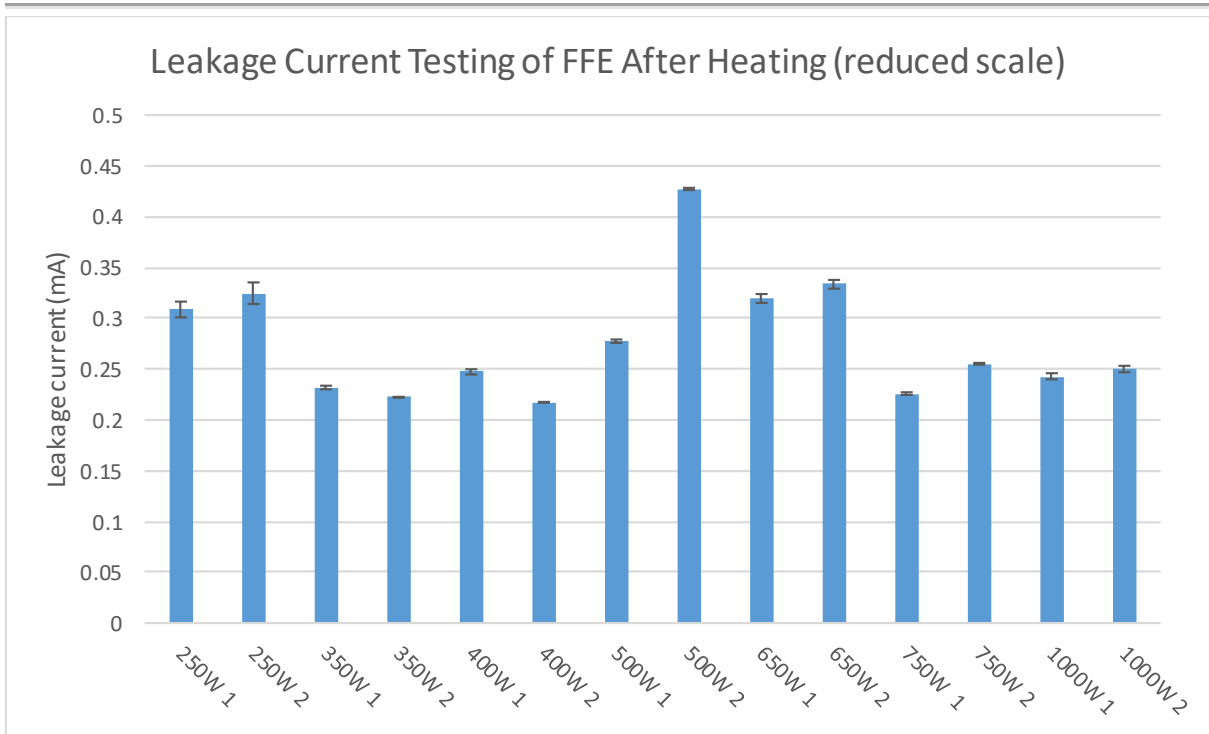
Figure 4.1-21 Closer examination of comparison test of various wattages after heating with reduced scale

- No overall connection between power and leakage current was apparent.
- The leakage current distribution had changed, with the highest recorded value from the 500W FFE and lowest from the 400W FFE.
- All other elements were distributed between 0.2 and 0.35mA of leakage current, with a concentration of 1000W, 750W and 250W between 0.22 and 0.26mA.

Power Test Conclusions:

Contrary to a view that larger electrical current draw as well as a greater quantity of heating coil should induce a larger leakage current or allow for greater earth leakage paths, there was no evidence in the results to suggest that the rated power had a bearing on the leakage current value. This result holds true when environmental effects are removed and adjusted for. The pre-heatup graph showed a large distribution across the 0.5-2mA range, consistent with all previous tests, while the post-heatup test showed a dramatic decrease in leakage current, again consistent with observed behaviour. As the IR elements cooled to ambient temperature, leakage current gradually rose back to pre-heated levels over a number of hours as the IR element absorbed and adsorbed moisture from the air.

4.1.3.3 Characterising the impact of surface area on leakage current.

Ceramicx IR heating elements are made in a range of profiles and sizes. These sizes range from the smallest at 60 x 60 x 8mm (QFE) to the largest at 250 x 125 x 25mm (LFTE). As the IR elements increase in size, more surface area is presented to the conductive foam pads of the hipot tester.

Test 7: Investigating the relationship between surface area and leakage current:

To measure the impact of surface area on leakage current, eight 250W IR elements in four sizes were selected. These flat profile IR elements were chosen to maximise coverage from the foam pads. Dimensions and technical specifications for the SFSE and FFE IR elements can be seen in fig. 4.1-9 and 4.1-18 above, and HFE and QFE IR elements in fig. 4.1-23 and 4.1-24 below.

No.	Type	Wattage	Serial no.	Dimensions: LxWxD	Surface Area
		IR elements tested:			
1.	Quarter Flat Element	250W	9415	60 x 60 x 8mm	0.0091m^2
2.	Half Flat Element	250W	3218	122 x 60 x 8mm	0.0175m^2
3.	Full Flat Element	250W	4682	245 x 60 x 8mm	0.0342m^2
4.	Square Flat Solid Element	250W	3975	122 x 122 x 8mm	0.0336 m^2

Figure 4.1-22 IR element types, dimensions and total surface area
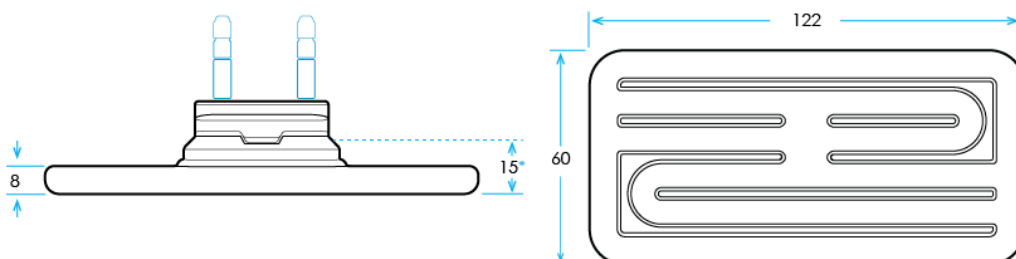
HFE Technical Details	125W	150W	250W	325W	400W	500W
Mean surface temperature(°C)	351	405	515	596	640	726
Max power density (kW/m^2)	15	18	30	39	48	60
Max permissible operating temperature(°C)	750					
Average weight	105 g					
Dimensions	122 x 60 x 26 mm					
Useful wavelength range	2 to 10 µm					

Figure 4.1-23 Half flat element (HFE) dimensions and technical data
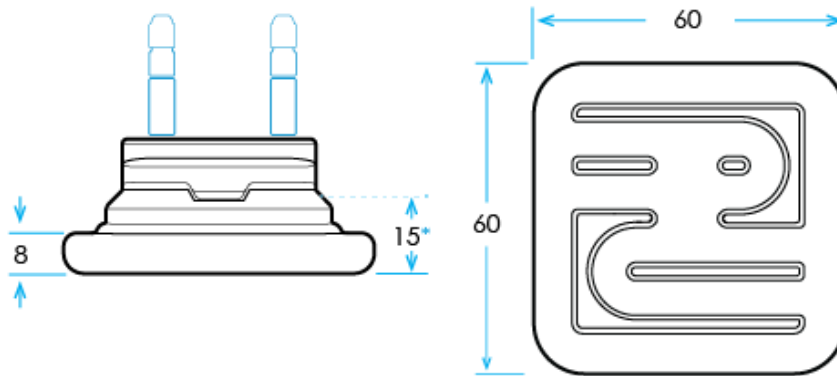
QFE Technical Details	125W	250W
Mean surface temperature(°C)	515	726
Max power density (kW/m^2)	30	60
Max permissible operating temperature(°C)	750	
Average weight	65 g	
Dimensions	60 x 60 x 26 mm	
Useful wavelength range	2 to 10 µm	

Figure 4.1-24 Quarter flat element (QFE) dimensions and technical data

The leakage current for each of these eight IR elements was measured 10 times and averaged to remove inconsistencies from environmental factors.
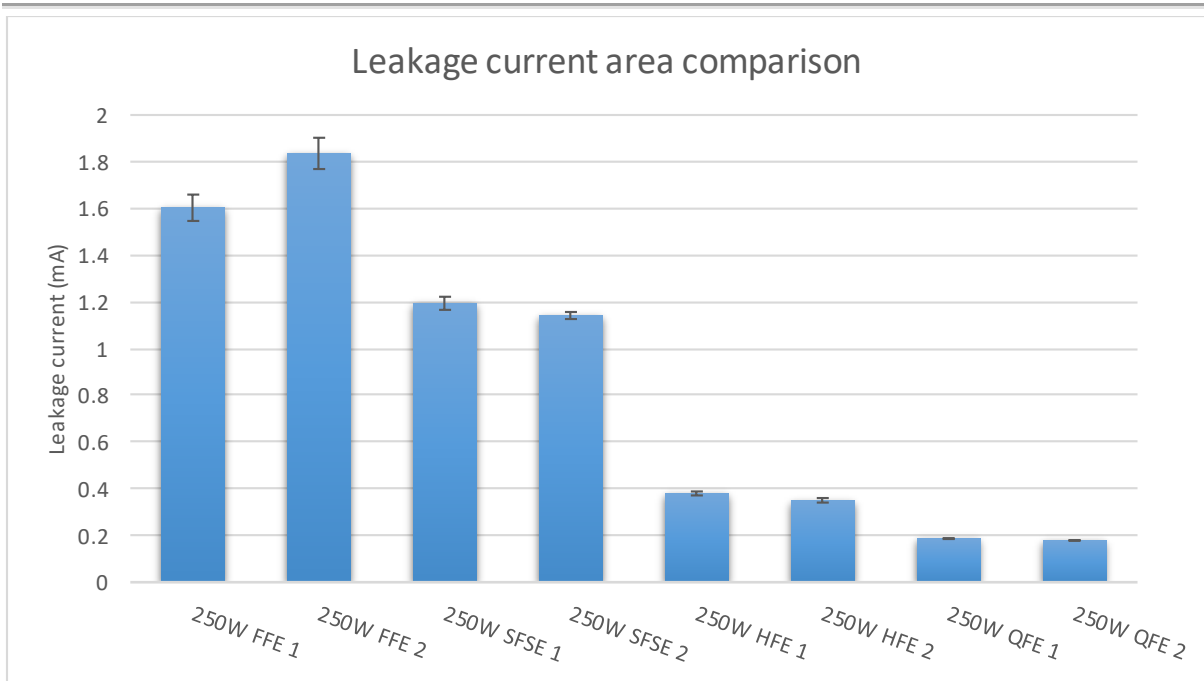
Figure 4.1-25 Comparison test of 250W IR elements with varying surface area

- Each result is an average of 10 measurements.

- Each element had an identical power rating of 250W.

- The maximum leakage current was 1.81mA (FFE 2) while the minimum leakage current was 0.19mA (QFE 2).

- The results indicated that there is a non-linear relationship between surface area and leakage current. This may result from the greater moisture absorption capacity in large surface area IR elements or that leakage current increased as more surface area was available to the testing pads.

- Although the FFE and SFSE elements have similar surface areas, the FFE has >0.4mA higher leakage current and larger distribution of results.

Test 8: Investigating the relationship between surface area and leakage current in moisture-free IR elements:

As before, each IR element was heated for 3 minutes to remove moisture and other contaminants. These IR elements were then retested as shown in fig. 4.1-26:
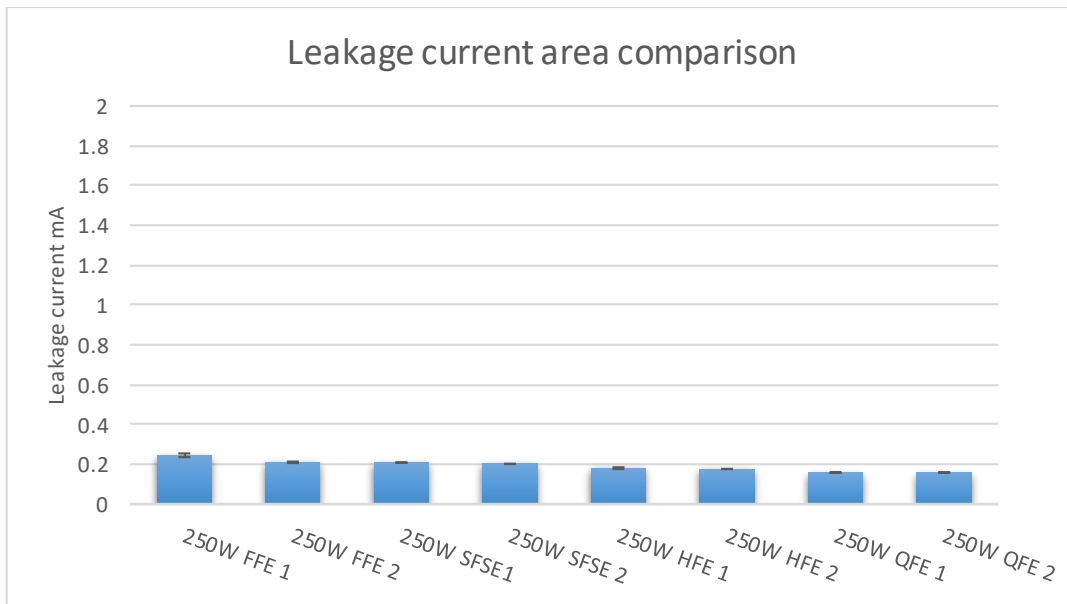
Figure 4.1-26 Comparison test of 250W IR elements with varying surface area after heating

- The leakage current for each element has been greatly reduced due to the elimination of moisture.

- There was less deviation in the leakage current measurements between different IR element sizes. However, the trend established in the previous test remains. A closer view of this trend can be seen in fig. 4.1-27.

- The leakage current value for the QFE IR elements have remained static. This may indicate a size limitation in the hipot test station or that the quantity of moisture in the IR element was insufficient to skew the measurements.
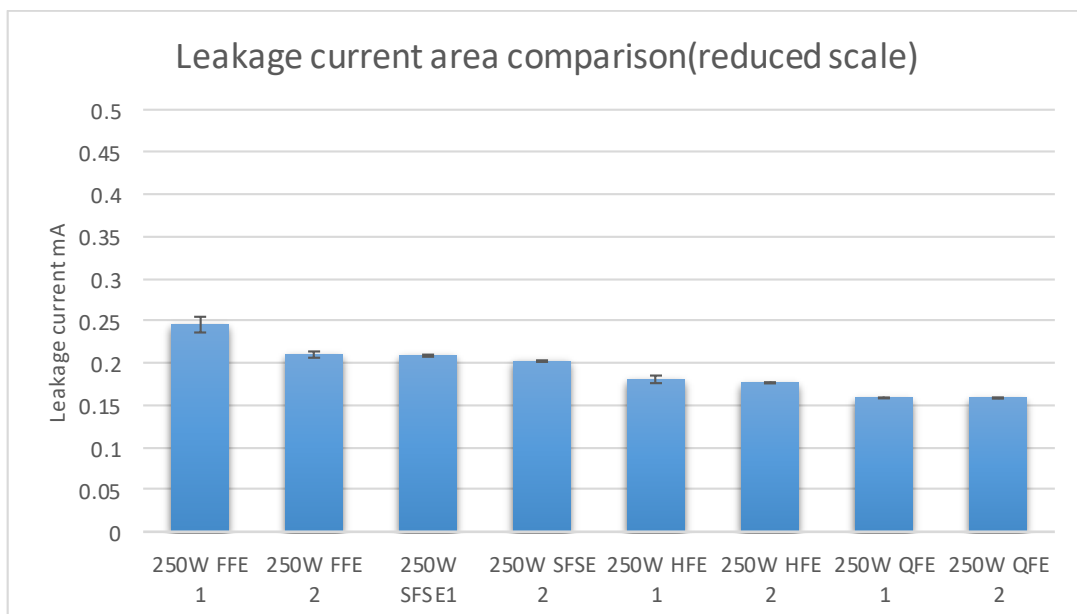
Figure 4.1-27 Comparison test of 250W IR elements with varying surface area after heating with reduced scale

Area test conclusions

81

These investigations indicated that leakage current increases with surface area. However, this increase was non-linear, as seen by the small difference in leakage current between the QFE and the HFE which has twice the surface area, while the SFSE and FFE have a larger distribution, despite having similar surface areas. The larger surface area in contact with the pads indicated that more current was permitted to leak to the earthed foam pads, however this must be countered with the physical construction of the heating element and the ease of which the foam pad can deform to the element profile.

Lack of a controlled environment caused variations in leakage current as seen in the previous test section. This test indicated that IR elements with greater surface area have greater leakage current measurements, but larger scale testing is needed in a controlled environment to attain a conclusive result.

Test 9: Characterising neck leakage current

The neck section is the location where the resistance wire enters the rear of the ceramic IR element and is the most common area for a wire breakout. This section is contoured to mate with a fixture retaining clip when the IR element is installed. Failure in the neck section may expose the customer to injury and is a critical test point. This was tested separately to measure the integrity and consistency of the clip mechanism which holds the IR element to the test pallet.
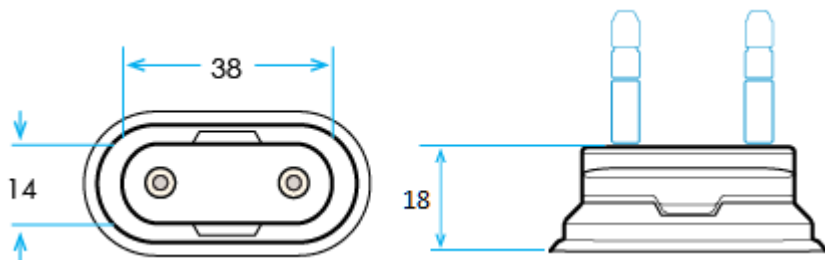
Figure 4.1-28 IR element neck dimensions
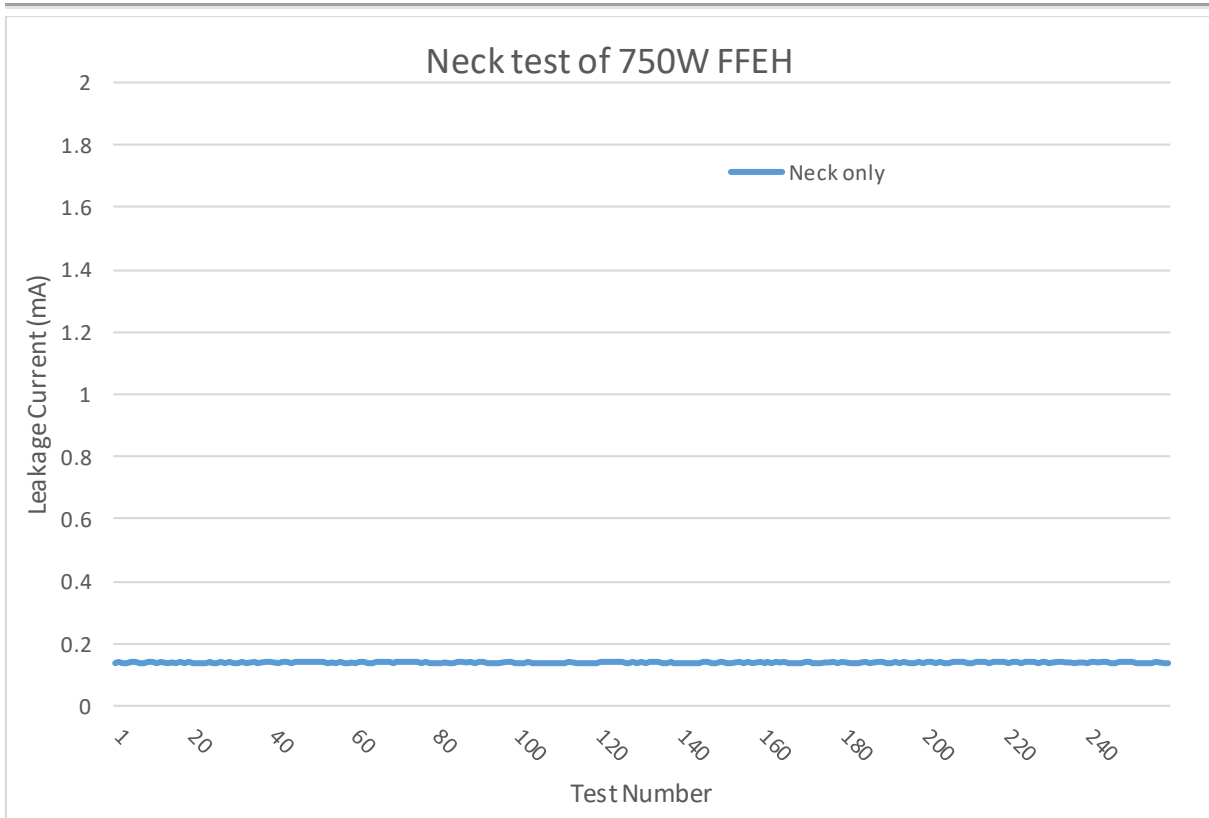
Figure 4.1-29 Testing Neck Section of 750W FFEH

- The neck section was tested over 250 times and gave consistent results.
- As seen in fig. 4.1-29, the leakage current value measured an average 0.14mA and varied by only 0.002mA across all tests, regardless of environmental factors.
- As the neck comprised a small fraction of total area tested by the hipot station, the leakage current measurements are minute compared to other, more comprehensive tests.

Test 10: Testing hipot response to common fault conditions:

The dielectric voltage withstand test is used to determine whether the degree of insulation used in a product is adequate to protect the user from injury. Given that the hipot test measures current flow to earth, it should be able to indicate whether a wire coil is exposed on the surface of the IR element either through damage or improper assembly. Due to hand assembly of the IR elements, several common failure points have emerged. These points mainly relate to issues with heating coil placement, where the coil lifts from the pre-fired ceramic mix and becomes exposed. This failure is a potential shock hazard. Most of these failures are identified in manual inspection

throughout the manufacturing process, but the coil may lie just below the surface of the IR element or be obscured by the glaze coating.

Artificial failure:

To replicate a damaged IR element, a section of glaze on an 800W FFEH element was removed. The IR element was placed into the hipot test station to measure what degree of damage could be detected. For this test, the hipot threshold limit was set to 5mA. This method was repeated three times, with increasing amounts of glaze removed.

Figure 4.1-30 Scraping successive portions of glaze from 800W FFEH IR element

The IR element was tested at each stage to induce a hipot failure. It was observed that leakage current increased only slightly with each subsequent test until the resistance coil was exposed, as seen in fig. 4.1-30(c). This caused the Kikusui TOS5200 to exceed the 5mA threshold limit and trigger a failure. A second test was carried out to

measure whether a small coil exposure would trigger a hipot failure. A small coil section located at the bottom of the trough on a 500W FTE IR element was exposed and tested.

Figure 4.1-31 Chipped 500W FTE IR element

This artificial defect did not exceed the threshold on the hipot test. It was determined that the concave shape of the FTE prevented the foam pads from deforming into the recess chipped into the face of the IR element and making contact with the exposed wire coil.

Legitimate IR element failures:

During testing, an FTEL IR element was repeatedly failed in the hipot test station. The cause of failure was determined to be a wire coil that had moved close to the surface of the ceramic. This failure can be seen below in fig. 4.1-32:

(a)   *(b)*

Figure 4.1-32 Failed FTEL IR element

85

In this example, the resistance wire has moved close to the surface of the element. The hipot test was repeated several times to burn the affected area, pinpointing the failure area, seen in fig.4.1-32(a). This showed a hairline crack at the intersection of the IR element neck and body. The glaze at the affected area was scraped back slightly to expose the heating coil, located just under the surface as shown in fig. 4.1-32(b).

Artificial failure conclusions:

While the hipot test is not designed to detect localised flaws in the ceramic IR elements, in certain circumstances it is possible to identify these defects. The required criteria to detect these defects relate to the ability of the conductive foam pads to deform to the contours on the face and rear of the IR element. Given a close proximity, the high voltage present on the resistance coil will spark to the foam pad, resulting in current flow which exceeds the hipot threshold value. This spark is a destructive force, which will damage the ceramic, as seen in the burn in fig. 4.1-32(a), and may potentially damage the foam pad. Both foam and fabric are fire retardant, but may need to be replaced in the event of repeated damage.

4.1.4 Leakage current investigation conclusions

The Al_2O_3 used in Ceramicx IR elements is of a relatively low grade, with a porosity of 3-6% and a density of 3.3-3.6g/mm^2[85]. Both SiO_2 and Al_2O_3 is classed as hygroscopic[92][93]. These properties, in tandem with porosity created by the manufacturing process, encourages the absorption of environmental moisture which leads to changes in the material structure and resistivity. This added moisture has been quantified in two weight measurement tests, where it was observed that the weight of IR elements fluctuated when heated and cooled, indicating a physical loss of mass. The effects of environmental factors have been observed in each of the leakage current tests, from exponential decay curves in fresh IR elements seen in test 1 and test 2, while acclimatised IR elements in test 3 showed linear results due to an adjustment to ambient conditions. While the adjusted results exhibited a linear, repeatable test result, a dramatic decrease in leakage current was introduced by removing all moisture from the IR element as seen in test 4 and test 6. These results show that environmental factors must be accounted for when performing leakage current tests.

Other factors, such as power and surface area were also tested. The results of Test 5 showed that there is no evidence to correlate rated power with leakage current, even

after discounting the aforementioned environmental influence. There is a correlation between leakage current and area, as shown in Test 7. However, the relationship is not strictly linear and showed variances with part types.

Finally, in addition to measuring leakage current, the hipot tester was capable to detect several flaws in the IR elements, such as a partially exposed heating coil and structural weaknesses in the element. However, as the hipot test station is not purposely designed for this task it should not be used as a substitute for other, more reliable methods such as visual inspection.

4.2   Characterising thermal analysis in test station 2

Introduction:

Thermal cameras are powerful and non-invasive tools for monitoring and diagnosing the condition of electrical and mechanical products and components[94]. Temperature is a critical parameter in various industrial processes. In-line, non-contact temperature measurement to identify abnormal temperature patterns can assist in early diagnosis of product faults and manufacturing flaws. Thermographic findings can be compared to thermocouple and power monitoring tools for versatile condition monitoring to ensure reliability and accuracy. The main benefit of infrared thermography is that it enables simultaneous monitoring of a large area through non-contact and non-invasive techniques while interpretations of the acquired false-colour thermal images are more informative than non-imaging techniques. Thermal cameras also provide video recording of dynamical variations of temperature in real time. Due to these advantages, thermal imaging has been established as an effective condition monitoring tool in both manufacturing and test industries[95].

4.2.1   Test methodology

Test station 2 measurement validation explored the IR element's thermal accuracy, repeatability, and characteristics due to thermal changes in the heating coil. The IR heating elements which form the use-case for this test execution system provide an interesting test case for the characterisation of the thermal camera performance. As seen in the previous section, the IR elements are available in a range of power, area and shape options, each with a unique heating profile. This variation forms the basis of the test methodology used in this study as illustrated in fig. 4.2-1 below:

Figure 4.2-1 Test methodology for thermal camera station validation

4.2.1.1 Test Setup

A Labview test routine was created to analyse the heat-up of the IR element. Mains voltage at 230V was applied to the IR element through the electrical contacter. The Optris PI400 thermal camera shown in fig. 4.2-2, was used to capture a series of images which showed the IR element in various stages of heat up. This camera was chosen due to the following specifications:

- The detectable temperature ranges from -20°C to 900°C, which was within the expected temperature output of all IR elements

- The spectral range of 7.5-13 μm closely match the IR element's emission wavelength.

- A 62° x 49° wide angle lens provides the necessary spatial resolution to view all IR elements while maintaining a reasonably short focal distance of 250mm.

- The thermal resolution of the Optris PI400 is 0.04K, and accuracy is ±2% which is an acceptable margin of error, given the temperature range expected from the IR elements.

- The Optris PI400 is capable of recording video, which may be required for future in-depth product analysis[95].
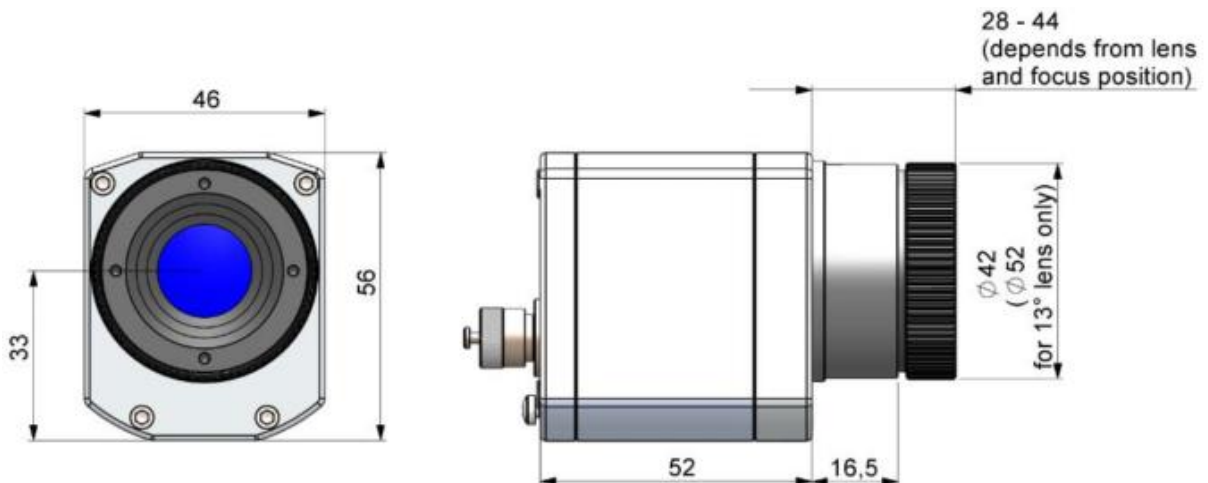
	PI 400	PI 450	PI 450 G7
Temperature ranges	-20...100 °C; 0...250 °C; 150...900 °C; Option: 200...1500 °C	-20...100 °C; 0...250 °C; 150...900 °C	200...1500 °C
Spectral range	7.5 - 13 µm		7.9 µm
Detector	UFPA, 382 x 288 pixel @ 80 Hz (switchable to 27 Hz)	UFPA, 382 x 288 pixel @ 80 Hz (switchable to 27 Hz)	UFPA, 382 x 288 pixel @ 80 Hz (switchable to 27 Hz)
Lenses (FOV)	13° x 10°, 29° x 22°, 38° x 29°; 53° x 40°; 62° x 49°; 80° x 56°	13° x 10°, 29° x 22°, 38° x 29°; 53° x 40°; 62° x 49°; 80° x 56°	13° x 10°, 29° x 22°; 53° x 40°; 80° x 56°
System accuracy[2)]	±2°C or ±2 %		

Figure 4.2-2 Optris PI400 thermal camera dimensions and technical specifications

These images were input to a Labview VI for analysis. This VI leveraged the Optris Connect software package through a plugin and was capable of exporting the following information:

1. Thermal Images (.tiff, .jpeg, .png)
2. Thermal video at 27 or 50Hz, depending on required resolution (.avi)
3. Text files with complete temperature information including max, min, mean and standard deviation for analysis in excel.
4. Heat up graph available as image or .csv file.
5. RAW data file, which provides a spreadsheet of individual pixel intensity.

4.2.1.2 Test Procedure

The flowchart for this test procedure can be seen in Fig. 4.2-3, where it is shown that the IR element mounted on the pallet fixture was lifted by test station 2 into the thermal camera's field of view (FOV). The electrical contacter extended and applied 230V to the IR element. The thermal camera recorded information relating to the IR elements heating profile, then measured the resistance of the hot wire coil. The electrical contacter retracted and the pallet was returned to the conveyor. Fig. 4.2-4 shows the IR element as it is brought into the thermal camera's FOV.
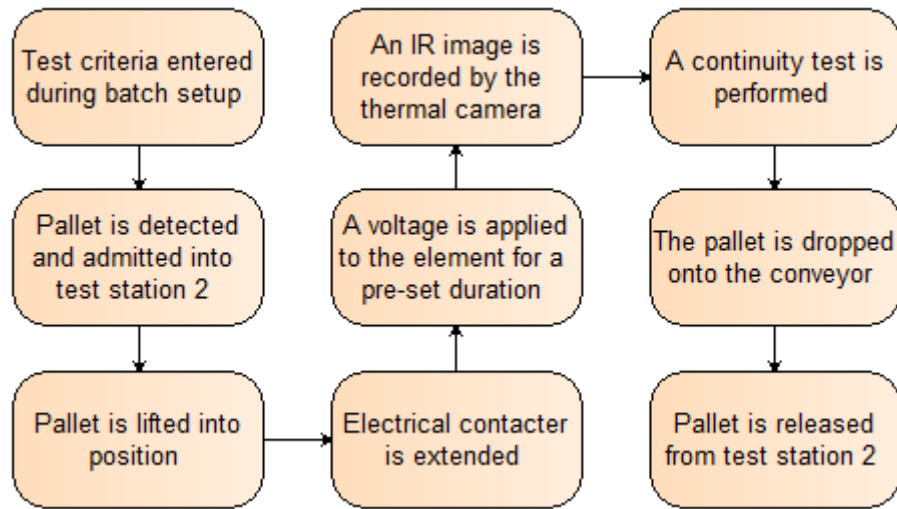
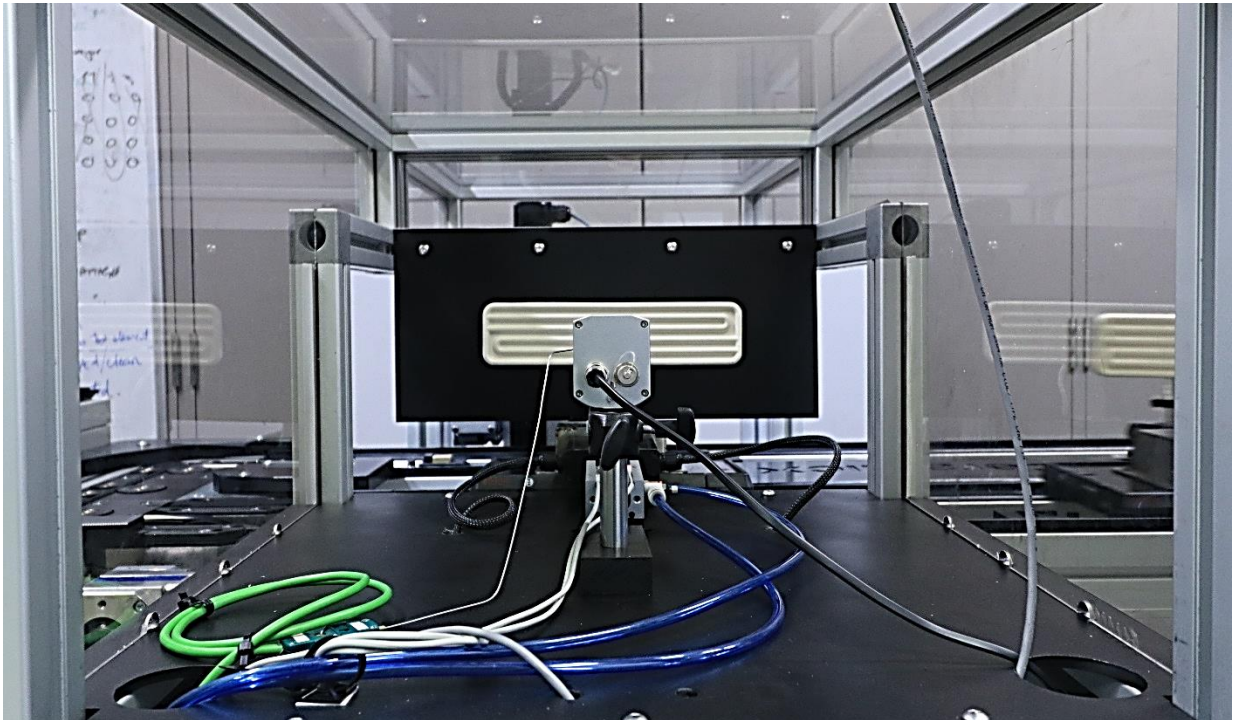*Figure 4.2-3 Station 2 Test Procedure.*

Figure 4.2-4 Rear view of test station 2 with FFE in test area. Black background provides false colour contrast and prevents erroneous heat signatures in IR image results.

4.2.2   Baseline investigations

Test 1: IR element emissivity measurements:

Before an accurate measurement baseline was established, the emissivity of the white ceramic IR element was determined. Emissivity is a representation of the actual value of radiated infrared compared to that of an ideal object. The emissivity of similar materials is shown in fig. 4.2-5 below:

Materials	Temperature (K)	Wavelength (lm)	Emissivity
Clay (fired)	298	8–14	0.91
Concrete (dry)	309	5	0.95
Masonry brick	273	5	0.94
Limestone	311	–	0.95

Figure 4.2-5 Emissivity values for common clay based materials

To determine the emissivity of the 150W FFE IR element, a portion was sprayed with a matt black high temperature paint in accordance to the specification described by Optris GmbH[61] to create a black body section.

Figure 4.2-6 150W FFE with portion painted black

Power was applied to the IR element for 10 minutes to reach max temperature of 262°C. The Optris thermal camera was placed 250mm from the IR element, resulting a field of view of 315mm x 240mm[96].

Two inclusion zones were selected to measure the IR differential between the black (Area 1) and white (Area 2). The mean temperature for the inclusion zones can be seen from fig.4.2-7. A distinct line between black and white sections can also be seen from this thermal image. The temperature difference of 9°C between Area 1 and Area 2 is a result of incorrect emissivity setting of Area 2.
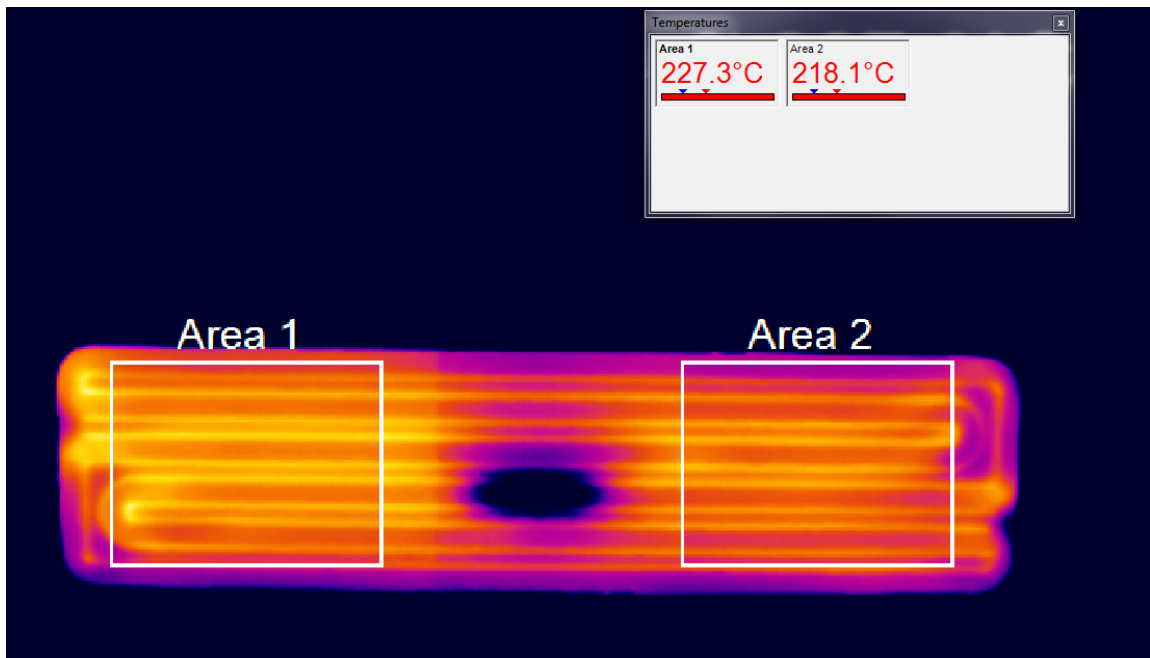
Figure 4.2-7 Thermal image showing mean temperature as emissivity = 1

The emissivity for the black region (Area 1) was assumed to be 0.98 as per the specification. The emissivity for Area 2 was then decreased from 0.98 until the temperature of both regions matched. The calibrated emissivity value was found to be 0.93.
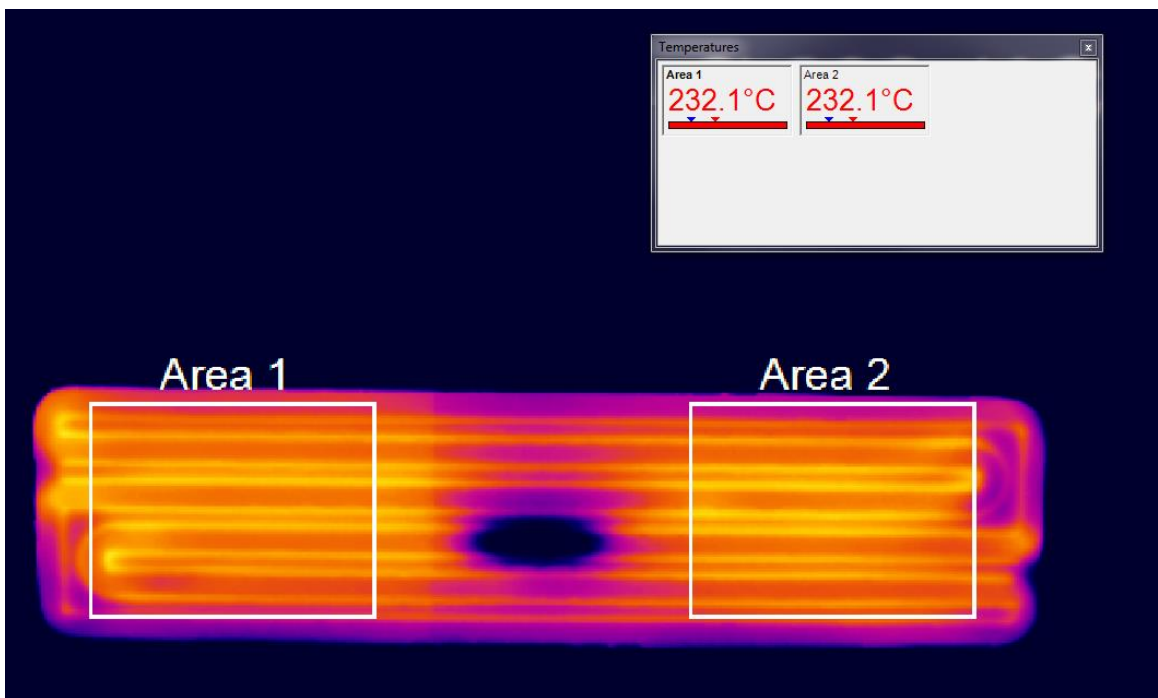
Figure 4.2-8 Thermal image showing mean temperature with calculated emissivity of 0.93

Test 2: Comparison of IR elements with identical shape and wattage:

93

To measure the consistency of the thermal camera's results against recorded measurements taken by Ceramicx, three identical 250W full trough elements (FTE) were heated for 30 minutes to generate a full heat-up curve. This was captured by the thermal camera (150 – 900°C range) and the K-type thermocouples embedded in the elements.
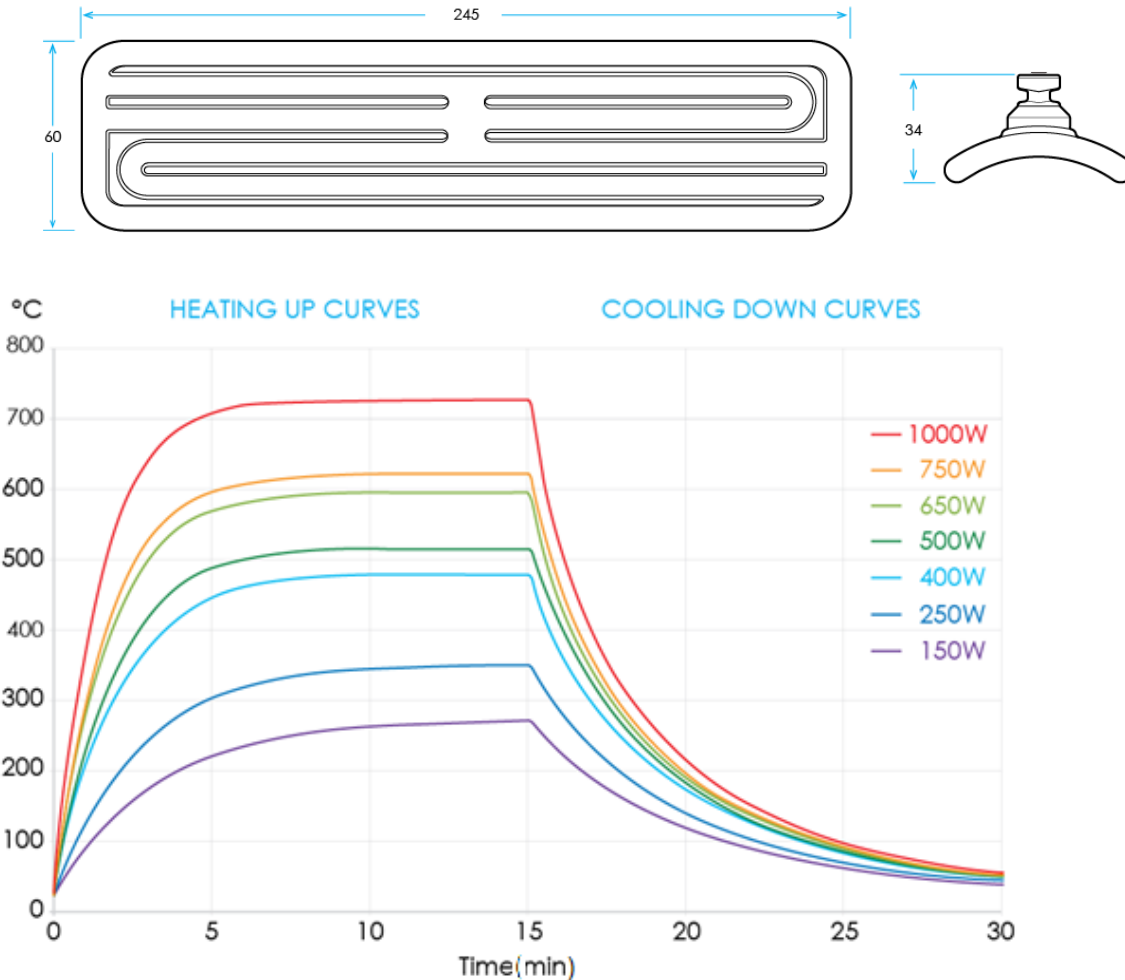
Figure 4.2-9 250W FTE dimensions and heat up curve taken from datasheet

No.	Type	Wattage	Serial No.	Coil length	Coil diameter (mm)	Power Density (kW/m^2)
			IR Elements Tested:			
1	FTE	250W	4759	61" (1549mm)	0.28	15
2	FTE	250W	2198	61" (1549mm)	0.28	15
3	FTE	250W	2207	61" (1549mm)	0.28	15
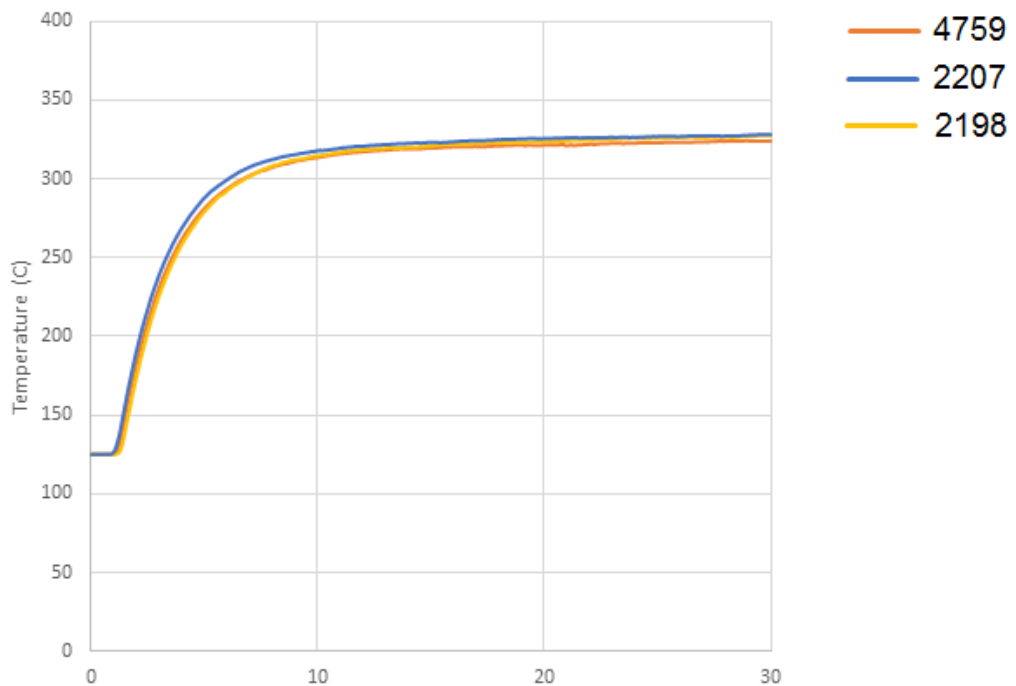
Figure 4.2-10 Thermal camera measurements of three 250W FTE over 30 mins (150-900°C range)

The resulting heat up curve captured by the thermal camera can be seen in fig. 4.2-10. The camera range was set to 150°-900°C as lower measurement ranges would saturate before the IR element reached its maximum temperature. This graph showed a high initial ramp that reaches a steady state after 15 mins.

- All IR elements exhibited an identical heat up curve while the Δ temperature is identical than the Ceramicx datasheet heat up curve.
- The IR elements reach a steady state temperature of ~330°C, 20°C less than the steady state value recorded by Ceramicx. This margin of error may be related to specific emissivity values used by Ceramicx, natural convection loss or accuracy issues between the Optris thermal camera and that used by Ceramicx.

Fig. 4.2-11 shows the IR element temperature as measured by the embedded thermocouple. The thermocouple is placed between in the centre of the IR element in an area devoid of resistance wire. This can be seen in fig. 4.2-8 as the dark circle in the centre of the IR element. As there is no resistance coil present, this area heats more slowly than the rest of the IR element.

95
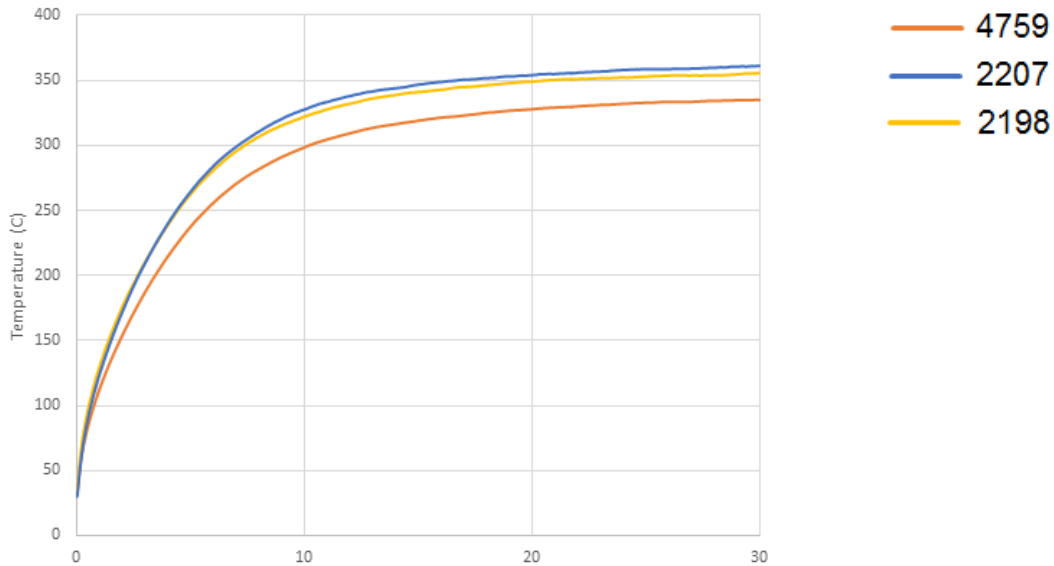
Figure 4.2-11 Thermocouple measurements of three 250W FTE over 30 mins

The thermocouple measurement differs considerably when compared with the thermal camera and Ceramicx results.

- There is a noticeable lag between camera and thermocouple, mainly due to thermocouple placement. The thermocouple is also used in an ungrounded configuration, which may contribute to the deviation in response time.
- FTE 4759 has a lower IR output than 2198 and 2207. This deviation was determined to be a defect in the uncalibrated K-type thermocouple as weight, coil resistance and the thermal image were consistent with other IR elements in this test.
- The IR elements reach a mean temperature of ~350°C, consistent with the mean value recorded by Ceramicx in fig. 4.2-9.

4.2.3 Investigations in thermal response characteristics in IR elements:

Multiple tests were performed on the IR heating elements to characterise thermal responses across a range of criteria using the following parameters:

Testing Parameters	
Voltage	230V
Duration	15 seconds
Camera scaling	0 – 250°C
Distance from IR element	250mm
Reference ambient temperature	24°C

Figure 4.2-12 Thermal camera testing parameters

To focus on temperature changes in the resistance coil, short 15 second tests were conducted to provide a comparable rate of change curves for analysis. This also limited temperatures to within a single scale on the Optris PI400 thermal camera and allow clearer visualisation of the heating coil before the surrounding ceramic mass heated and obfuscated the coil.

Test 3: Thermal analysis on IR elements of various wattage

A test was carried out to measure the heating responses of IR elements with varying wattages. Four FFE elements were heated in accordance to the testing parameters outlined above.

IR Elements Tested:						
No.	Type	Wattage	Serial No.	Coil length	Coil diameter (mm)	Power Density (kW/m^2)
1	FFE	250W	7385	61" (1549mm)	0.28	15
2	FFE	400W	1811	61" (1549mm)	0.35	24
3	FFE	650W	1660	61" (1549mm)	0.40	39
4	FFE	1000W	7324	61" (1549mm)	0.42	60

250W (a)

400W (b)

650W (c)

1000W (d)
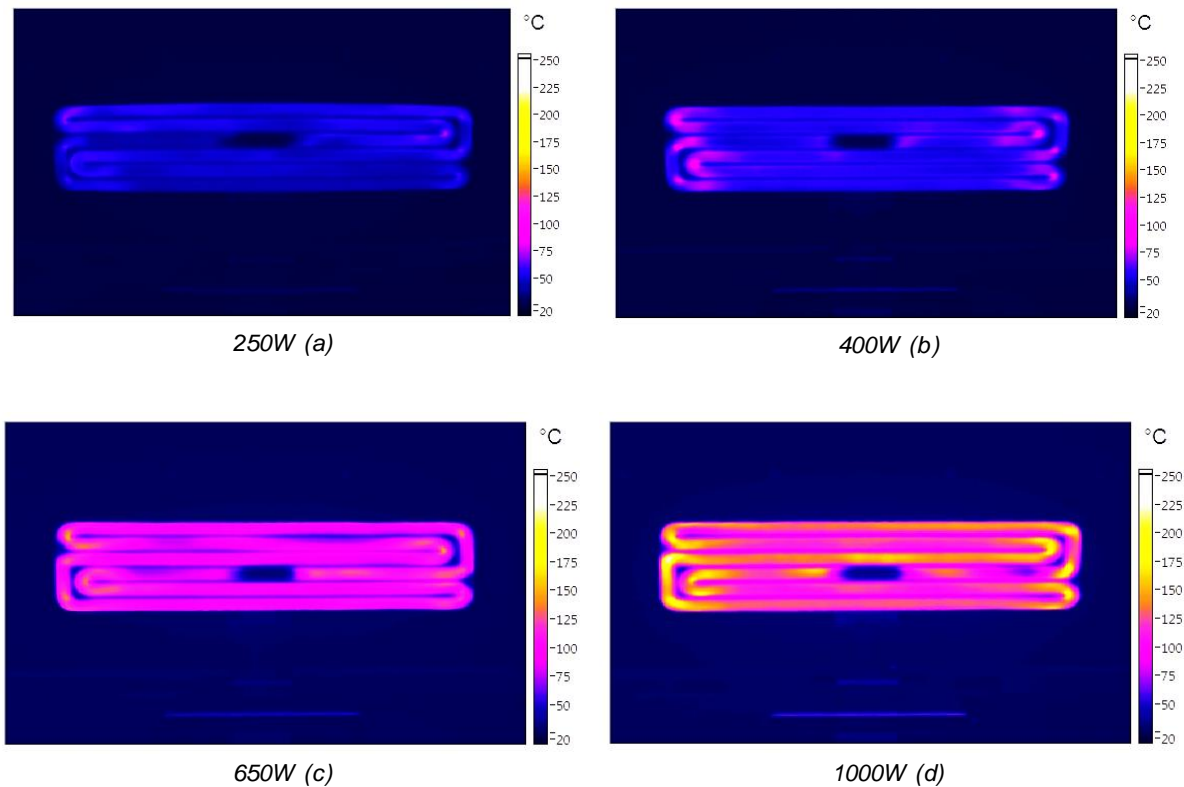
Figure 4.2-13 Thermal images of FFE IR elements (+20% brightness)

Fig. 4.2-13 shows the thermal profile of the four IR elements after 15 seconds.

- The path of the heating wire coil in each case is clearly visible. There is no coil placement across the centre of the IR element resulting in a cold spot. This is the point at which the resistance wire enters the rear of the IR element and is where the thermocouple is located.

- Hot spots are created at each turn in the coil, as the windings are tightly bunched, while areas between the coils remain cold. These effects can be clearly seen in fig. 4.2-13(b) and (d) where localised heating is shown as yellow patches. This also causes the temperature at the edges of the IR element to heat faster than the centre, creating an imbalanced heating profile.

The average temperature values throughout each test were then graphed as shown in fig. 4.2-14:

Heatup comparison: 250W, 400W, 650W and 1000W FFE
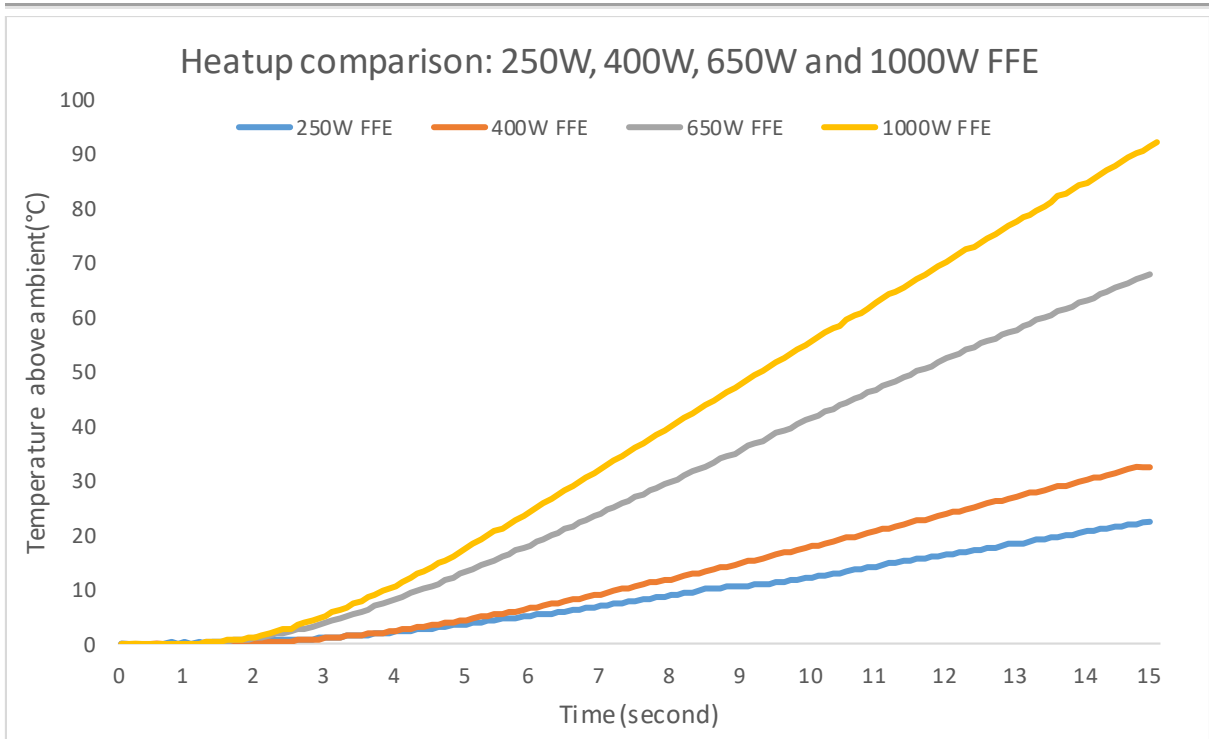
Figure 4.2-14 Surface temperature rise from ambient for four FFE IR elements

This graph confirms expectations that a greater current flow will result in a proportionally greater heating response.

- The change in temperature is first registered by the thermal camera at 0.5 seconds and each IR element has a linear response at this scale. The slope of these heat-up curves was calculated and found to correspond to the rated power density.

Type	Power Density (kW/m²)	Slope
250W FFE	15	1.9
400W FFE	24	3
650W FFE	39	5.6
1000W FFE	60	7.5

Figure 4.2-15 Test 3: Comparison of power density to slope

Test 4: Thermal analysis on IR elements of various surface area

A test was carried out to measure the heating responses on IR elements with differing surface areas. Four 250W IR elements of various surface area were heated in accordance to the testing parameters outlined in fig. 4.2-12.

No.	Type	Wattage	Coil length	Coil diameter (mm)	Surface Area	Power Density (kW/m²)
1	FFE	250W	61" (1549mm)	0.28	0.0342m2	15
2	HFE	250W	32" (813mm)	0.25	$0.0175m^2$	30
3	QFE	250W	15" (381mm)	0.22	$0.0091m^2$	60
4	SFSE	250W	53" (1346mm)	0.28	$0.0336m^2$	15

FFE (a)

HFE (b)

SFSE (c)

QFE (d)
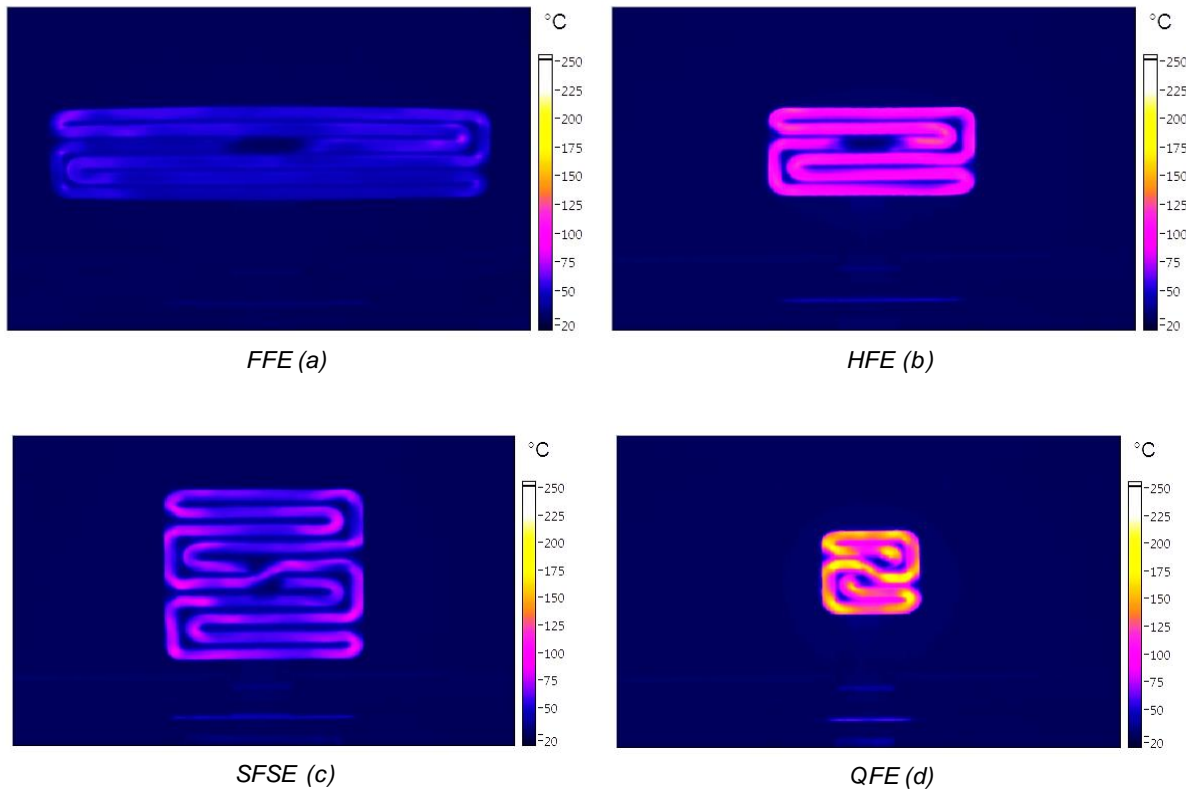
Figure 4.2-16 Thermal images of 250W IR elements of various shapes (+20% brightness)

Fig. 4.2-16 shows the heat up results of four 250W IR elements of various shape.

- To maintain the 250W power rating, the heating coil length and diameter must be altered to account for the change in volume. This concentrates the heating potential of the IR element and increases power density. The difference can be seen in fig.4-46 (a) and (d), where the QFE has ¼ the volume and therefore four times power density.

- The heating wire in both the SFSE and QFE have been routed differently to remove the centre cold spot and improve heating uniformity.

The average temperature values throughout each test were then graphed as shown in fig. 4.2-17:
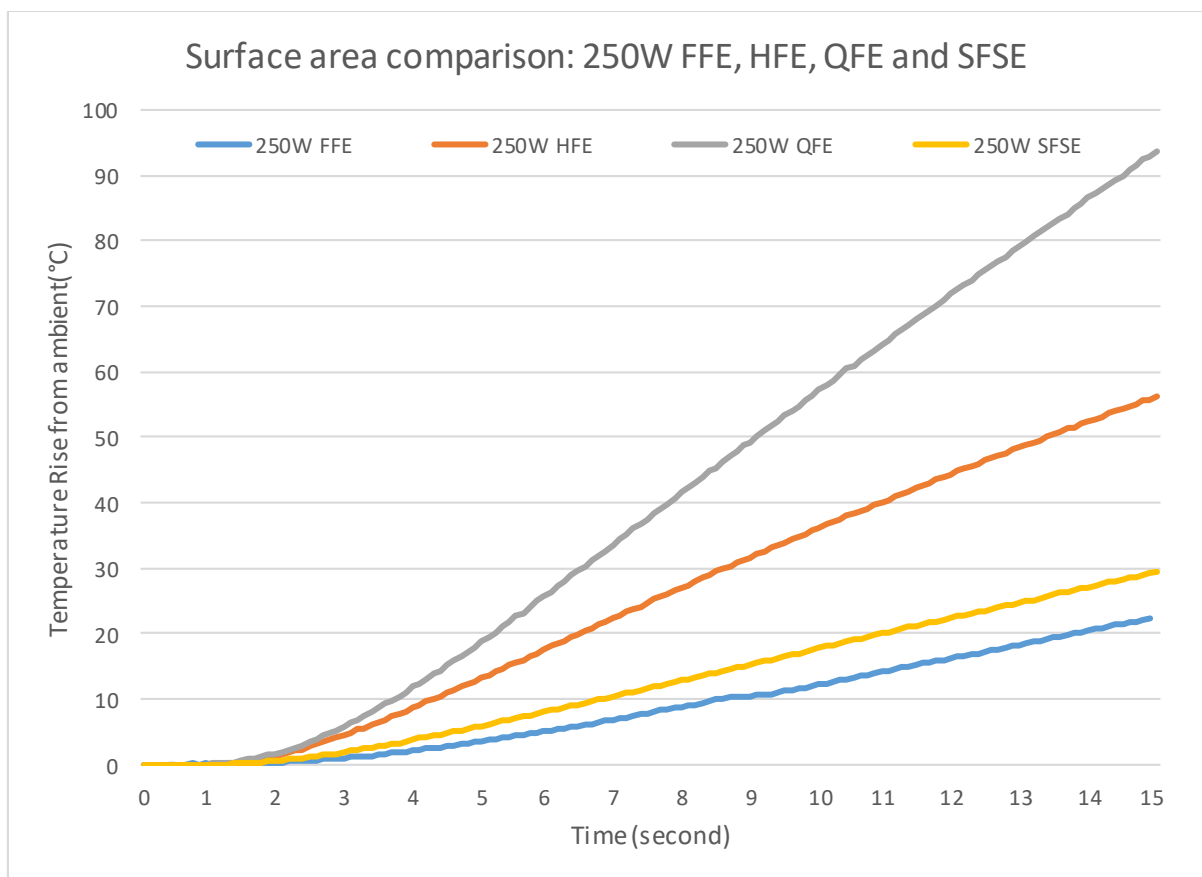
Figure 4.2-17 Surface temperature rise from ambient for four 250W IR elements

As current flow in each IR element is constant, power density is the determining factor in average temperature measurements in this test. Fig. 4.2-17 shows the deviation in average temperature between the four IR elements tested.

- Due to the reduced size of the IR element, less thermal camera resolution is available to measure the QFE and HFE to the same accuracy as FFE. This may introduce a small experimental error that could not be eliminated due to the fixed

focal length of the thermal camera and environmental temperature at close proximity to the IR element.

- The ratio of front surface area emissions to side perimeter emissions can also impact these results. The front surface area of the FFE element is 0.0147m^2 while its perimeter is 0.61m compared to a SFSE, which has a similar surface area of 0.0148m^2, but a smaller perimeter of 0.488m. This reduces the available area for side IR transmissions and therefore more is available for frontal emission.

- The slope of each heat up response from 5-15 seconds was calculated and compared to the power density:

Type	Power Density (kW/m^2)	Slope
FFE	15	1.9
SFSE	15	2.36
HFE	30	4.31
QFE	60	7.55

Figure 4.2-18 Test 4: Comparison of power density to slope

Test 5: Thermal analysis on FFE and FTE IR elements.

Two FFE, one FTE and one FTEL IR elements were heated in accordance to the testing parameters outlined above. The FTEL is a physically longer version of the FTE and measures 285 x 60mm compared to the FTE which measures 245 x 60mm.

IR Elements Tested:						
No.	Type	Wattage	Serial No.	Coil length	Coil diameter (mm)	Power Density (kW/m^2)
1	FFE	250W	7385	61" (1549mm)	0.28	15
2	FTE	250W	0325	61" (1549mm)	0.28	15
3	FFE	1000W	2167	61" (1549mm)	0.42	60
4	FTEL	1000W	9999	61" (1549mm)	0.42	-
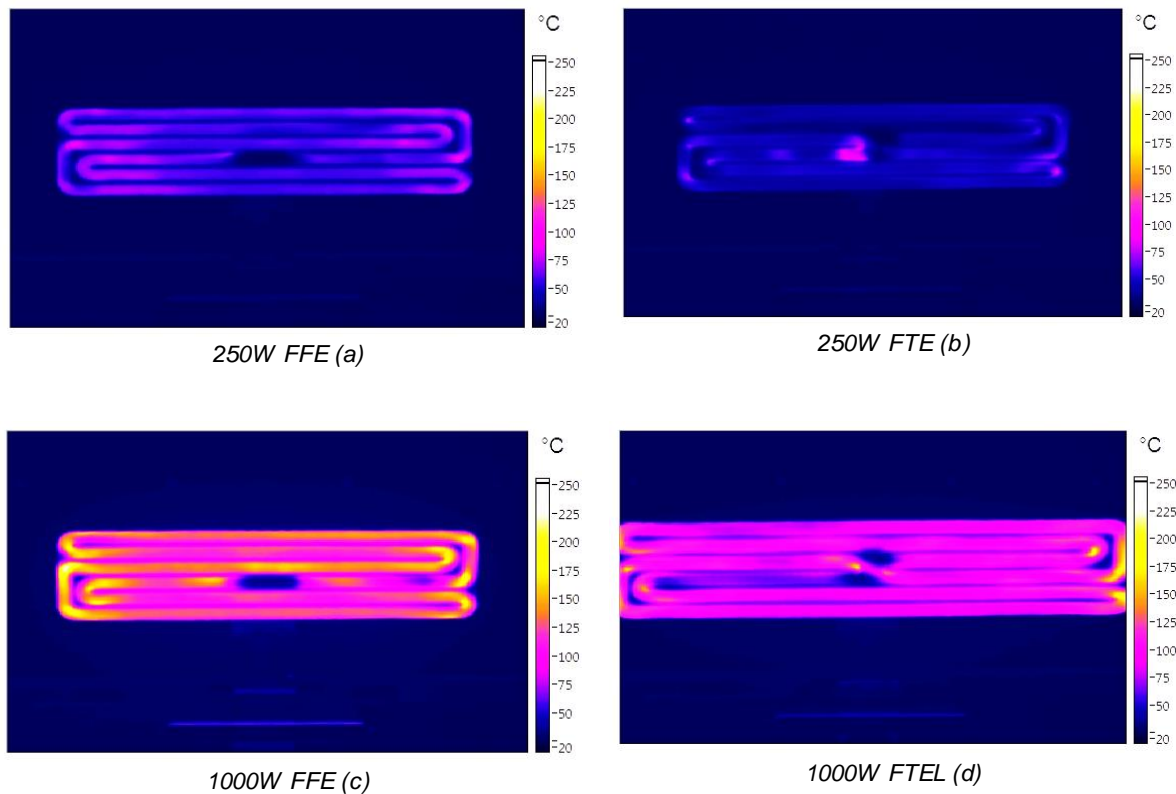
Figure 4.2-19 Thermal images of FFE FTE and FTEL IR elements (+20% brightness)

- The FTE has increased mass compared to the FFE in order to maintain similar dimensions while retaining a concave shape. The increased mass, in addition to the non-perpendicular angle of radiation to the thermal camera reduced the measurable power output, and caused the FTEs to appear colder than FFE of identical size and power.

- The heating coil in the FTE and FTEL is routed to minimize the cold spot in the centre of the IR element.

- Each IR element type exhibits dissimilar heat up characteristics. The FFE heats quickly at the edges, while the centre remains cool, due to the cold spot caused by heating wire routing. The FTE has small areas of localised heating in the centre, while the top and bottom edges appear colder.

- By increasing the size of the FTEL, the power density is proportionally reduced.

4.2.4 Thermal analysis reponse investigation conclusions:

The IR element assembly has certain features such as bunched or misplaced heating coils. These tests illustrate the wealth of information available on the behaviour of the heating coil, post manufacture. Once the emissivity was established in test 1 it was possible to characterise the IR emissions from each element and correlate these with

expected power output. Each IR element has been shown to have an individual thermal profile which is directly related to shape, size and wattage as seen in fig. 4.2-13 and 4.2-16.

The IR elements also exhibit interesting variances in heat up behaviour, where concentrations of coil windings reach higher temperatures, as seen in hot spots at 90° and 180° turns. Several straight sections also react in a similar manner, indicating that the coil has not been stretched uniformly before it was inserted into the IR element. This observation may also be attributed to the pressure applied to the coil when it is pressed into the soft pre-fired clay, pushing sections closer to the face of the IR element. As IR elements of different wattage show identical thermal patterns, seen in fig. 4.2-19 (a) and (c), this may be attributed to a manufacturing technique.

While it may be expected that IR elements made from identical materials should exhibit uniform heating profiles, it can be seen that size have a measureable impact on the ability of the thermal camera to visualise IR emissions. The 250W SFSE in test 4 recorded a heat up curve 20% higher than a comparable 250W FFE, which may be explained through increased ratio of frontal to side surface area, concentrating more IR emissions into the thermal camera's field of view. Shape too, has a noticeable impact. Less IR emissions are recorded when the heating plane is not perpendicular to the camera lens, as seen in test 5. This can lead to distortions in the heating profile and lower than expected thermal responses. This may be countered by altering the mounting angle of the IR element, or using a lens which incorporates a Scheimpflug tilt adjustment.

The Labview VI allows for inclusion zones to be assigned to the face of each style of IR element, similar to the method employed to measure different regions in test 1. These zones are designated with temperature threshold values obtained by analysing approved IR elements. These thresholds can be used to create a measurement baseline for test. Similar measurements, such as maximum, minimum, mean, heat up response times and thermocouple verified temperatures are also available for full characterisation of IR heating elements in and automated test process.

4.3   Image processing feasibility study

Introduction:

IR elements suffer from several manufacturing defects which may take the form of hairline cracks, visible lines formed during casting, lumps due to mould wear, flashing along the perimeter of the element and imperfections in glazing. Currently, these defects are spotted during routine inspection throughout the manufacturing process. However, the prevalence of these imperfections are not recorded. Therefore, the cause may not be identified which may lead to reoccurrences and wastage in production.

Computer vision and image processing offer a solution to these issues by providing and empirical test routine which can identify and categorise flaws by type and location, then log results to a database. The image processing technique used in this study is based on the use of low cost hardware and open source software. Images of the IR elements were captured with a webcam, then imported to ImageJ, an open-source software package. This images were cropped, post-processed and then compared to reference dimension measurements. ImageJ is a multi-platform, Java-based image processing software and able to import nearly all common image formats used in engineering, medical and scientific fields. It is capable of processing captured images through a wide variety of common processing tools, supplemented with a large library of custom, application specific plugins[97].

4.3.1   Test methodology

Due to the variation in quality of the IR elements, it is necessary to record and measure the physical characteristics of each product during the end-of-line test process. This test routine incorporated three low cost webcams with 1280x720 HD resolution and ImageJ to measure physical dimensions and quantify product flaws and defects. This section will examine the accuracy and repeatability of this process under the following headings:
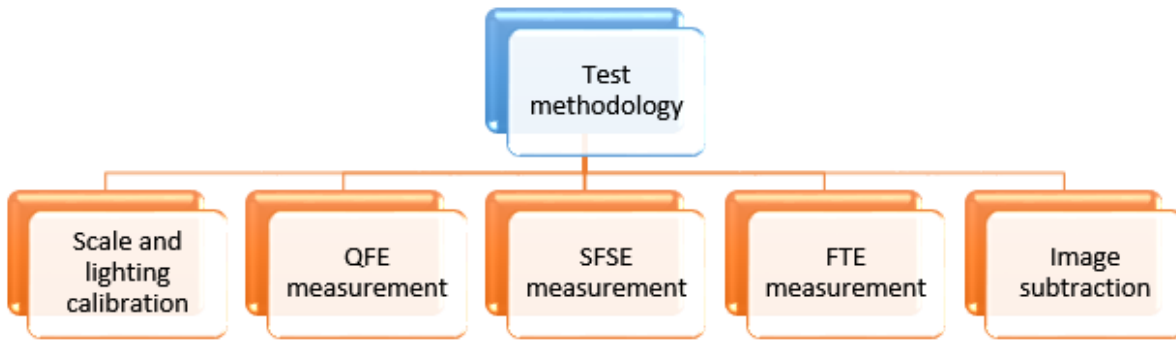
Figure 4.3-1 Image capture test methodology

4.3.1.1 Test setup

To accurately measure multiple dimensions of the IR element, three webcams were positioned onto an extruded aluminium frame. Each webcam was oriented to capture a different face of the IR element, which was mounted onto a stand and surrounded by a black backdrop, as seen in fig. 4.3-2.
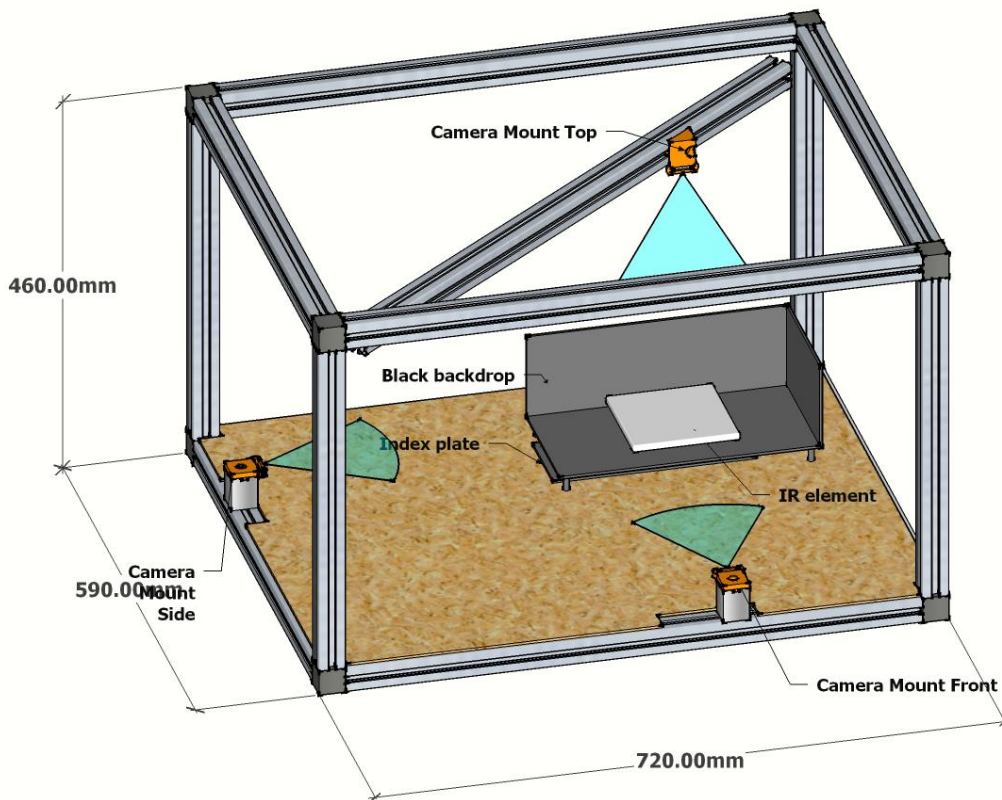
Figure 4.3-2 Image capture testing apparatus

The apparatus was sized to ensure the IR element is situated within the focal distance and field of view (FOV) of the camera. The webcams used in this experiment were Microsoft® Lifecam 3000, which have a fixed focus of 0.3m to 1.5m and a horizontal FOV of 60°.

Imaging Features	
Sensor	CMOS sensor technology
Resolution	• Motion Video: 1280 X 720 pixel resolution*
	• Still Image: 1280 X 800
Imaging Rate	Up to 30 frames per second
Field of View	68.5° diagonal field of view
Imaging Features	• Digital pan, digital tilt, vertical tilt, swivel pan,
	• Fixed focus from 0.3m to 1.5m
	• True Color - Automatic image adjustment
	• 16:9 widescreen
	• 24-bit color depth

Figure 4.3-3 Microsoft® Lifecam 3000 image and technical specifications

The webcams were connected to a PC via a USB hub. The ImageJ plugin WebcamCapture was used to interface with the webcams. A series of 12V warm white LED strips were positioned around the black backdrop to provide controlled lighting. The LEDs had a colour temperature of 2700-3300K and were powered from an EL301 bench power supply.

4.3.1.2 Test procedure

The WebcamCapture plugin was used to record still images, which were imported into ImageJ for further analysis. A macro was created to automate image capture, greyscaling and cropping. Further post-processing, such as thresholding and measurement was done manually according to the nature of the test.

4.3.2   Baseline investigations

Test 1: Setting scale values for each axis.

To accurately measure the dimensions of each IR element, a scale was needed to convert pixel measurement to millimetres. 10mm black lines were marked on each side of a quarter flat element. Still images of the IR element were taken from each camera and the scale lines were measured in ImageJ then used to calibrate each camera.

83.92x81.25 mm (189x183); 8-bit; 3

(a) Top view

65.71x25.75 mm (148x58); 8

(b) Front view

66.41x23.58 mm (138x49)
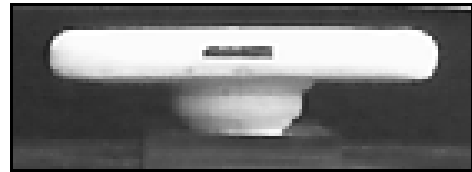
(c) Side view

ImageJ Scale for FFE IR elements using 10mm reference line		
View	Distance in pixels	Millimetres per pixel:
(a) Top	23.4	0.427
(b) Front	22.13	0.452
(c) Side	19.8	0.505

Figure 4.3-4 Reference scale of QFE IR element imported to ImageJ

An indexing table, seen in fig. 4.3-5 was designed to reduce calibration time between parts types. The indexing table maintains the distance from the front and side edges of an IR element to their respective cameras, regardless of the IR element size.

Figure 4.3-5 Indexing plate used to maintain IR element distance from camera

Test 2: Establishing optimal lighting parameters

ImageJ features a threshold system, which uses segmentation to separate an object of interest from the background based on pixel intensity. Captured images are converted to 8-bit greyscale, which has 256 (2^8) intensity graduations ranging from black (0) to white (255). Every graduation between these extremes is a shade of grey[98]. Thresholding works by separating pixels which fall into a desired range of intensity values from those who do not. The greater the contrast between background and subject, the greater the accuracy to which the subject can be visualised and separated. A backdrop was constructed from matt black acrylic, to improve the contrast between the white IR elements and background. LED lighting was installed to remove unwanted shadows and highlight the edges of the IR elements. Voltage control was used to tailor the intensity of the LEDs to the scene. To determine the optimal LED intensity, a SFSE IR element was mounted onto the indexing plate. The voltage was incrementally increased and a series of images were captured of the IR element, as seen in fig. 4.3-6:
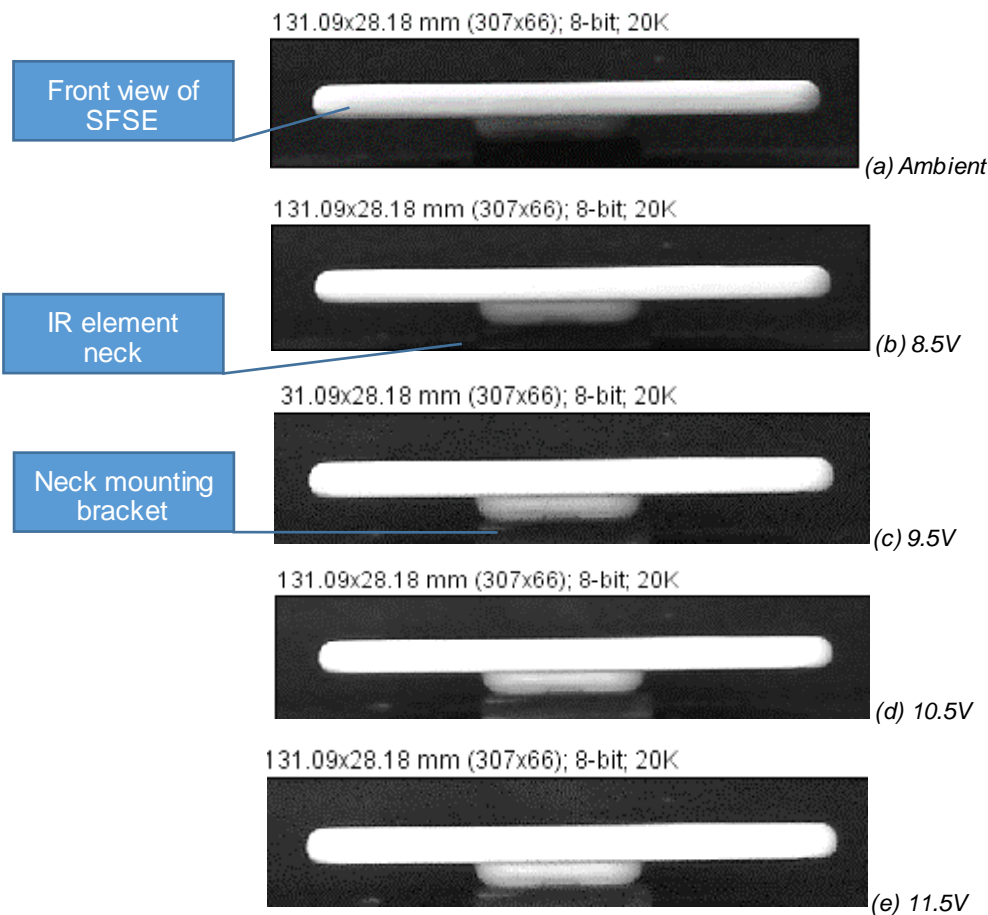

Figure 4.3-6 Front view of SFSE under varying lighting conditions

From these images it can be seen that the face of the IR element contrasted well with the black backdrop. However, under ambient conditions (fig. 4.3-6*(a)*) the neck section

blended into the neck mount. The contrast between neck and mount increased as the light intensity increases (fig. 4.3-6*(b-d)*), until the mount begins to reflect light (fig. 4.3-6*(e)*). It was determined that 10.5V was the optimal conditions for further tests.

4.3.3 Investigations in dimensional measurements of IR elements.

When the IR elements were mounted into the apparatus it could not be assumed their placement was square to the FOV of the webcam. Therefore, an alternative to measurements along the X and Y axis of the image was found. Feret's diameter is the furthest distance between any two parallel tangents, while minimum Feret's diameter is the shortest distance between any two parallel tangents. By using Feret's diameter to dynamically measure distance on the face of IR element, the issue of non-uniform placement was overcome. ImageJ uses a rotating callipers algorithm to determine Feret's diameter, where a region of interest is rotated in 2° increments along a central axis and the maximum and minimum distance values are recorded as seen in fig. 4.3-7. In addition, both area and perimeter were recorded.

259.74x104.34 mm (585x235); 8-bit (inverting LUT); 134K

Perimeter

Minimum Feret's Diameter

Feret's Diameter

Area
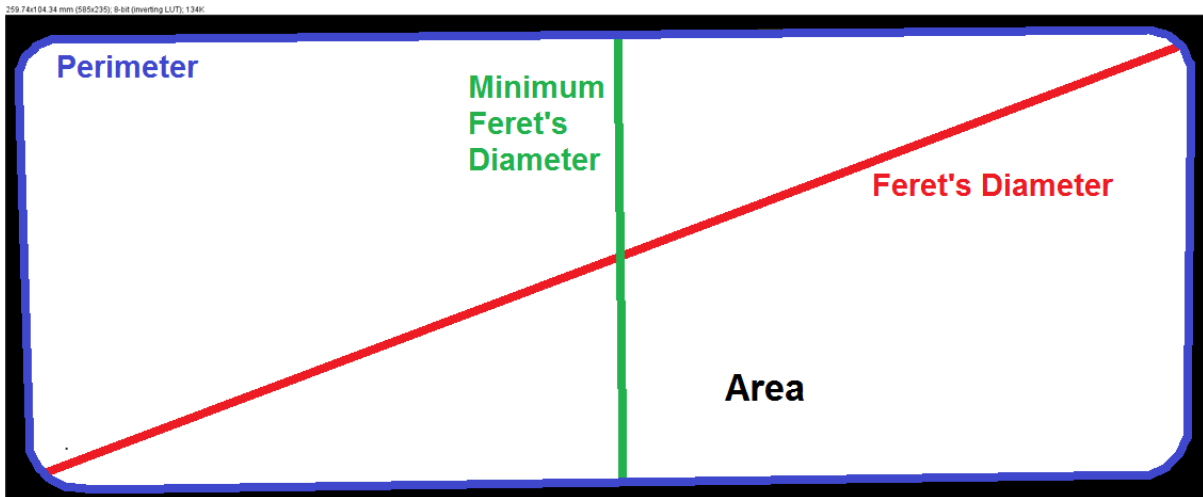
Figure 4.3-7 Top view measurements taken from FFEL IR element

Test 3: Dimensional measurement of reference QFE element

The reference QFE used in Test 1 was used to determine the accuracy of this system. The QFE has nominal dimensions of 60 x 60 x 8m, as seen in the figure below:
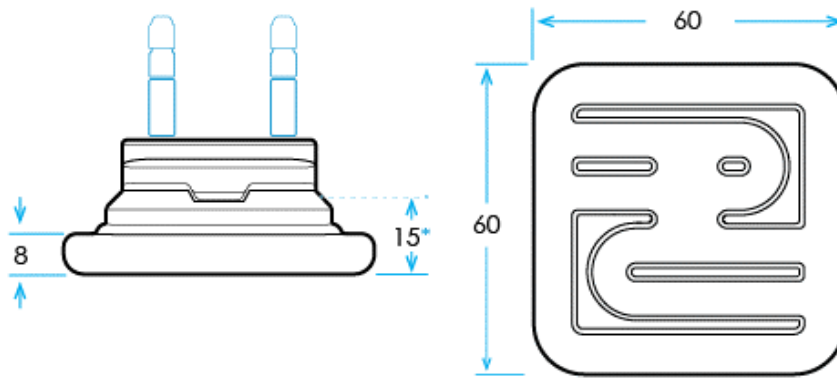
Figure 4.3-8 QFE dimensional diagram

The reference QFE was measured with digital callipers which gave dimensions of 59.18 x 58.88 x 7.92mm. This IR element was placed into the measurement apparatus. Three images were taken with WebcamCapture, then imported to ImageJ. Thresholding was used to create a binary image which was then traced and measured.

(a) Top view

(b) Front view

(c) Side view
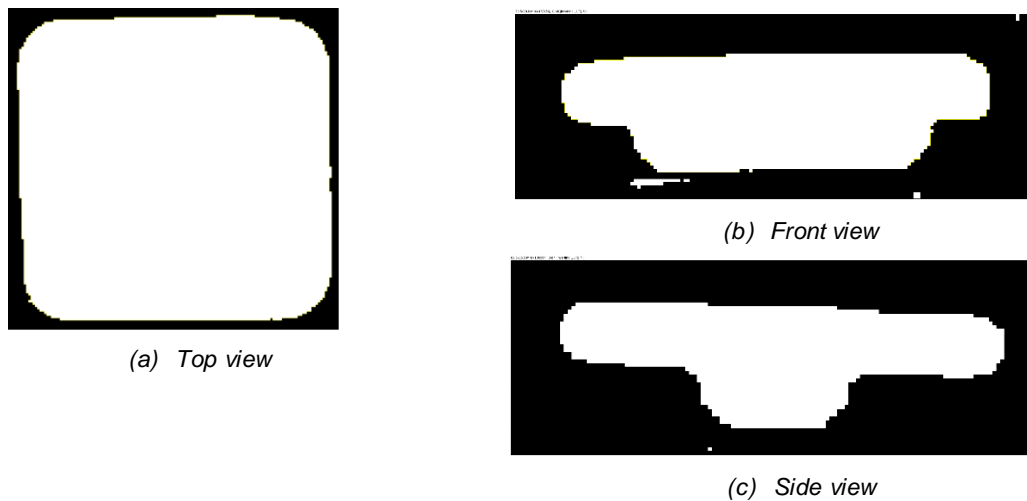
Figure 4.3-9 Thresholded view of QFE element

Measurements of QFE reference IR element			
View	Top	Front	Side
Measured X axis	59.15	59.15	58.88
Measured Y axis	58.88	16.64	16.64
ImageJ min. Feret's diameter	58.591	16.587	16.58
Measured Feret's diameter	75.66	59.15	58.88
ImageJ Feret's diameter	75.705	60.041	59.3
ImageJ perimeter	224.199	141.857	138.902
ImageJ Area (mm^2)	3350.63	815.196	623.281
Threshold (min, max)	0,98	0,61	0,61

*all measurements in mm unless otherwise specified

111

From the table above it can be seen that the ImageJ results closely match those measured with callipers:

- The reference QFE was smaller than the reference dimensions given in the datasheet.

- Each image has jagged, pixellated edges as a result of the limited resolution of the webcam.

- Erroneous white areas are visible on fig. 4.3-9(b) due to light reflections from the IR element mount. These were excluded when the region of interest was defined.

- None of the images line up precisely with the webcam's FOV. A 2.2° deviation from parallel can be seen in fig. 4.3-9(c).

- The measured Y-axis and minimum Feret's diameter measurements are within 0.3mm using the scale determined in test 1 and lighting parameters established in test 2.

- The measured Feret's diameters are within 0.9mm of the ImageJ results. This error may be a result of camera resolution, where one pixel = 0.505mm.

Test 4: Dimensional measurement of SFSE element

As the cameras are held in a fixed position, the inclusion zone selected when measuring a small IR element encompasses only a small portion of available camera resolution. To measure if resolution had a quantifiable impact on dimensions, a SFSE with a nominal dimension of 120 x 120 x 8mm was tested using the same parameters as the previous test. The SFSE has four times the surface area of the QFE.
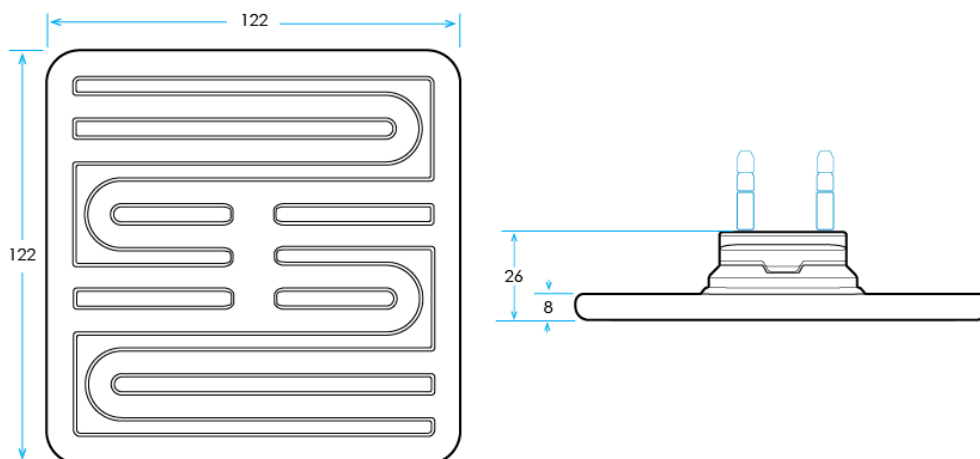
Figure 4.3-10 SFSE dimensional diagram

(a) Top view

(b) Front view

(c) Side view
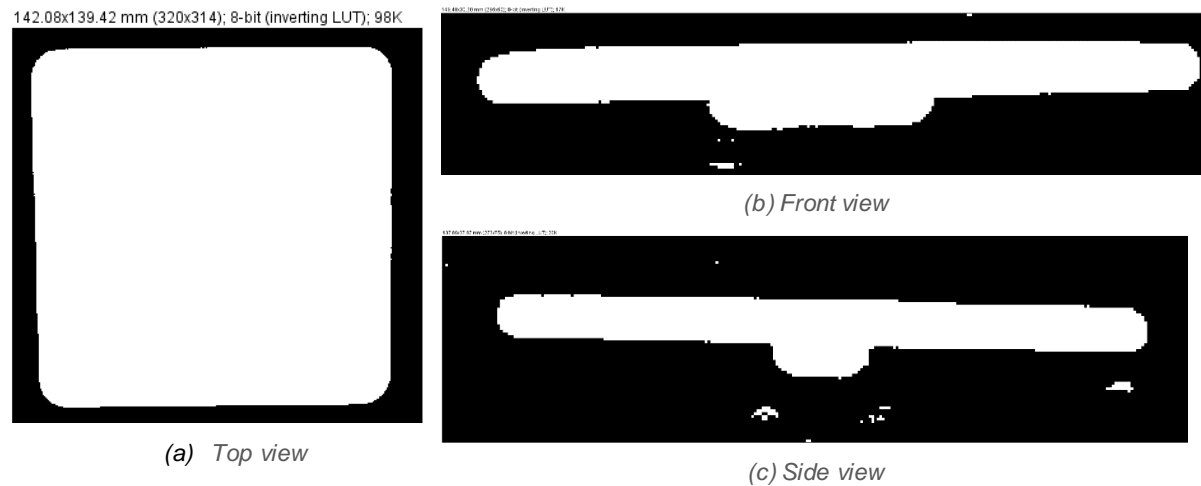
Figure 4.3-11 Thresholded view of SFSE element

Measurements of SFSE IR element			
View	Top	Front	Side
Measured X axis	120.6	120.6	120.9
Measured Y axis	120.9	16.4	16.4
ImageJ min. Feret's diameter	120.440	14.523	14.894
Measured Feret's diameter	162.06	120.6	120.9
ImageJ Feret's diameter	161.500	120.709	120.38
ImageJ perimeter	469.640	261.621	263.230
ImageJ Area (mm²)	14220.6	1204.809	1076.166
Threshold (min, max)	0,96	0,60	0,62

*all measurements are in mm unless otherwise specified

These measurements correlate closely with the previous test.

- The top view results for measured Y-axis and minimum Feret's diameter were within 0.46mm. This is within the 0.505mm single pixel margin of error, observed in test 3, and which was now established as a minimum margin of error induced by the limited resolution of the camera.

- However, the results for the front and side view differ substantially. This was attributed a shadow that was not completely eliminated by the LED lighting, which caused the thresholding algorithm to remove a portion of the IR element's neck when segmenting the image.

- The measured Feret's diameter and ImageJ Feret's diameter are within the 0.5mm tolerance band.

Test 5: Dimensional measurements of FTE element

All previous tests have used flat element positioned perpendicular to the camera's FOV. This test used a FTE IR element to measure the capability of the system to account for a curved profile.
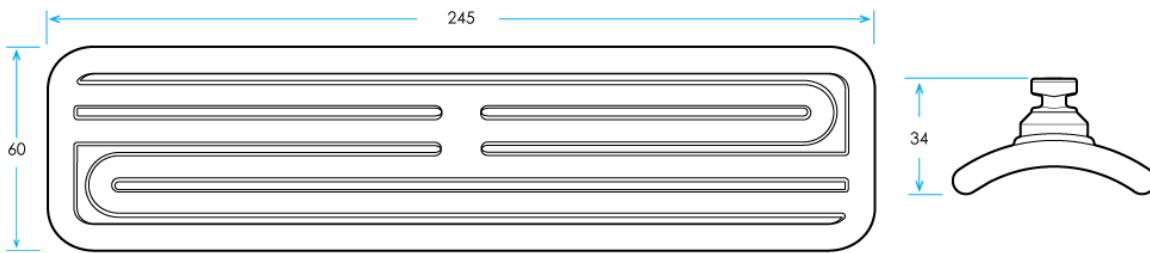
Figure 4.3-12 FTE element dimensional diagram

(a) Side view

(b) Top view
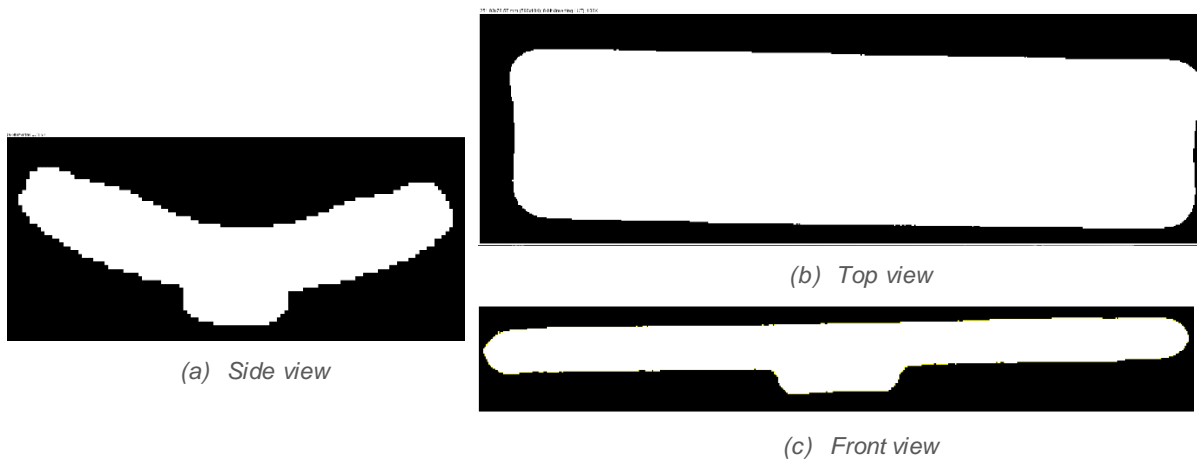
(c) Front view

Figure 4.3-13 Thresholded view of FTE element

Measurements of FTE IR element			
View	Top	Front	Side
Measured X axis	242.7	242.7	59.9
Measured Y axis	59.9	23.3	18.4
ImageJ min. Feret's diameter	59.234	24.620	21.379
Measured Feret's diameter	242.9	242.7	59.9
ImageJ Feret's diameter	242.09	243.096	59.197
ImageJ perimeter	583.199	523.971	148.539
ImageJ Area (mm²)	13633.1	3897.735	599.429
Threshold	0,112	0,60	0,45

*all measurements are in mm unless otherwise specified

The results of this test fall in line with previous observations. However, the curved profile of the FTE is a source of inaccuracy in several measurements.

- Each camera was calibrated according to scale markers placed on the face of the IR element. As the FTE has a curved profile, the top camera is calibrated to the lowest point of the curve.

- As the camera has a fixed focal distance, the curved profile creates a perspective distortion, as seen by the curved effect in fig. 4.3-14 below:

Figure 4.3-14 Perspective distortion in FTE

- This distortion, in tandem with the pixel error, increased the error margin when comparing measured and ImageJ Feret's diameter where the maximum error recorded was 0.8mm.

- The long, narrow shape of the FTE also created a perspective issue when viewed from the side it was required to adjust the camera height until both camera and the bottom of the trough were positioned on the same plane. As the position of the neck moves further from camera its dimensional value decreases, leading to error.
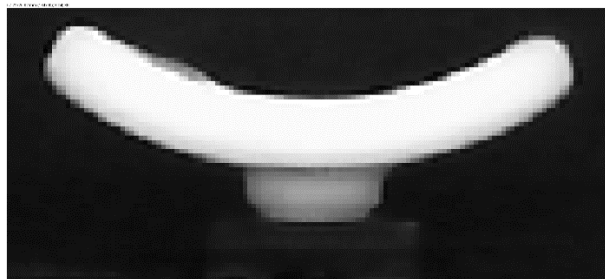
Figure 4.3-15 Side view of FTE

- These distortions impacted on minimum Feret's diameter results. The side view perspective error added to the overall height resulting in a value nearly 3mm larger than measured.

Test 6: Dimensional measurement of black HFEH element

Ceramicx manufacture IR elements in white, yellow and black coloured glaze. In this experiment, a black HFEH IR element was used to test the ability of the imaging system to acquire dimensional information from a black object. The black HFEH was mounted into the system and three images were taken and thresholded.
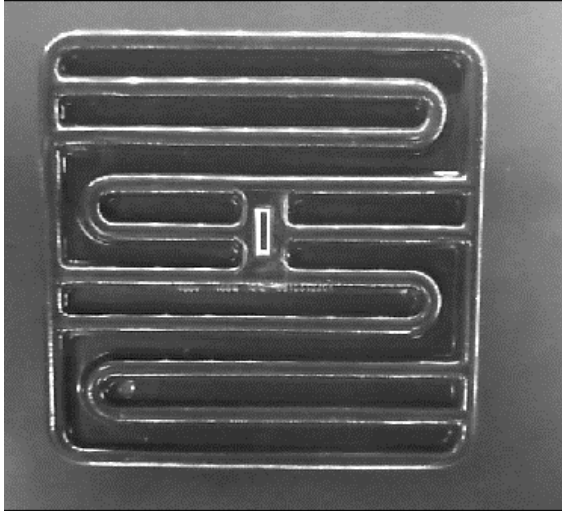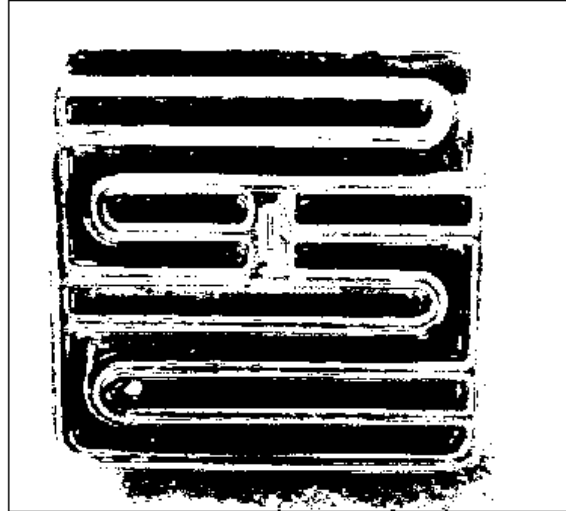
(a) Before   (b) After

Figure 4.3-16 Image of black HFEH before and after thresholding

From fig. 4.3-16 it is clear that the system cannot wholly distinguish between the black background and the black object. Directed LED lighting was used to create glare on the face of the IR element in an attempt to highlight edges and contours. However, this was insufficient to create a significant contrast to differentiate between the IR element and background. Similar results were recorded from front and side views:
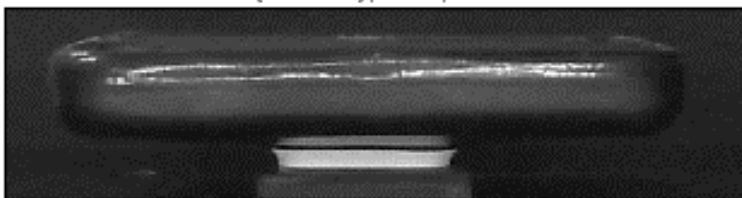
(a) front view before threshold
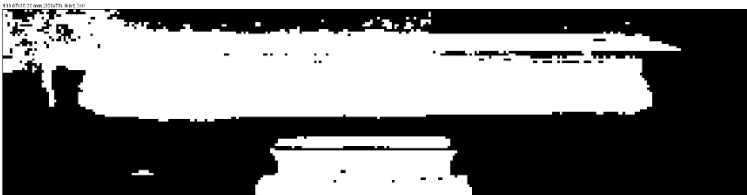
(b) front view after threshold

130.29x34.84 mm (258x69); 8-bit; 17K
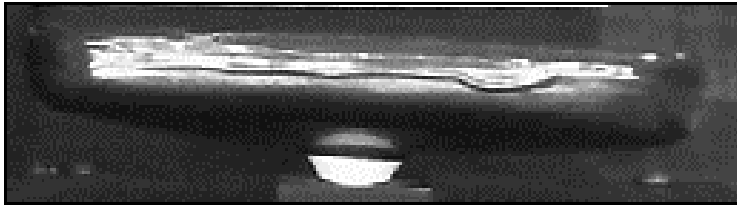
(c) side view before threshold

(d) side view before threshold

Figure 4.3-17 Images of failed threshold analysis on black HFEH

This issue can be resolved by mounting the black IR elements on a white backdrop. To prevent reflections from white LED light, an alternative wavelength, such as ultraviolet or near infrared may be required and a camera with the capability to visualise this wavelength.

Test 7: Image Subtraction

ImageJ has several image calculation algorithms which can perform addition, subtraction or logic operator functions. This test focussed on using image subtraction to locate imperfections on the face of the IR element, with a view to identify manufacturing flaws at the end-of-line test. A SFSE was imaged using the top camera, then the face was marked with three 'X' shapes, using a black sharpie. The IR element was imaged again and both images were imported to ImageJ:

145.61x138.35 mm (341x324); 8-bit; 108K   148.60x136.21 mm (348x319); 8-bit; 108K
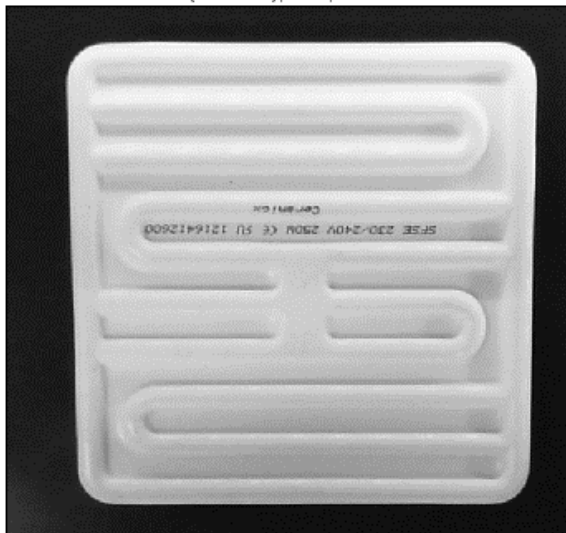
(a) Before marking   (b) After marking

Figure 4.3-18 Marking the face of a SFSE IR element

117

Image subtraction involves comparing the intensity of individual pixels and noting discrepancies. As seen in fig. 4-3.19, the three black X shapes were highlighted by the subtraction algorithm while other detail was removed:
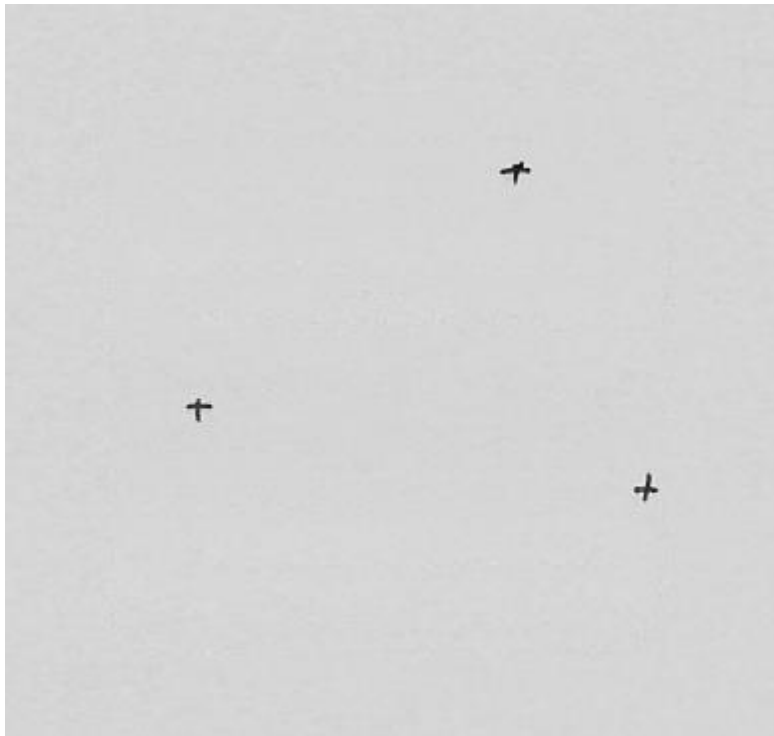
Figure 4.3-19 Subtracted image of SFSE element

Image subtraction operates best under controlled light conditions, which prevents changes in ambient lighting from generating signal noise, resulting in a ghosted image. An example of this is shown in fig. 4.3-20 where an image was captured of the SFSE under controlled LED lighting. A second image was taken under ambient lighting with controlled lighting removed. The same subtraction technique was then applied to both images which can be seen in fig. 4.3-21.

- *Low controlled light*

- *No controlled light*

Figure 4.3-20 Images of SFSE under controlled and non-controlled lighting

Figure 4.3-21 Ghosted image of SFSE after subtraction.

This image shows the effects of controlled LED lighting on highlighting edges and raised features on the face of the IR element. From this image it can be seen that the areas which were previously highlighted by controlled light have appeared as lighter areas. This test highlights the need for uniform, controlled light to counteract the changeable intensity of ambient lighting.

Test 8: Using subtraction to identify imperfections

Locating and highlighting imperfections on the face of an IR element is a key requirement for this study. In this test, an image of an FTE was subtracted from an FTE with several areas of damage. The resulting image was then thresholded to

remove noise and ghosting effects due to changes in position and lighting which resulted from the damage:

300.98x110.09 mm (596x218); 8-bit; 127K

(a) Intact FTE

296.43x102.51 mm (587x203); 8-bit; 116K

(b) Damaged FTE

297.44x103.52 mm (589x205); 32-bit; 472K

(c) Subtracted FTE

297.44x103.52 mm (589x205); 32-bit; 472K

(d) Thresholded FTE

Figure 4.3-22 Progression of FTE damage identification

Fig. 4.3-22 (b) shows a FTE with four areas of damage which include cracks and chipping. This image was subtracted from the undamaged FTE image shown in fig. 4.3-22(a). The resulting subtraction (fig. 4.3-22(d)) shows the four damaged areas in addition with several other areas which had changed from the original image. These include:

- An outline of white which was a result of movement when the IR element was reinserted into the mount. Two vertical cracks in the face of the IR element also resulted in deviation in placement from the original image.

- Several lines in the left of the image which were attributed to the left side of the IR element drooping due to the severity of the crack.

- A white spot between the two cracks, which showed that the IR element had been turned 180° in the interval between image capture.

Subtraction in ImageJ can be a useful tool in determining the integrity of the IR elements through an impartial, empirical analysis of faces and features. This test has shown that flaws can be visualised through a simple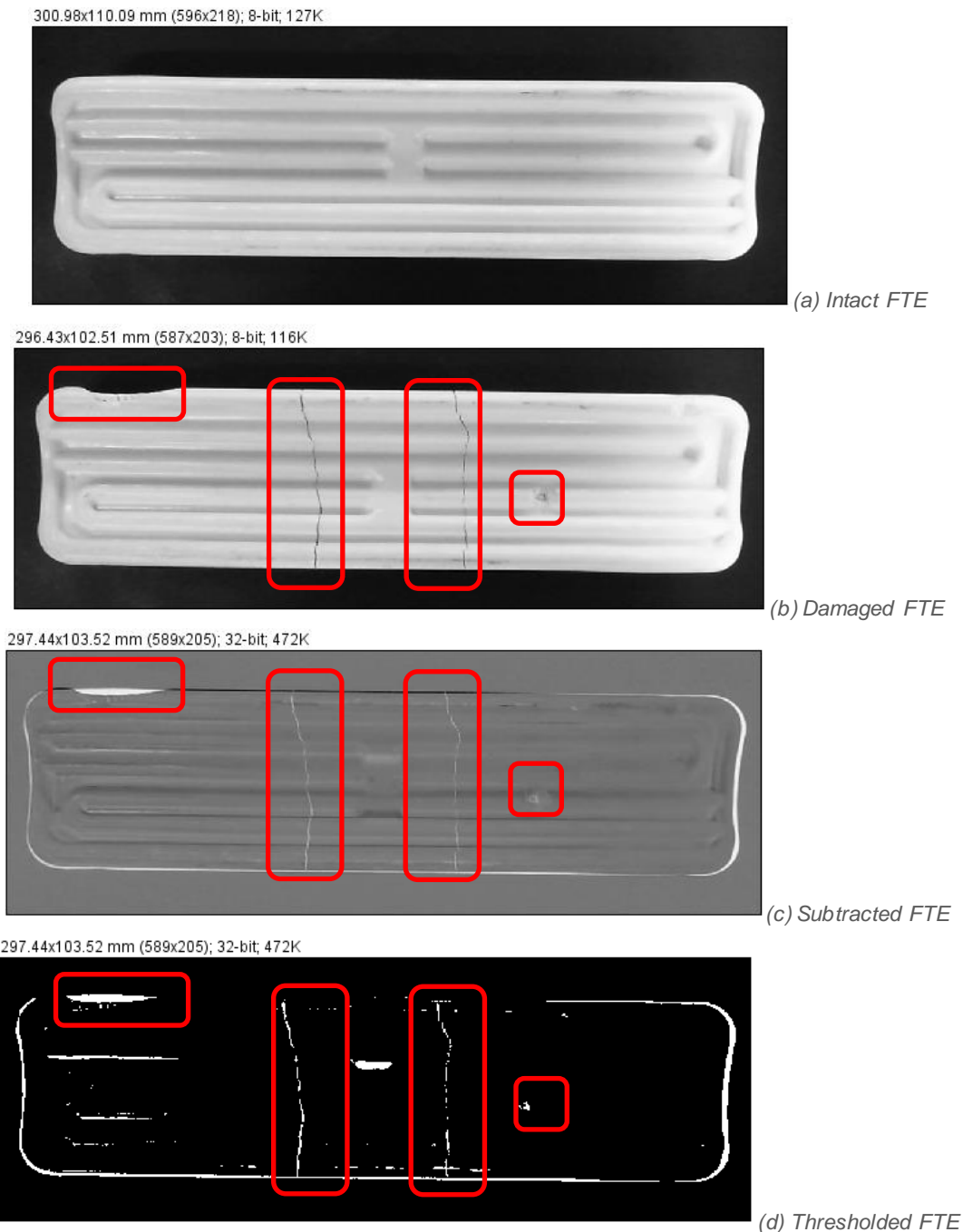 machine vision subtraction algorithm. Further analysis using higher resolution cameras and more dynamic lighting to highlight and shade specific features may increase the resolution of this system. Indicators which resulted from placement or movement, as seen in this test, were construed as false imperfections. It may be possible to avoid these by creating a larger reference library, which may average out common false positives.

4.3.4 Image processing investigations conclusions:

This study has shown that accurate sub-millimetre measurements can be achieved with limited investment in hardware and software. The measurement apparatus was constructed from off-the-shelf consumer electronics and free, open-source software. Care must be taken to optimise conditions in the imaging environment to best suit the object under test. As seen in test 4, lighting is the main factor used to tailor the scene to the specific requirements of the test. Maintaining consistency in lighting parameters between tests is crucial in image comparisons and subtraction. Inconsistencies may create noisy images which require more comprehensive post-processing as shown in test 7. In addition to lighting, it was observed that error was induced due to the limited resolution of the Lifecam 3000 webcams used. By utilising cameras or imaging system more specific to this task, with higher resolution and macro lenses, this error may be reduced to a negligible value. Consideration must be given to the background to ensure that sufficient contrast is present to easily distinguish between background and object. The black background used in these tests was ideally suited to white IR elements, but failed in test 6 when a black IR element was tested.

Imaging systems for automated test have been implemented in manufacturing since the advent industrial robot vision in the 1980's[99]. However, low cost systems with

easy implementation have the potential to drastically increase the range of available test and measurement that can be to increase product and process quality. ImageJ allows the creation of custom plugins to leverage other software components in acquiring and processing specific information and objectives. Macros can be used to fully automate this process, resulting in immediate objective and empirical results, without the requirement for specific operator training or knowledge.

5 Conclusions

Introduction:

This study has shown a range of positive impact from the successful implementation of reconfigurable manufacturing and test systems, especially for companies who predict rapid changes in growth and changeable product requirements. The last decade has seen a "Cambrian explosion" in the number and range of new hardware start-ups, hackerspaces and accelerators programs, each requiring manufacturing system[100]. Established companies are also moving to integrate more holistic, modular manufacturing systems to improve efficiency, quality and yield. There is an as yet unrecognised potential for these companies to leverage the modular, integrable and scalable RMS which can develop and scale in tandem with the product.

Properly implemented, the RMS can create a system of continuous feedback, providing physical product data at every stage of manufacture and test by leveraging the concepts of Industry 4.0, the Internet of Things and Big Data. This feedback loop is completed by the test execution system (TES), explored in this study. The data captured by the TES can be utilised in several ways such as:

- Constant improvement of the product and process, improving yield, reducing waste and trimming process time and increasing throughput.
- Providing real-time information to other stake-holders in manufacturing chain for more accurate product forecasting and streamlined product delivery.
- Allowing customisation of products through web-enable customer interfaces tied to flexible manufacturing systems.
- Accurate and comprehensive technical data on individual products.
- Analysis on long term product and process trends through Big Data analytics.
- Predictive maintenance and fault finding systems.

Given recent developments in low cost sensors, the ubiquity of high bandwidth communications, increased computing speeds and powerful software development environments, the potential for reconfigurable manufacturing and test based on the concept of Industry 4.0 is limitless. Future adoption of RMS's may eventually lead to decentralised or local manufacturing, portable and easily deployable manufacturing systems and a design anywhere, make anywhere, sell anywhere paradigm where

businesses are freed from economic constraints which are current limiting factors in manufacturing[27].

Machine development:

The reconfigurable test execution system was designed around a stadium shaped Bosch asynchronous conveyor which functioned as the backbone of the system, providing power, compressed air and communication to eight equally spaced slots along the perimeter of the conveyor. Each slot was capable of accommodating a single test station. Three test stations were provided with the system and each was designed in isolation using a common footprint and system architecture.

Test station 1: Dielectric test and resistance measurement

Test station 2: Heat-up and thermal image test

Test station 3: Serial number printing station.

The stations interfaced with the conveyor infrastructure and communicated to a central control computer, located at one end of the conveyor. The operator controlled the system through a HMI and input test parameters specific to the product under test. These parameters were communicated to each test station which then operated autonomously in testing each product on the conveyor line. An operator station allowed the operator to place untested products on the line. This station also gave the operator the capability to view test information from each product as they moved through the system.

The unassigned slots on the TES allowed future upgrades and expansions. Test stations with new features and functionality can be quickly constructed based on standardised architecture and seamlessly interfaced with the TES. Duplicate test stations can also be added to increase product throughput and add redundancy.

Leakage current investigation conclusion:

In validating the TES, a series of investigations were undertaken to characterise the dielectric voltage withstand test in test station 1. These tests uncovered interesting factors which related to the materials used to construct the IR elements. The IR elements were discovered to be highly hygroscopic and capable of absorbing moisture from the environment. This resulted in higher than expected leakage current results. It was also found that rated power could not be directly correlated with leakage current

results, while comparisons of leakage current to surface area showed a non-linear relationship. The hipot test was also capable of detecting a series of electrical faults such as exposed wires, although only under certain test conditions. Recommendations from this study concluded that ambient conditions be maintained when conducting leakage current measurements and that the IR elements should be allowed to acclimatise to these conditions over a 48-hour period. While this protocol will give stable results, the actual leakage current values can only be uncovered when the IR element has undergone a heating cycle, although this may not be possible in a high throughput manufacturing environment.

Thermal analysis investigation conclusion:

Test station 2 incorporated a thermal imaging system which allows the operator to verify the integrity of the heating coil embedded in each IR element. Several heating tests were undertaken to characterise the thermal response of the IR elements and to correlate the resultant heating curves to datasheet values. These investigations indicated a relationship between physical size, rated power and power density. The thermal analysis tests also highlighted several other features of interest such as hot spots caused by bunched wires, differences in wire routing and differences in heating patterns. Thermocouple placement was found to adversely impact heating response times. It was also surmised that specific shapes lend themselves to better thermal imaging analysis by projecting a larger proportion of IR towards region detectable by the IR camera.

Image processing feasibility conclusion:

Image processing tests utilised low cost hardware and open source software to attain dimensional measurements from a series of IR elements. The accuracy of this system fell to <500 microns. However, tests showed that camera placement, quality and ambient lighting conditions can significantly impact the accuracy and repeatability of these measurements. Fixed camera positions and controlled lighting techniques were incorporated into the image processing apparatus to provide uniform test conditions. Further development of this system with more advanced cameras and software development could potentially remove the requirement for several stages of visual inspection, streamlining manufacture and provide a comprehensive measure of IR element cosmetic quality.

Future work:

Future developments in the area of test execution systems could follow a number of paths:

Development of additional test stations:

Test station 2 was identified as a potential system bottleneck due to the duration of the test. The current TES can output a full tested part every 12-16 seconds depending on part type. This may be increased by adding a second heat up station to operate in parallel with test station 2. The addition of this station may reduce test times to 8-12 seconds.

Integration into other manufacturing processes:

An early concept for the TES was to integrate the final assembly stage and packaging stage with end-of-line testing to achieve continuous, streamlined product movement. The Bosch conveyor used in this system is capable of being integrated into other conveyor systems. Successful implementation of this integration would part handover times and increase overall production throughput, consistent with lean manufacturing concepts

Integration of image processing test station:

The image processing system described in Ch. 4.3 was a proof of concept exploration into the potential of machine vision for quality control using IR elements as a use case. This system has a huge potential to empirically identify and map IR element faults leading to higher quality control. In addition to functional analysis, a grading system, leveraging the power of image processing could ensure that IR element are sorted based on cosmetic issues, where IR element with surface defects which do not compromise the integrity of the product are integrated into larger ovens and space heaters, while perfect IR elements are sold individually.

Application of TES concepts to other products:

The TES was designed as a general purpose product test system that can be adapted to a range of individual products. Both hardware and software architectures are fully reconfigurable and modular. Each test station can accommodate a large volume of application specific test equipment and the conveyor system can be integrated into a

larger product transportation system. The true value of the TES will be seen in the adoption and deployment of the system across a range of product categories.

6   References & bibliography

[1]   George Chryssolouris, *Manufacturing Systems : Theory and Practice*. Verlag New York: Springer, 2006.

[2]   M. Groover, *Fundamentals of Modern Manufacturing: Materials, Processes, and Systems*. Wiley, 2010.

[3]   E. Puik, D. Telgen, L. Van Moergestel, and D. Ceglarek, "Robotics and Computer-Integrated Manufacturing Assessment of reconfiguration schemes for Reconfigurable Manufacturing Systems based on resources and lead time," 2016.

[4]   R. M. da Silva, F. Junqueira, D. J. S. Filho, and P. E. Miyagi, "Control architecture and design method of reconfigurable manufacturing systems," *Control Eng. Pract.*, vol. 49, pp. 87–100, 2016.

[5]   Y. Koren, U. Heisel, F. Jovane, T. Moriwaki, G. Pritschow, G. Ulsoy, and H. Van Brussel, "Reconfigurable Manufacturing Systems," *CIRP Ann. - Manuf. Technol.*, vol. 48, no. 2, pp. 527–540, 1999.

[6]   Y. Koren, "General RMS Characteristics. Comparison with Dedicated and Flexible Systems," in *Reconfigurable Manufacturing Systems and Transformable Factories*, Berlin, Heidelberg: Springer, 2006, pp. 27–45.

[7]   A. Botta, W. De Donato, V. Persico, and A. Pescapé, "Integration of Cloud computing and Internet of Things: A survey," *Futur. Gener. Comput. Syst.*, vol. 56, pp. 684–700, 2016.

[8]   A. Al-Fuqaha, M. Guizani, M. Mohammadi, M. Aledhari, and M. Ayyash, "Internet of Things: A Survey on Enabling Technologies, Protocols, and Applications," *IEEE Commun. Surv. Tutorials*, vol. 17, no. 4, pp. 2347–2376, 2015.

[9]   K. Henning, "Recommendations for implementing the strategic initiative INDUSTRIE 4.0," *Final Rep. Ind. 4.0 WG*, no. April, p. 82, 2013.

[10] D. Kolberg and D. Zühlke, "Lean Automation enabled by Industry 4.0 Technologies," *IFAC Proc. Vol.*, vol. 48, no. 3, pp. 1870–1875, 2015.

[11] L. Wang, M. Törngren, and M. Onori, "Current status and advancement of cyber-physical systems in manufacturing," *J. Manuf. Syst.*, vol. 37, pp. 517–527, 2015.

[12] S. Weyer, M. Schmitt, M. Ohmer, and D. Gorecky, "Towards industry 4.0 - Standardization as the crucial challenge for highly modular, multi-vendor production systems," *IFAC Proc. Vol.*, vol. 48, no. 3, pp. 579–584, 2015.

[13] B. Esmaeilian, S. Behdad, and B. Wang, "The evolution and future of manufacturing: A review," *J. Manuf. Syst.*, vol. 39, pp. 79–100, 2016.

[14] R. Ayres, "The impacts of industrial robots," *Carnegie Melon Univ.*, no. November 1981, p. 60, 1981.

[15] E.Weisberg David, "Chapter 2 A Brief Overview of the History of CAD," *World*, 2008. [Online]. Available: http://www.cadhistory.net. [Accessed: 06-Jun-2016].

[16] P. Wright, *21st Century Manufacturing*. Prentice Hall, 2001.

[17] E. P. Degarmo, R. a Kohser, and B. E. Klamecki, "Materials and Process in

Manufactoring," *Mater. Process Manuf.*, p. 383, 2003.

[18] T. J. Goldsby, S. E. Griffis, and A. S. Roath, "Modeling Lean, Agile, and Leagile Supply Chain Strategies," *J. Bus. Logist.*, vol. 27, no. 1, pp. 57–80, 2006.

[19] R. B. S. Consultants, "Mastering Product Complexity," 2012.

[20] Z. M. Bi, S. Y. T. Lang, W. Shen, and L. Wang, "Reconfigurable manufacturing systems: the state of the art," *Int. J. Prod. Res.*, vol. 46, no. May, pp. 967–992, 2006.

[21] R. Ramaswamy and R. Rowthorn, "Deindustrialization: Causes and Implications," *IMF Working Papers*, vol. 97, no. 42. p. 1, 1997.

[22] A. Dujin, C. Geissler, and D. Horstkötter, "Industry 4.0 The new industrial revolution How Europe will succeed," *Rol. Berger Strateg. Consult.*, no. March, pp. 1–24, 2014.

[23] C. A. Giffi, "Global Manufacturing Competitiveness Index," *Deloitte*, p. 40, 2013.

[24] R. Berger, "The Industrie 4.0 transition quantified," p. 19, 2015.

[25] S. Heng, "Industry 4.0: Huge potential for value creation waiting to be tapped.," *Dtsch. Bank Res.*, vol. 0, pp. 8–10, 2014.

[26] S. B. Rate, "Automation Industry : Industry 4 . 0 Challenges and Solutions for Storage Devices," vol. 0, 2011.

[27] T. Chen and H.-R. Tsai, "Ubiquitous manufacturing: Current practices, challenges, and opportunities," *Robot. Comput. Integr. Manuf.*, vol. 45, pp. 126–132, 2016.

[28] A. Blanter and M. Holman, "Silicon Valley Thought Leaders Series. Internet of Things 2020: A Glimpse into the Future.," 2014.

[29] L. Monostori, "Cyber-physical production systems: Roots, expectations and R&D challenges," *Procedia CIRP*, vol. 17, pp. 9–13, 2014.

[30] L. Monostori, B. Kádár, T. Bauernhansl, S. Kondoh, S. Kumara, G. Reinhart, O. Sauer, G. Schuh, W. Sihn, and K. Ueda, "Cyber-physical systems in manufacturing," *CIRP Ann. - Manuf. Technol.*, vol. 65, no. 2, pp. 621–641, 2016.

[31] B. Bagheri, S. Yang, H. A. Kao, and J. Lee, "Cyber-physical systems architecture for self-aware machines in industry 4.0 environment," *IFAC-PapersOnLine*, vol. 28, no. 3, pp. 1622–1627, 2015.

[32] R. Rajkumar, I. Lee, L. Sha, and J. Stankovic, "Cyber-physical systems: The next computing revolution," *47th ACM/IEEE Des. Autom. Conf.*, pp. 731–736, 2010.

[33] E. A. Lee, "Cyber physical systems: Design challenges," *Object Oriented Real-Time Distrib. Comput. (ISORC), 11th IEEE Int. Symp.*, pp. 363–369, 2008.

[34] D. H. Liles and B. L. Huff, "A computer based production scheduling architecture suitable for driving a reconfigurable manufacturing system," *Comput. Ind. Eng.*, vol. 19, no. 1–4, pp. 1–5, 1990.

[35] M. G. Mehrabi, G. Ulsoy, and Y. Koren, "Reconfigurable manufacturing systems and their enabling technologies," *Int. J. Manuf. Technol. Manag.*, vol. 1, no. 1, pp. 114–131, 2000.

[36] M. R. A. and A. W. Labib, "Feasibility study of the tactical design justification for reconfigurable manufacturing systems using the fuzzy analytical hierarchical process," *Int. J. Prod. Res.*, vol. Vol. 42 , no. 15, 2004.

[37] T. Alix, Y. Benama, and N. Perry, "Reconfigurable Manufacturing System Design: The Case of Mobile Manufacturing System," *IFIP Adv. Inf. Commun. Technol.*, vol. 440, no. PART 3, 2014.

[38] A. M. Deif and W. H. ElMaraghy, "A control approach to explore the dynamics of capacity scalability in reconfigurable manufacturing systems," *J. Manuf. Syst.*, vol. 25, no. 1, pp. 12–24, 2006.

[39] M. Duelli and J. Bartels, "Industrie 4.0," *Sonderbeil. Handel. vom 12.03.2014*, no. 5, p. 18, 2014.

[40] E. Abele, J. Metternich, M. Tisch, G. Chryssolouris, W. Sihn, H. ElMaraghy, V. Hummel, and F. Ranz, "Learning factories for research, education, and training," *Procedia CIRP*, vol. 32, no. Clf, pp. 1–6, 2015.

[41] U. Wagner, T. AlGeddawy, H. ElMaraghy, and E. Müller, "The state-of-the-art and prospects of learning factories," *Procedia CIRP*, vol. 3, no. 1, pp. 109–114, 2012.

[42] M. Tisch, C. Hertle, J. Cachay, E. Abele, J. Metternich, and R. Tenberg, "A systematic approach on developing action-oriented, competency-based Learning Factories," *Procedia CIRP*, vol. 7, pp. 580–585, 2013.

[43] J. Vanian, "Why Data Is The New Oil," *Forbes*, 2016. [Online]. Available: http://fortune.com/2016/07/11/data-oil-brainstorm-tech/. [Accessed: 16-Jan-2017].

[44] GE Intelligent Platforms, "The Rise of Industrial Big Data," 2012.

[45] Tata Consultancy Services(TCS), "TCS Big Data Conclave," 2012.

[46] M. Troester, "Big Data Meets Big Data Analytics," *SAS Inst.*, 2012.

[47] J. Lee, B. Bagheri, and C. Jin, "ScienceDirect Introduction to cyber manufacturing," *Manuf. Lett.*, vol. 8, pp. 11–15, 2016.

[48] M. Schuval, "Manufacturing for the Future: The Customer Centric Manufacturer," *Datix ERP & CRM*, 2012. [Online]. Available: http://www.datixinc.com/wp-content/uploads/2014/03/cloud-and-big-data-ms-manufacturing.jpg. [Accessed: 02-Jan-2017].

[49] A. A. Brian, "Measurement Science Roadmap for Prognostics and Health Management for Smart Manufacturing Systems Prepared for."

[50] K. Stevenson, "2012-2013 Intel IT Performance Report," 2013.

[51] B. Marr, "Big Data At Tesco: Real Time Analytics At The UK Grocery Retail Giant," *Forbes*, 2016.

[52] W. Hauschild and E. Lemke, *High-Voltage Test and Measuring Techniques*. 2014.

[53] P. W. Brazis, *The Dielectric Voltage Withstand Test: Benefits and Limitations*. Underwriters Limited LLC, 2012.

[54] *UL 499 Electric Heating Appliances*. Underwriters Limited Inc., 2005.

[55] B. S. En, "Information technology equipment — Routine electrical safety testing in production," vol. 3, 2006.

[56] "Standard Test Mehod for Dielectric Breakdown Voltage adn Dielectric Strength of Solid Electrical Insulating Materials at Commercial Power Frequencies," *Am. Soc. Test. Mater.*, vol. D149–97a, 2004.

[57] P. Still, "PAT testing of equipment having high protective leakage curretnt," 2005.

[58] "SI No. 299 Safety, health and welfare at work," vol. 2007, no. 299, 2007.

[59] CENELEC, "Iec 950 Safety of information technology equipment," vol. 60950.

[60] Megger, "' A Stitch in Time ...' The Complete Guide to Electrical Insulation Testing," *Megger*, pp. 21–22, 2006.

[61] Optris GmbH, "Basic principles of non-contact temperature measurement," Berlin, Germany.

[62] O. GmbH, "Basic principles of non-contact temperature measurement."

[63] A. Rogalski, "History of infrared detectors," *Opto-Electronics Rev.*, vol. 18, no. 2, pp. 121–136, 2010.

[64] W. L. Wolfe and P. W. Kruse, "Thermal Detectors," *Handb. Phys.*, pp. 1–14, 1995.

[65] A. Rogalski, "Infrared detectors: An overview," *Infrared Phys. Technol.*, vol. 43, no. 3–5, pp. 187–210, 2002.

[66] A. Rogalski, "Progress in focal plane array technologies," *Prog. Quantum Electron.*, vol. 36, no. 2–3, pp. 342–473, 2012.

[67] M. R. Montgomery, "Using IR Thermography as a Predictive Maintenance Tool in an Electronics Manufacturing Facility." [Online]. Available: http://www.irinfo.org/07-01-2010-montgomery/.

[68] J. Wardlaw, F. Wanner, and G. Brostow, "EngD Group Project A New Approach to Thermal Imaging Visualisation," 2010.

[69] F. Ke, J. Xie, and Y. Chen, "A flexible and high precision calibration method for the structured light vision system," *Optik (Stuttg).*, vol. 127, no. 1, pp. 310–314, 2016.

[70] T. Luhmann, "ISPRS Journal of Photogrammetry and Remote Sensing Close range photogrammetry for industrial applications," *ISPRS J. Photogramm. Remote Sens.*, vol. 65, no. 6, pp. 558–569, 2010.

[71] Z. M. Bi and L. Wang, "Advances in 3D data acquisition and processing for industrial applications," *Robot. Comput. Integr. Manuf.*, vol. 26, no. 5, pp. 403–413, 2010.

[72] F. Ke, J. Xie, and Y. Chen, "A flexible and high precision calibration method for the structured light vision system," *Optik (Stuttg).*, vol. 127, no. 1, pp. 310–314, 2016.

[73] Creaform, "Measurement technologies in quality control," no. March, 2014.

[74] H. Fathi, F. Dai, and M. Lourakis, "Advanced Engineering Informatics Automated as-built 3D reconstruction of civil infrastructure using computer vision : Achievements , opportunities , and challenges," *Adv. Eng. Informatics*, vol. 29, no. 2, pp. 149–161, 2015.

[75] M. K. Johnson and E. H. Adelson, "Shape estimation in natural illumination," *Proc. IEEE Comput. Soc. Conf. Comput. Vis. Pattern Recognit.*, pp. 2553–2560, 2011.

[76] Z. M. Bi and L. Wang, "Advances in 3D data acquisition and processing for industrial applications," *Robot. Comput. Integr. Manuf.*, vol. 26, no. 5, pp. 403–413, 2010.

[77] S. Van der Jeught and J. J. J. Dirckx, "Real-time structured light profilometry: A review," *Opt. Lasers Eng.*, vol. 87, pp. 18–31, 2015.

[78] R. Boridy, "TeleDyne 3D Laser Triangulation Calibration," 2013. [Online]. Available: http://blog.teledynedalsa.com/2013/02/calibrating-2d-cameras-for-3d-machine-vision-inspection/.

[79] S. Van der Jeught and J. J. J. Dirckx, "Real-time structured light profilometry: A review," *Opt. Lasers Eng.*, vol. 87, pp. 18–31, 2015.

[80] K. Leuven, "Structured Light." [Online]. Available: http://www.esat.kuleuven.be/psi/research/structured-light.

[81] S. Gerbino, D. M. Del Giudice, G. Staiano, A. Lanzotti, and M. Martorelli, "On the influence of scanning factors on the laser scanner-based 3D inspection process," *Int. J. Adv. Manuf. Technol.*, vol. 84, no. 9–12, pp. 1787–1799, 2016.

[82] J. Baqersad, P. Poozesh, C. Niezrecki, and P. Avitabile, "Photogrammetry and optical methods in structural dynamics – A review," *Mech. Syst. Signal Process.*, pp. 1–18, 2016.

[83] National Instruments, "Automated Test Outlook," 2016.

[84] S. J. Meyer, "Using Big Data in Manufacturing at Intel ' s Smart Factories IT @ Intel Intel ' s Long-Term Vision of," no. April, 2016.

[85] P. Auerkari, "Mechanical and physical properties of engineering alumina ceramics," *Tech. Res. Cent. Finl.*, vol. 1792, p. 26, 1996.

[86] Z. Chen and C. Lu, "Humidity Sensors: A Review of Materials and Mechanisms," *Sens. Lett.*, vol. 3, no. 4, pp. 274–295, 2005.

[87] GE measurement and control, "Panametrics Aluminium Exide Moisture Probe," 2014.

[88] K. Davis, "Material Review: Alumina (Al 2 O 3).," *Sch. Dr. Stud. Eur. Union J.*, pp. 109–114, 2010.

[89] E. B. G. Donald A. McQuarrie, Peter A. Rock, *McQuarrie General Chemistry*. 2011.

[90] F. Wilson, *HeatWorks*, no. February. Ceramicx, 2015.

[91] Statex Productions, "Shieldex Bremen technical datasheet," 2010.

[92] D. Pont, "Material Safety Data Sheet Material Safety Data Sheet," vol. 3, pp. 1–

5, 2010.

[93]   Iolitec Nanomaterials, "Aluminium Oxide MSDS," 2010.

[94]   FLIR Systems UK, "Thermal imaging for electrical / mechanical diagnostics."

[95]   S. Bagavathiappan, B. B. Lahiri, T. Saravanan, J. Philip, and T. Jayakumar, "Infrared thermography for condition monitoring - A review," *Infrared Phys. Technol.*, vol. 60, pp. 35–55, 2013.

[96]   Optris Gmbh, *Optris PI Thermal Camera Manual*. Berlin, 2015.

[97]   M. D. Abràmoff, P. J. Magalhães, and S. J. Ram, "Image processing with imageJ," *Biophotonics Int.*, vol. 11, no. 7, pp. 36–41, 2004.

[98]   A. McNaughton, "Image J Thresholding - Measuring Area Using Thresholds," vol. 256, no. 0, pp. 8–10, 2010.

[99]   A. Gruen, "Recent advances of photogrammetry in robot vision," vol. 47, pp. 307–323, 1992.

[100] L. Siegele, "A Cambrian moment," *The Economist*, 2014. .

7 Appendices

Wiring block diagrams:

1) Conveyor cabinet electrical
2) Conveyor cabinet pneumatic
3) Hi-Pot test station
4) Heat-Up test station

Software flowcharts

1) Hi-pot test station
2) Heat-Up test station
3) ImageJ image processing macro

Mains In

Mains Disconnect Switch

MCB

RCD

Power Meter

Operator Control
- ON
- OFF
- E-Stop

Conveyor E-Stop

Safety Relay

24V PSU

NI DAQ

Conveyor Motor 1

EMI Filter 1

Lenke VFD 1

Conveyor Motor 2

EMI Filter 2

Lenke VFD 1

Cabinet Monitor

Network Switch

HMI

Industrial PC

230V Socket Station 1-7

Ethernet Socket Station 1-7

Conveyor Comm port 1-7

Conveyor Prox Sensor 1-7

Status Traffic Light

Prepared By:	Cian Martin
Date:	5 April 2018
Description:	
CIRCLE Main Cabinet Block Diagram	
Rev: 1	Trinity College Dublin Coláiste na Tríonóide, Baile Átha Cliath The University of Dublin
Description:	

| 7 Bar In | → | Manual Shutoff Valve | → | Pressure Regulator | → | Dump Valve | → | Air Socket Station 1-7 |

Prepared By:	Cian Martin
Date:	5 April 2018
Description:	
CIRCLE Main Cabinet Pneumatic Block Diagram	
Rev: 1	Trinity College Dublin Coláiste na Tríonóide, Baile Átha Cliath The University of Dublin
Description:	

CIRCLE Hipot Station Block Diagram

Prepared By:	Cian Martin
Date:	5 April 2018
Description:	
CIRCLE Hipot Station Block Diagram	
Rev: 1	

230V In

Ethernet Socket

Pneumatic Socket

Solid State Relay

24V PSU

Pressure Regulator

Ethernet To USB Converter

NI CompactRIO

Thermal Camera

NI DAQ

Pneumatic Controller

Lift Actuator

NI Thermocouple

Stop Gate

Contact Actuator

Proximity Sensor

Electrical Contactor

Pallet

Prepared By:	Cian Martin
Date:	5 April 2018
Description:	
CIRCLE Heat-Up Station Block Diagram	
Rev: 1	

Trinity College Dublin
Coláiste na Tríonóide, Baile Átha Cliath
The University of Dublin

Set Resistance Limit (± 1,2,5,10%)
Set Leakage Current Limit (± X mA)
Set Voltage Applied (V)
Set HiPot Test time (S)

Lower Station Input Gate:
Proximity Sensor
Triggered?

Y

N

Wait

Raise Station Exit Gate.
Raise Pallet Lift Actuator.
Extend Electrical Contactor Actuator

Lower Station Exit Gate
Pallet moves to next test
station

Switch contact to
"Resistance"

**Part Pass
Retract Electrical Contactor
Lower Pallet Lift Actuator**

Extend Compression
Actuator

Y

Measure Cold Resistance
Pass?

Y

Switch contact to "Hi-Pot"

Perform Hi-Pot Test
Pass?

N

N

Part Fail
Retract Electrical Contactor
Lower Pallet Lift Actuator

Part Fail
Retract Electrical Contactor
Lower Pallet Lift Actuator

Lower Station Exit Gate
Pallet skips subsequent
testing and is removed.

Lower Station Exit Gate
Pallet skips subsequent
testing and is removed.

Prepared By:	Cian Martin
Date:	5 April 2018
Description:	
	HiPot Station Software Flowchart
Rev: 1	

Trinity College Dublin
Coláiste na Tríonóide, Baile Átha Cliath
The University of Dublin

5

Perform Thermocouple Test? (Boolean)
Set Thermocouple Type (K, T, J)
Set Thermal Image Interrogation Window
Set acceptable IR-cam temperature change
Set Resistance Limit (± 1,2,5,10%)

Lower Station Input Gate:
Proximity Sensor
Triggered?

Y

N

Wait

Raise Station Exit Gate.
Raise Pallet Lift Actuator.
Extend Electrical Contactor Actuator

Switch Relay to Mains
Voltage.
Apply Power to DUT

Initiate IR Cam
Measurement
Pass?

Record Thermocouple
Measurement
Pass?

N

Y

Switch Relay to Resistance

Measure Hot Resistance.
Pass?

Y

N

Lower Station Exit Gate
Pallet moves to next test
station

Part Pass
Retract Electrical Contactor
Lower Pallet Lift Actuator

Part Fail
Retract Electrical Contactor
Lower Pallet Lift Actuator

Lower Station Exit Gate
Pallet skips subsequent
testing and is removed.

Part Fail
Retract Electrical Contactor
Lower Pallet Lift Actuator

Lower Station Exit Gate
Pallet skips subsequent
testing and is removed.

Prepared By:	Cian Martin
Date:	5 April 2018
Description:	
	Heat-Up Station Software Flowchart
Rev: 1	

Trinity College Dublin
Coláiste na Tríonóide, Baile Átha Cliath
The University of Dublin

Flowchart steps (top to bottom):
- Open camera feed for X/Y/Z web cam
- Wait 2 seconds for image to stabilize
- Capture image from each web cam
- Convert image from colour to black & white
- Convert image from 32-bit B&W to 8-bit B&W
- Run threshold analysis to convert to binary image
- Run Feret's diameter, Feret's minimum diameter, perimeter and area measurement

Labels on final image:
- Perimeter
- Minimum Feret's Diameter
- Feret's Diameter
- Area

Prepared By:	Cian Martin
Date:	5 April 2018
Description:	
	ImageJ Macro Flowchart
Rev: 1	

Trinity College Dublin
Coláiste na Tríonóide, Baile Átha Cliath
The University of Dublin